DEPARTMENT OF PHYSICS, UNIVERSITY OF JYVÄSKYLÄ
RESEARCH REPORT No. 4/1998

DECAY STUDIES OF EXOTIC NUCLEI NEAR THE Z = N LINE

BY
MARKKU OINONEN

Academic Dissertation
for the Degree of
Doctor of Philosophy

Jyväskylä, Finland
April 1998

URN:ISBN:978-951-39-9737-3
ISBN 978-951-39-9737-3 (PDF)
ISSN 0075-465X

Jyväskylän yliopisto, 2023

ISBN 951-39-0218-8
ISSN 0075-465X

KOPIJYVÄ OY – Jyväskylä 1998

DEPARTMENT OF PHYSICS, UNIVERSITY OF JYVÄSKYLÄ
RESEARCH REPORT No. 4/1998

DECAY STUDIES OF EXOTIC NUCLEI NEAR THE Z = N LINE

BY
MARKKU OINONEN

Academic Dissertation
for the Degree of
Doctor of Philosophy

To be presented, by permission of the
Faculty of Mathematics and Natural Sciences
of the University of Jyväskylä,
for public examination in Auditorium FYS-1
of the University of Jyväskylä on April 24, 1998,
at 12 o'clock noon

Jyväskylä, Finland
April 1998

Preface

Experimental studies for this work have been performed in three major laboratories around Europe during the years 1994-1997. Most of the experiments have been carried out at European Laboratory of Particle Physics(CERN) in Geneva. In addition, studies have been done at Accelerator Laboratory of University of Jyväskylä and at Gesellschaft für Schwerionenforschung(GSI) in Darmstadt. Regardless of the international nature of these studies, the most important part of the work of preparation and analyzing the experimental data has been carried out at Department of Physics in Jyväskylä. I am very grateful of this support of the whole Department and want to thank, especially, Dr. Pete Jones, who patiently guided me into the mysteries of the data analysis software.

It has been a pleasure to work with the international collaborators taking part in the experiments. I would like to thank especially professor Ernst Roeckl, professor Piet Van Duppen and Dr. Guy Walter for the helpful discussions with them during recent years and for the effort they have put on my career. Also, I want to express my gratitude to all of the other collaborators in these experiments performed abroad and in Jyväskylä. Without their hard labour this thesis would not have been completed.

The IGISOL group at JYFL deserves a special thanks. Useful, and sometimes quite intensive, discussions especially with Dr. Antti Honkanen, Dr. Ari Jokinen and Mr. Kari Peräjärvi stimulated my mind during this work. Most of all, I want to thank my supervisor professor Juha Äystö, who dynamically leads the group and has offered me a possibility to participate in this extremely interesting research. Experimental physicists would not exist without theoretical modelling of the nuclear properties. Therefore, emeritus professor and real gentleman, Pertti Lipas merits very special thanks for introducing me the basics of the nuclear shell model.

Finally, I would like to thank Maarit for the support whenever it has been necessary.

Jyväskylä, April 1998
Markku Oinonen

Abstract

This thesis is based on beta-decay studies performed during 1994-1997 in three mass-separator facilities in Europe. Most of the experiments have been done at the ISOLDE facility at CERN. In addition, experiments were carried out at the GSI On-Line Mass Separator in Darmstadt and the Heavy-ion Ion-Guide Isotope Separator On-Line (HIGISOL) in Jyväskylä. The production methods used were fusion-evaporation reactions at GSI and JYFL as well as fragmentation and spallation at ISOLDE. Production of refractory elements from Y to Mo was proved successful using the heavy-ion fusion-evaporation reactions in connection with the ion-guide technique at JYFL. These complementary facilities offered means to obtain new information on several beta-decaying isotopes along Z = N line in the region A = 55 - 85 by using beta-delayed gamma and proton spectroscopy. The Gamow-Teller strengths for the low-energy final states could be determined for four isotopes leading to a comparison of the results of the beta-decay and charge-exchange reaction studies in the case of ^{58}Zn. The systematics of the ground-state Gamow-Teller matrix elements could be extended for the mirror decays in fp shell. The proton drip line was reached for Rb isotopes and new information was obtained for refractory elements above A = 80. In addition to the nuclear structure studies, the output of these studies can be straightly used as an input for the astrophysical reaction flow calculations.

Table of Contents

1. Introduction

Studies of exotic nuclei near the proton drip line in the *fp* shell have gained interest during recent years due to several reasons. These nuclei are characterized by the nearly equal number of protons and neutrons in the same shell-model orbitals. Thus, the role of N = Z symmetry in determining the properties of low-lying states in nuclei is enhanced. Especially, proton-neutron pairing leading to an additional binding energy for N = Z nuclei determines the ground-state energies of the nuclei. Therefore, the position of the proton drip line is also affected by the p-n pairing. Ordering of $T = 0$ and $T = 1$ states in odd-odd N = Z nuclei is determined by the interaction strengths involved in the pairing. Above A = 60, increased number of valence nucleons give rise to deformations. The deformation can alter the level structure at low energies and even shape coexistence may occur. The position of the high-lying states can also be affected by deformation and could even be a tool to discriminate between different shapes of nuclei. Theoretical interest has moved towards higher masses above the *sd* shell. Computational capacity for full-space shell-model calculations has already reached region A ~ 50 [Mar97]. Although full-space calculations in the whole *fp* shell are still limited, one can obtain relevant information for example on binding energies using a truncated configuration space [Orm97]. Other approaches such as shell-model Monte Carlo [Joh92, Lan93] or Hartree-Fock calculations [Fri95] have also proven to be reasonable tools in predicting properties of proton-rich nuclei. From the astrophysical point of view, nuclei between A = 60 and 100 are heavily involved in the rapid proton capture process. This process may be responsible for producing certain isotopes of high abundancies in the solar system. Model calculations for the capture path need experimental information on the states in participating nuclei.

Beta decay probing the low-lying structure in nuclei provides important information for testing model predictions. Beta-decay studies based on beta-delayed gamma emission have been successful for the studies of the lowest-lying states. Near the proton drip line beta-delayed proton emission becomes important and offers a sensitive method for studies of higher-lying states. Experimental information near the drip line above A = 60 has been scarce. As an example of this Fig.1 shows the beta-decay Q values for mirror decays above A = 40. Values based on the systematics of Audi and Wapstra [Aud95] above A = 60 do not seem to follow

the behaviour observed between the shell closures at A = 40 and 56. The smooth line corresponds to the fit to experimental Coulomb displacement energies giving good agreement between A = 40 and 56. However, the global nature of the fit does not reproduce the experimental energies at the shell closures. The need for experimental information above A = 60 is evident not only for energetics, but for half-lives and decay strengths as well.

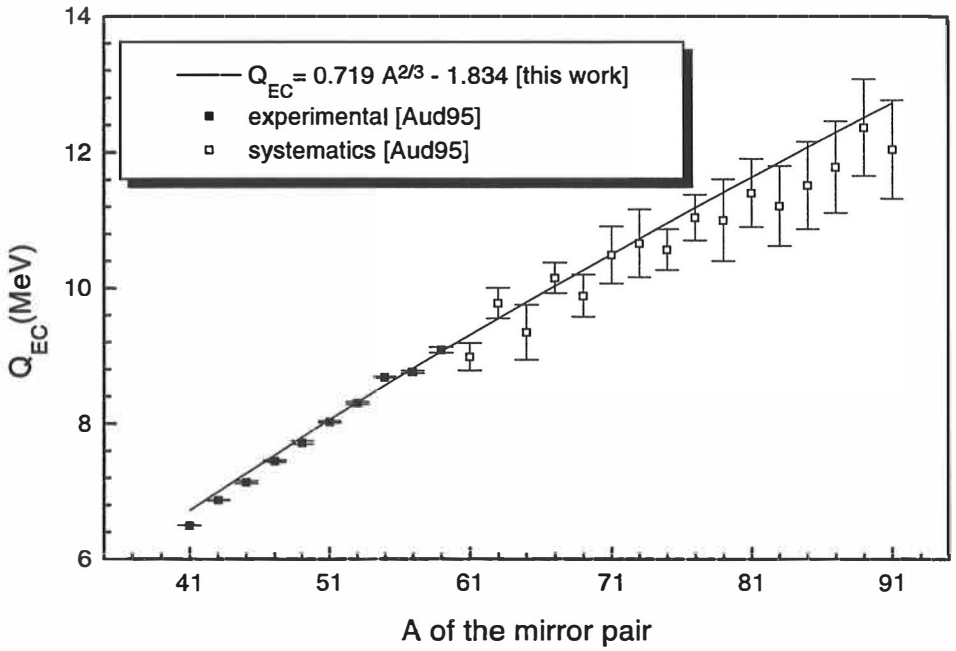

Figure 1. *Systematical trend of beta-decay energies above A = 40 for mirror pairs.*

In this work beta decays of proton-rich isotopes in the mass region A = 55-85 have been studied experimentally. These studies have been performed using different mass-separator facilities in Europe. Isotopes ^{58}Zn, ^{70}Kr, ^{71}Kr, ^{73}Rb and ^{74}Rb have been investigated at ISOLDE, CERN. In addition, the beta decay of ^{61}Ga was studied using the On-line Mass Separator at GSI, Darmstadt. Extension of studies towards mass region A = 80 - 88 has been carried out using the IGISOL mass separator at JYFL, Jyväskylä. These complementary facilities with sophisticated target/ion-source techniques provide tools which can be used for spectroscopic studies of exotic nuclei in the whole mass region between the doubly-magic ^{40}Ca and ^{100}Sn.

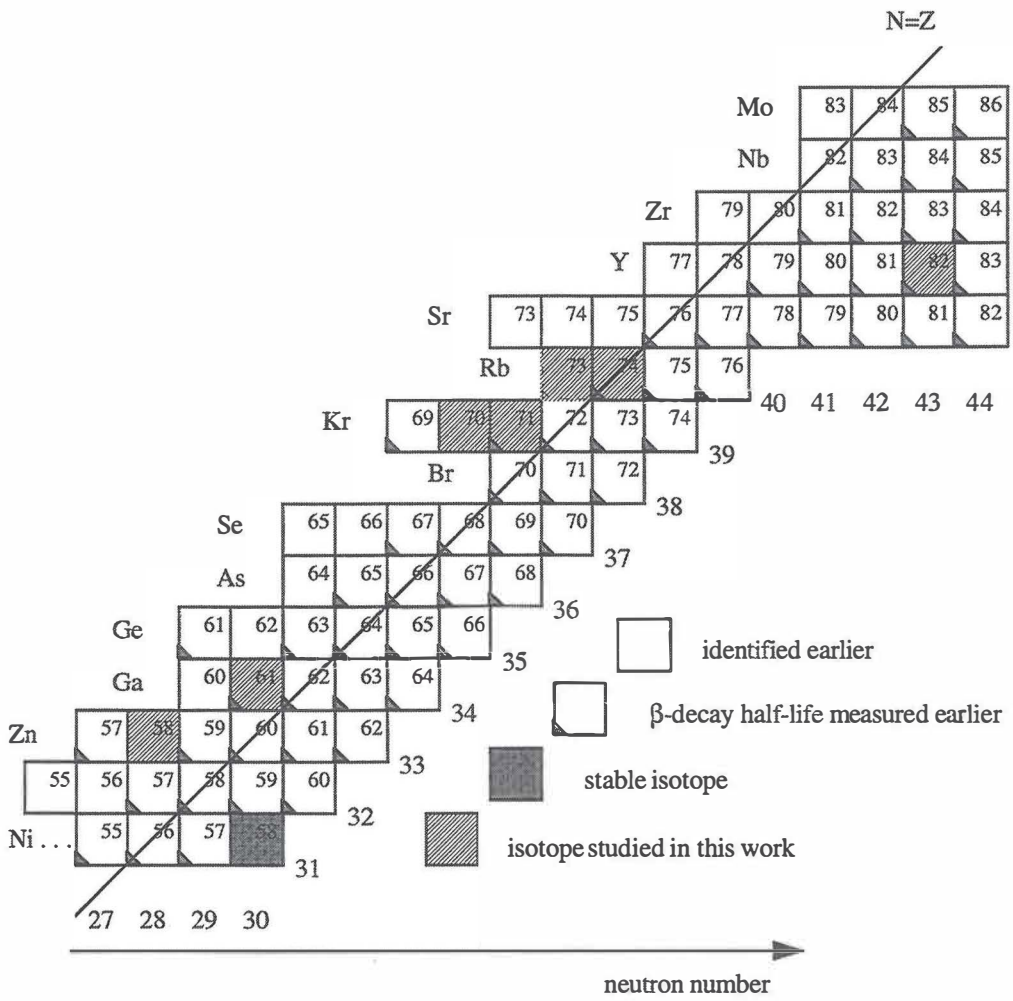

Figure 2. *Part of the nuclide chart near the proton drip line. Isotopes studied in this work have been marked by hatched squares.*

Figure 2 shows the part of the nuclide chart studied in this work. The production of these isotopes is characterized by low production cross sections. The isotopes from Zn to Sr can be, however, produced in measurable amounts using the mass-separator ISOLDE at CERN or the On-line Mass Separator at GSI. These facilities exploit conventional ion-source techniques. Production of refractory elements is problematic in these facilities due to the slow release times of the reaction products out of the target. The mass-separator IGISOL at JYFL provides a successful production method for these elements ranging from Y to Pd.

There is a long tradition in studies of proton-rich nuclei at the Physics Department of the University of Jyväskylä among both *sd*- and *fp*-shell nuclei [Hon81a, Hon81b, Hon82, Äys84, Hon87, Hon89, Hon98]. This work extends these studies towards the end of the *fp* shell and beyond.

This thesis is based on the following publications:

1. Proton instability of ^{73}Rb

A.Jokinen, M.Oinonen, J.Äystö, P.Baumann, F.Didierjean, P.Hoff, A.Huck, A.Knipper, G.Marguier, Yu.N.Novikov, A.V.Popov, M.Ramdhane, D.M.Seliverstov, P.Van Duppen, G.Walter and the ISOLDE Collaboration, Z. Phys. A **355**(1996)227.
https://doi.org/10.1007/BF02769690

2. Beta decay of the proton-rich T_z = -1/2 nucleus, ^{71}Kr

M.Oinonen, A.Jokinen, J.Äystö, P.Baumann, F.Didierjean, A.Honkanen, A.Huck, M.Huyse, A.Knipper, G.Marguier, Yu.Novikov, A.Popov, M.Ramdhane, D.M.Seliverstov, P.Van Duppen, G.Walter and the ISOLDE Collaboration, Phys. Rev. C **56**(1997)745.
https://doi.org/10.1103/PhysRevC.56.745

3. Study of the beta decay of a M_T = -1 nucleus ^{58}Zn using selective laser ionization

A.Jokinen, M.Oinonen, J.Äystö, P.Baumann, P.Dendooven F.Didierjean, V.Fedoseyev, A.Huck, Y.Jading, A.Knipper, M.Koizumi, U.Köster, J.Lettry, P.Lipas, W.Liu, V.Mishin, M.Ramdhane, H.Ravn, E.Roeckl, V.Sebastian, G.Walter and the ISOLDE Collaboration, submitted to The European Physical Journal A (1998).
https://doi.org/10.1007/s100500050177

4. Beta decay of ^{61}Ga

M.Oinonen, P.Baumann, P.Dendooven, Y.Fujita, M.Górska, H.Grawe, Z.Hu, Z.Janas, A.Jokinen, R.Kirchner, O.Klepper, A.Knipper, W.Liu, H.Penttilä, A.Plochocki, M.Ramdhane, E.Roeckl, G.Walter and J.Äystö, submitted to The European Physical Journal A (1998).
https://doi.org/10.1007/s100500050271

5. Production of refractory elements close to Z = N line using the ion-guide technique
M.Oinonen, R.Beraud, G.Canchel, E.Chabanat, P.Dendooven, A.Emsallem, S.Hankonen, A.Honkanen, J.Huikari, A.Jokinen, G.Lhersonneau, Ch.Miehé, A.Nieminen, Yu.Novikov, H.Penttilä, K.Peräjärvi, A.Popov, D.M.Seliverstov, J.C.Wang and J.Äystö, submitted to Nucl. Instr. and Meth. in Phys. Res. A (1998).
https://doi.org/10.1016/S0168-9002(98)00613-5

2. Theoretical background

2. 1. Shell model in the region A > 56

The nuclear shell model (SM) has been successful in explaining the basic properties of nuclei near the closed shells. The original shell model for spherical nuclei has to be modified for the region between the closed shells for collective effects. This has been done using the Nilsson model where single-particle states are generated using a deformed potential. In the *sd* shell, where deformations do not play a significant role, the success of the spherical SM has been undisputable. Limitations in the use of the SM in the *fp* shell are mainly computational since the dimensions of the shell-model spaces rapidly grow as the number of valence nucleons increases.

2.1.1. Shell structure above Z = N = 28

The nuclear shell model is based on the assumption that each nucleon moves independently in an average potential created by the other nucleons. Qualitatively, this assumption has its groundings on the short range of the nucleon-nucleon interaction and on the Pauli principle. Striking evidence for the shell structure in nuclei can be seen in Fig. 2 where the energies of the lowest 2^+ states have been plotted for certain even-even nuclei above A = 40. The excitation energy of the lowest state is remarkably large for the $M_T = 0$ nucleus with Z = 28, i.e. for ^{56}Ni. This is due to the doubly-magic structure of this particular nuclide. The difference in energies between the ground state and the first excited state for doubly-magic nuclei corresponds roughly to the difference in energy between two major shells in the framework of the single-particle shell model. Nucleons in the closed-shell nuclei are evenly distributed spatially and drive the nuclei into spherical ground-state shape. The low excitation energies between the filled shells near Z = 40 are due to angular-momentum coupling in excitations involving several nucleons. The increased number of valence nucleons forces the nucleus to deform since the attractive nucleon-nucleon interaction favours nucleons to be spatially concentrated in certain regions. The highly deformed region near ^{80}Zr shown in Fig. 3 with $E(2^+)$ = 250-300 keV corresponds to a magnitude of quadrupole deformation $\beta_2 \sim 0.4$ [Lis87].

When going towards the doubly-magic ^{100}Sn, effects of collectivity decrease and a shape transition from a deformed to spherical nucleus occurs.

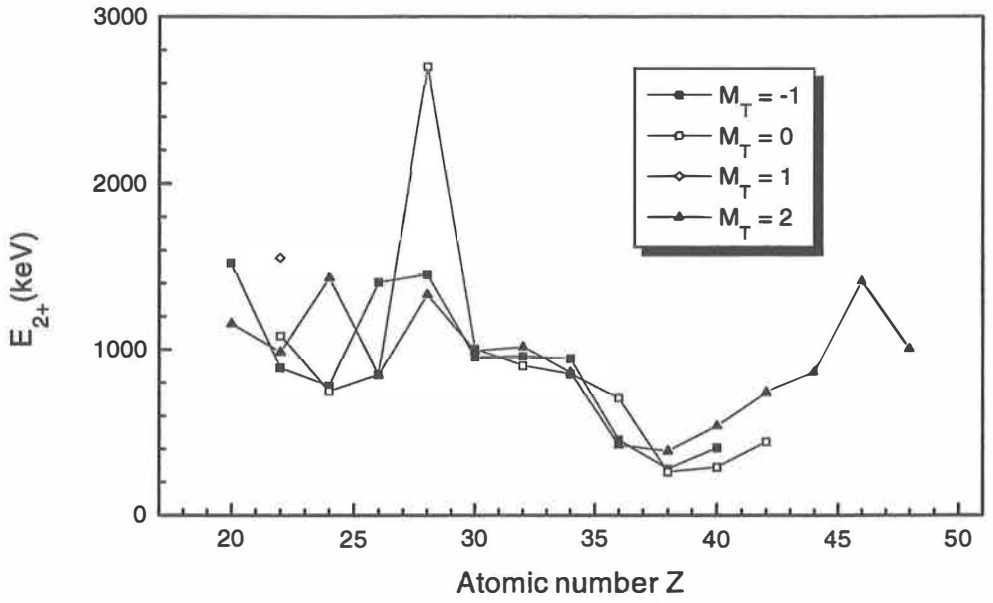

Figure 3. *Energies of the lowest 2^+ states in even-even nuclei near the N = Z line above A = 40.*

Under the assumption of an average potential inside the spherical nucleus, energies for single-particle states can be calculated. Figure 4 shows schematically occupation of single-particle states of nuclei studied in this work. In the case of ^{58}Zn, the single-particle picture is justified since only two protons occupy the $2p_{3/2}$ orbital. However, the increase of collectivity due to the increased number of valence nucleons in heavier nuclei cause a substantial increase in the number of states due to angular-momentum coupling between the valence nucleons. Configuration mixing between these states lead to altered level energies and thus affect transition strengths. Calculated deformation parameters indicate an increase of deformation from ^{58}Zn to ^{74}Rb. Only a moderate deformation is predicted for ^{82}Y whereas ^{81}Y is expected to possess large deformation again [Möl95]. This is an example of expected rapid changes of shapes among nuclei being involved in an interplay between the *fp* shell and higher orbitals.

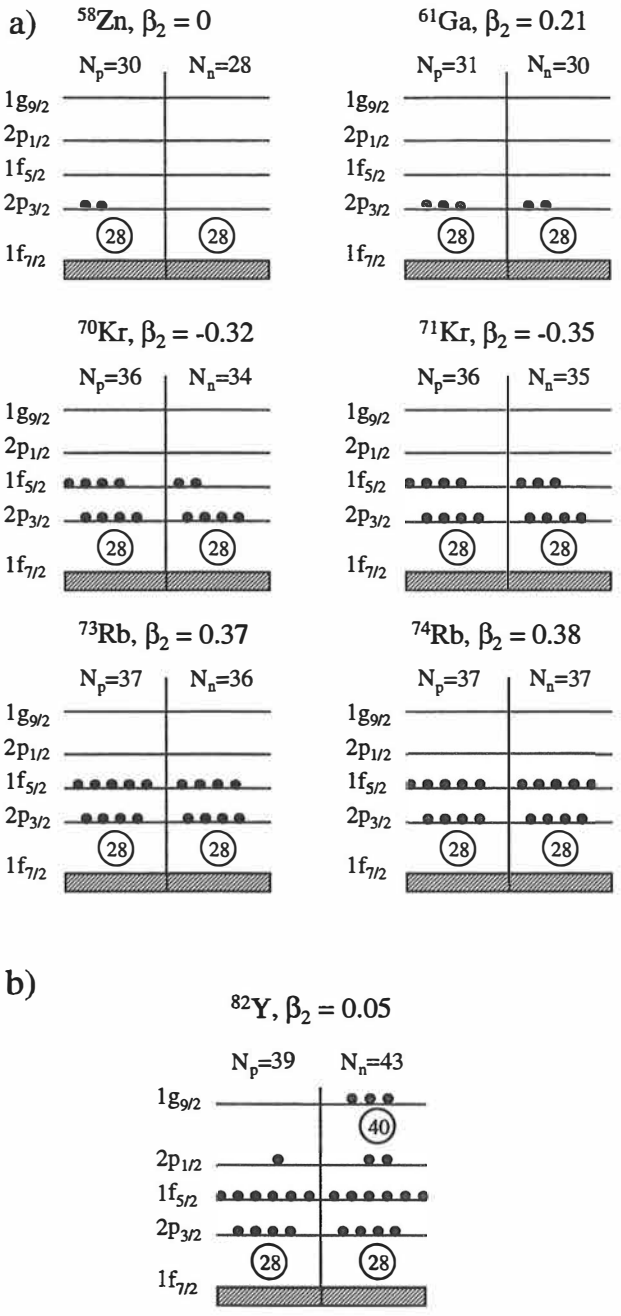

Figure 4. *Schematic view of occupation of single-particle states in spherical potential for nuclei studied in this work. a) studied fp-shell nuclei. b) contribution of the $1g_{9/2}$ orbital in the case of ^{82}Y. Calculated deformation parameters are also shown with minus sign indicating oblate (disc-shaped) and plus sign indicating prolate (cigar-shaped) deformation [Möl95].*

The role of proton-neutron interactions in determining the structure of nuclei have been stated a long time ago [Tal62]. The success of the so-called N_pN_n scheme in parametrizing the strength of the interaction, as well as the magnitude of deformation, illustrates its importance [Cas85]. Systematics of deformation effects in this scheme can be studied as a function of the product of number of valence nucleons. The role of the $1g_{9/2}$ orbit for driving the nucleus into deformation in the upper *fp* shell becomes evident within this approach since the number of possible nucleons in the orbital is as large as ten.

2.1.2. Single-particle energies in deformed potential: Nilsson model

A model for single-particle states in deformed nuclei was developed by Nilsson [Nil55] and by Mottelson and Nilsson [Mot55]. It is based on an axially-deformed core which is surrounded by a valence nucleon. Due to a non-spherical shape, the magnitude of the total angular momentum j of the single nucleon is not conserved but its projection Ω on the symmetry axis is. Also the $(2j+1)$ degeneracy associated with a certain j orbital is broken by deformation. Nilsson model leads to single-particle orbitals with a degeneracy of 2 and they are labelled by asymptotic quantum numbers $[Nn_z\Lambda]\Omega$ (see App.1). As an example, the $1f_{5/2}$ orbital in spherical potential is split into $\Omega = 1/2^-, 3/2^-, 5/2^-$ orbitals in the deformed potential.

A simple rule is that for prolate ($\beta_2 > 0$) deformations, the smallest possible Ω interacts most strongly with the core and is lowest in energy. With oblate ($\beta_2 < 0$) deformations, the rule is reversed. A sign of deformation in odd-A nuclei in the *fp* shell is thus observation of a $\Omega^\pi = 9/2^+$ state lowest in energy due to oblate deformation and a low lying $\Omega^\pi = 1/2^+$ state in the case of prolate deformation. In even-A nuclei, the excitation of a nucleon pair to the $1g_{9/2}$ orbit leads to a low-lying 0^+ intruder state. An interplay between the *fp* shell and the $1g_{9/2}$ orbit strengthening along the N = Z line towards A ~ 80 might lead to such an ordering of states that isomerism becomes possible. Isomerism requires a lack of suitable final states for the feeding and, indeed, in the vicinity of full *fp* shell for protons or neutrons many isomeric states have been observed.

2.1.3. Configuration mixing

In general, for A-nucleon systems the total Hamiltonian for particle motion is written as

$$H = H^{(0)} + H^{(1)} = \sum_{k=1}^{A} \left[T(k) + U(k) \right] + \left[\sum_{l=k<l}^{A} W(k,l) - \sum_{k=1}^{A} U(k) \right] \qquad (1)$$

where the independent particle motion is described by $H^{(0)}$. However, particles do not move independently inside the nucleus but are subject to a residual interaction $H^{(1)}$. This interaction arises from two-body interactions $W(k,l)$ between nucleons. The smaller the residual interaction, the better the motion of a nucleon is described by the independent particle approach. The usual method to obtain the best possible independent particle wave functions and corresponding eigenenergies is the Hartree-Fock method where the influence of the residual interaction is minimized.

If the energies of the A-particle states with the same J^{π} or Ω^{π} are close to each other in energy the residual interaction can cause scattering from one state to another. This is called configuration mixing and the state can be expressed as a linear combination of the individual A-body states Φ_k

$$\Psi_p = \sum_{k=1}^{g} a_{kp} \Phi_k \qquad (2)$$

where g = number of individual states, p = 1,...,g. The probability of having a nucleus in a state described by Φ_k is given by the square of the amplitude a_{kp}. The energy matrix following from the Schrödinger equation for mixed configurations can be diagonalized to obtain final eigenfunctions and eigenenergies, which characterize the state p. The diagonalization can never be performed taking into account all possible configurations since the dimensions of the matrix will then increase to infinity. Computing capacity sets the limits for available configuration spaces. The number of states involved in the calculation can be reduced by assuming an inert core with doubly-magic character and only a few active nucleons participating in the excitations. As an extreme example, the low-lying states of ^{58}Zn can be

expressed as ^{56}Ni core together with 2 protons in the $2p_{3/2}$ orbital leading to a ground state with $J^{\pi} = 0^{+}$ and an excited state with $J^{\pi} = 2^{+}$.

2.2. Isospin in the fp shell

The concept of isospin is used to identify two charge states of nucleons, protons and neutrons. It is defined such that protons have an isospin projection m_t = -1/2 and neutrons have m_t = +1/2. The definition of isospin relies on the fact that the proton and neutron have almost equal mass and their nuclear interactions are almost identical. Evidence for charge symmetry of nuclear force can be found in mirror nuclei which are characterized by nearly identical states at low energies. This chapter gives a basis for isospin-related subjects in nuclear physics studies among the *fp*-shell nuclei. The main results originating from isospin algebra are given and the role of isospin in nucleon-nucleon correlations is also discussed.

2.2.1. Isospin formalism

The total isospin of a nucleus can be obtained by summing the isospins of the constituent nucleons as in the case of angular momentum. The detailed algebra can be found, for example, in [Bru77, Hey94a]. Individual isospin vectors can be summed as:

$$\boldsymbol{T} = \sum_{k=1}^{A} \boldsymbol{t}(k) \tag{3}$$

It follows from the commutation relations that the eigenvalues for isospin operator $\boldsymbol{T}$ are:

$$\boldsymbol{T}^2 \Rightarrow T(T+1) \tag{4}$$

and for the isospin projection eigenvalue M_T, the possible values are between -T and T. So, for each value of T there is an isospin multiplet with $2T+1$ members which have different M_T components. For a particular nucleus the eigenvalue of the isospin projection is $M_T = 1/2(\mathrm{N}-\mathrm{Z})$ and it is often used as a measure of neutron deficiency of nuclei. The total

isospin T is at least as large as its projection $|M_T|$. Thus the states in a nucleus are characterized by isospins $T = |M_T|, |M_T|+1, \ldots, A/2$. Experimentally it has been observed that almost all of the ground states of the nuclei have the lowest possible value of the isospin $T = |M_T|$. The corresponding states among the isobars with the same T are called isobaric analog states (IAS) and consequently the wave functions of these states are identical. The absolute binding energies of these states should also be the same when correcting for Coulomb effects and for the mass difference between the proton and the neutron.

2.2.2. Isospin and nucleon-nucleon interaction near N = Z

The study of isospin triplets in two nucleon systems provides information on the nucleon-nucleon interaction. The simplest possible combinations are n-n, d and ^{2}He of which only the deuteron is bound. In the framework of the shell model, the simplest possible cases to study are systems with a doubly-magic Z = N core surrounded by a n-n, p-n or p-p pair. As an example, Fig. 5 shows the low-lying states of ^{58}Zn, ^{58}Cu and ^{58}Ni, which form an isospin mass triplet built on the doubly-magic nucleus ^{56}Ni. For two-nucleon systems with particles in the same orbit only states with $J + T$ = odd are possible because of the Pauli exclusion principle which requires the total wave function to be antisymmetric with respect to changing the particles. This leads to only $T = 1$ states in the case of n-n or p-p interactions but allows also $T = 0$ states for deuteron-like p-n pair. This can be seen in Fig.5 where the odd-J states in ^{58}Cu are $T = 0$ states generated by p-n coupling.

The ground-state spins of odd-odd N = Z nuclei are determined by the strengths of $T = 0$ and $T = 1$ pairing. All such nuclei with A < 40, except ^{34}Cl, have a $T = 0$ ground state with an odd value of spin. For A > 40 the ground-state isospin $T = 1$, except for ^{58}Cu, which has a $T = 0$ ground state with $J = 1$. In some cases low-lying $T = 0$ states among odd-odd N = Z nuclei are characterized by relatively long lifetimes since there are no suitable final states for a fast transition and thus isomers are found in nuclei such as ^{42}Sc, ^{50}Mn, ^{54}Co and ^{70}Br. The role of the p-n interaction is clearly visible in the masses of N = Z nuclei. Additional binding known as the Wigner-energy term found among *sd*-shell nuclei has been explained to arise mainly from the contribution of $T = 0$ pairing within SDI interaction [Bre90] as well as within

realistic KB3 interaction [Sat97]. In the *fp* shell the $T = 1$ pairing starts to dominate leading to $J = 0$ ground states.

The fact that the energies of the states within an isospin multiplet are almost equal indicates charge independence in nuclear configurations. However, the nuclear Hamiltonian is not fully charge independent i.e. scalar in isospin space (isoscalar), but may consist of higher order Coulomb terms as isovector and isotensor terms which violate the charge independence.

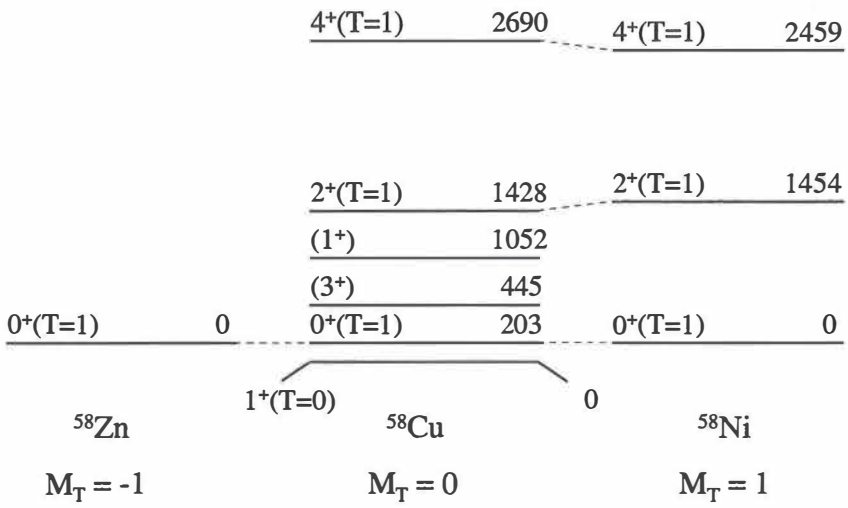

Figure 5. *Low-lying states of ^{58}Zn, ^{58}Cu and ^{58}Ni. Only low-lying $T = 0$ and $T = 1$ states are shown.*

The effect of higher-order terms is usually so small that it can be treated as a perturbation and thus the isospin can be considered as a good quantum number up to A = 100. In addition to pure Coulomb effects, also the charge-dependent part of the nuclear interaction has its contribution in the total charge-symmetry violating interaction H_{CV}. One of the effects due to H_{CV} is the mixing between $T' \neq T$ and T states called isospin mixing. Since the main contribution to H_{CV} comes from the Coulomb term and especially from the isovector part of it, the strongest mixing occurs between the states with T and $T' = T + 1$ [Aue83]. The amount of isospin impurities can be estimated using various methods [Aue83]. Isospin mixing plays important role in the case of $0^+ \rightarrow 0^+$ beta decays which are used to test conserved vector current hypothesis (CVC) in The Standard Model.

2.3. Mass predictions in the fp shell

Mass predictions for unknown nuclei have been compiled in [Hau88]. The most important ones for proton-rich *fp*-shell nuclei are the isobaric multiplet mass equation (IMME), the mass relations of Kelson-Garvey [Kel66] and Jänecke-Masson [Jän88] as well as the microscopic-macroscopic model of Möller and Nix [Möl81]. The last one gives a useful basis for astrophysical network calculations and the former two have been found to be the most accurate methods for the predictions of masses of neutron-deficient nuclei. In shell-model calculations, the nuclear binding energies are obtained with high accuracy among other quantities. Near the proton drip line single-particle wave functions of loosely bound protons extend further away compared to neutrons reducing the Coulomb energy. This reduction is called the Thomas-Ehrman shift [Tho51, Ehr51] and it can have a magnitude between a few tens of keV [Aue83] and even few hundred keV [Naz96]. This shift is partly taken into account in mass relations due to their local nature, but is left usually without consideration in other models. In this chapter, a short description of each of the methods mentioned above are given and a comparison of these models are made for *fp*-shell nuclei.

2.3.1. Isobaric multiplet mass equation, IMME

Energies of the members of an isospin multiplet are no longer degenerate in the precence of charge-symmetry violating interaction H_{CV}. The energy splitting between the members of the multiplet is given in first-order perturbation theory by:

$$E(\alpha\ T, M_T) \equiv \langle \alpha\ T, M_T | H_{CV} | \alpha\ T, M_T \rangle = \langle \alpha\ T, M_T \left| \sum_{k=0,1,2} H_{CV}^{(k)} \right| \alpha\ T, M_T \rangle \quad (5)$$

where $H_{CV}^{(0)}, H_{CV}^{(1)}$ and $H_{CV}^{(2)}$ are the isoscalar, isovector and isotensor components of the total Hamiltonian H_{CV}. α denotes other quantum numbers in addition to T and M_T. Using the well-known Wigner-Eckart theorem and the tabulated values for *3j* symbols one obtains for the masses or mass excesses within the isospin multiplet:

$$M(T, M_T) = a(\alpha, T) + b(\alpha, T) M_T + c(\alpha, T) M_T^2 \quad (6)$$

This quadratic relation is known as the isobaric multiplet mass equation (IMME). It can be used to predict the unknown masses of isospin multiplets provided that at least three masses of the multiplet are known. Fitting of the known energies of the IAS states give coefficients for IMME, and thus an extrapolation to the next members of the multiplet can be made. Fits for isoscalar (a), isovector (b) and isotensor (c) coefficients have been performed up to mass A = 60 [Ant84]. An improvement in detailed spectroscopic information above A = 60 has been slow and fitting of the isospin multiplets above it is no longer possible. Another way of predicting masses of proton-rich nuclei in the whole chart of nuclei is to use a global fit to the known mass differences between the isobaric analog states, i.e. Coulomb displacement energies ΔE_C, using:

$$\Delta E_C = k_1\left(Z_{av}/A^{1/3}\right) + k_2 \tag{7}$$

where Z_{av} is an average charge between the isobars. The isovector coefficient b in IMME can then be calculated from:

$$b = \Delta_{nH} - \left(k_1/2\right)A^{2/3} - k_2 \tag{8}$$

where Δ_{nH} = 782.3 keV is the neutron-hydrogen mass difference. The obtained b coefficient can then be used for projecting the mass of the proton-rich nucleus with M_T = -T from its neutron-rich mirror nucleus with M_T = +T [Ant84]:

$$M_{-M_T} = M_{+M_T} - 2bM_T \tag{9}$$

2.3.2. Mass relations

The Jänecke-Masson prediction for nuclei with $Z > N, T \geq 1$ is based also on the charge symmetry of the nuclear force and uses the so-called Kelson-Garvey relation [Kel66]. Instead of that, a transverse Garvey-Kelson relation has to be used for nuclei with $N \geq Z$ [Gar66]. Figure 6 shows the schematic presentation of these two relations.

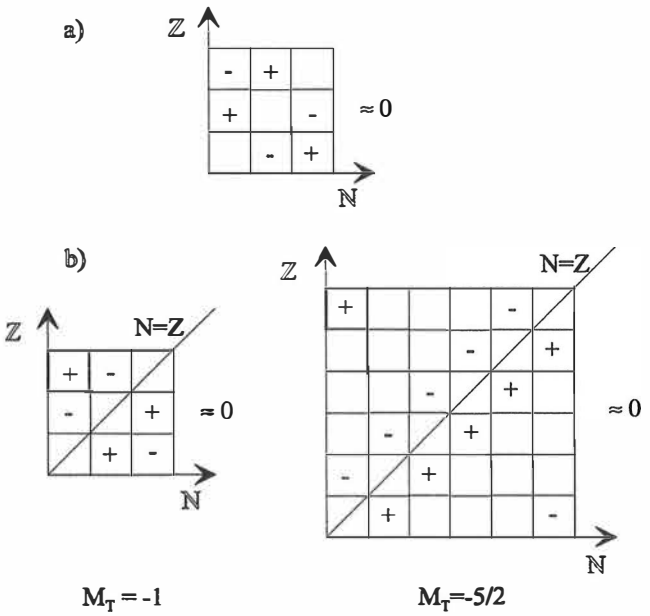

Figure 6. *Schematic presentation of a) transverse Garvey-Kelson relation and b) charge symmetric Kelson-Garvey relation for M_T = -1 and M_T = -5/2 nuclei. Plus and minus signs indicate whether the mass of the nucleus is to be added or subtracted.*

The applicability of these relations is limited because masses of M_T = -1/2 nuclei are presently known only up to A = 59. In predictions of [Jän88] these mass values were calculated using Coulomb-energy calculation [Com83].

2.3.3. Microscopic-macroscopic model of Möller and Nix

Mass formulae based on a liquid-drop model are frequently used in astrophysical reaction-flow calculations. A microscopic-macroscopic model of Möller et al. [Möl81, Möl95] uses the liquid-drop based macroscopic part and corrects it for shell effects using the Strutinsky method [Str67]. The total ground-state energy is determined as a sum of the macroscopic energy E_{mac} and the microscopic term E_{s+p} representing shell and pairing correction:

$$E_{tot}(Z, N, shape) = E_{mac}(Z, N, shape) + E_{s+p}(Z, N, shape) \qquad (10)$$

The macroscopic energy E_{mac} is calculated using either the finite-range droplet model (FRDM) or the finite-range liquid-drop model (FRLDM). The main difference between these is that FRDM takes into account effects on volume energy due to compressibility of the nuclear matter. However, the Thomas-Ehrman shift has not been taken into account. The finite-range droplet model is the preferred one and is adopted here for further use.

2.3.4. Masses from shell-model calculations

Recently, a study of nuclear masses for proton drip line nuclei with Z > N were completed up to A = 70 using Coulomb-energy calculations based on a shell-model approach [Orm97]. Some truncations of the shell-model space had to be included but they were found to affect the results by less than a few keV. Also, full *fp*-shell calculations have been performed for masses A = 47-49 through the whole isobaric chains [Cau94, Mar97]. The former calculations have estimated errors of 50-300 keV and the the values from the latter deviate less than 350 keV from measured values.

2.3.5. Comparison of models

Table 1 shows root mean square deviations of different mass predictions from known masses for *fp*-shell nuclei with $Z \geq N$ taken from [Aud95]. Only the cases where the experimental error is less than 200 keV have been included. It is clear that the experimental knowledge is limited and one cannot make comparisons beyond A ~ 60. A fit to obtain the value for the isovector parameter b have been made in this work by using Eqs. (7-9) and the region has been chosen to cover masses A = 40-124 and elements from Ca to Sn with the requirement that the experimental error in Coulomb displacement energy ΔE_C is smaller than 20 keV. The data set consisted of 531 experimental values for ΔE_C. The fits in ref. [Ant97] have been performed for the states with $T = 1/2$ and $T = 1$ separately using masses A = 3-60. The results indicate that the larger database corresponding to the whole *fp* shell gives a better fit than the fit including the lower mass region. This is understandable because the fit using light masses below A = 40 is more sensitive to shell effects present in the vicinity of closed proton or neutron shells with Z or N = 8 and 20.

Table 1. *Comparison of the mass predictions in the fp shell for* $Z \geq N$ *nuclei. The root mean square deviations have been given in keV. Fit to the experimental Coulomb displacement energies in this work resulted in the relation* $\Delta E_C = 1.438\left(Z_{av}/A^{1/3}\right) - 1.052$.

M_T	Mass region	Fit for *b*, this work	Fit for *b*, [Ant97].	Jänecke-Masson [Jän88].	FRDM [Möl95].
0	40-62			251	940
-1/2	41-59	96	195	58	1082
-1	42-62	197	219	163	1009

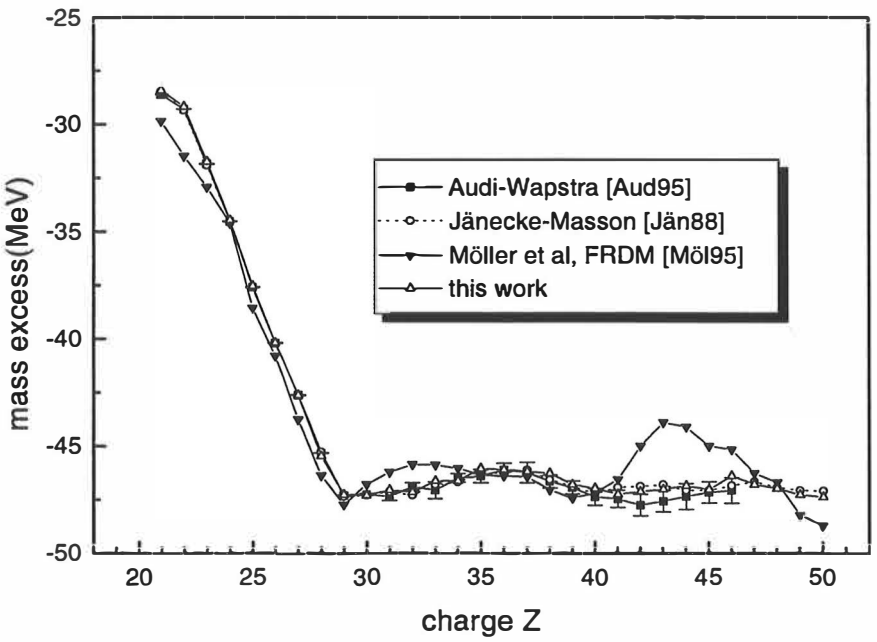

Figure 7. *Mass excesses for* M_T *= -1/2 nuclei in mass region A = 40-100 based on different predictions.*

The best agreement is obtained using Coulomb-energy calculations and mass relations [Com84, Jän88] which emphasize the importance of pure Coulomb part of the nuclear Hamiltonian. However, the predictive power of Jänecke-Masson method towards more proton-rich nuclei has been questioned recently [Sch98] by comparing the data from [Jän88] and the most recent mass measurements after compilation of Haustein [Hau88].

Figure 7 shows the mass excesses given by different predictions for $M_T = -1/2$ nuclei. As seen also from Table 1, the predictions based on Coulomb-energy differences agree within about 200 keV with the experimental values from [Aud95] but the model of Möller et al. shows serious deviations. Indeed, the model has been criticized for too small Coulomb energy differences between analog partners [Orm97].

2.3.6. Q_{EC} and S_p values for studied nuclei

The most crucial quantities describing the energetics of the decays near the N = Z line among *fp*-shell nuclei are the beta-decay energy Q_{EC} and the proton separation energy S_p. The proton separation energy defines the position of the proton drip line and its negative value indicates the proton-unbound character of the nucleus. Probability for beta-delayed proton emission depends on the proton separation energy in the daughter nucleus.

Table 2. *Beta-decay energies Q_{EC} and proton separation energies S_p for mother and daughter nuclei studied in this work. All the proton separation energies have been taken from [Aud95].*

Isotope	Q_{EC} (MeV)	ref.	S_p (MeV),mother	S_p (MeV),daughter
^{58}Zn	9.370(50)	[Aud95]	2.280(50)	2.874(4)
^{61}Ga	9.262(50)	[Orm97]	0.45(20)	5.290(17)
^{70}Kr	10.459(50)	[Orm97]	1.85(50)	2.58(37)
^{71}Kr	10.14(32)	this work	1.80(47)	1.94(37)
^{73}Rb	10.65(50)	[Aud95]	-0.59(40)	5.02(30)
^{74}Rb	10.44(72)	[Aud95]	2.13(74)	5.93(15)
^{82}Y	7.82(10)	[Aud95]	3.96(10)	7.841(9)

In Table 2, values of these quantities used in this work have been given. In most cases experimental values or values given by systematics were used [Aud95]. In the case of ^{61}Ga and ^{70}Kr values from shell-model calculations from [Orm97] were used and for ^{71}Kr the beta-decay energy was determined in this work. A comparison of the Q_{EC} and S_p values suggests the largest beta-delayed proton branch for ^{71}Kr. Negative proton separation energy implies unbound character for ^{73}Rb.

2.4. Beta decay near the proton drip line

Experimental studies of beta decay far from stability are concentrated mainly on allowed beta decay due to lower probability for forbidden transitions. States populated by these beta decays can further decay by electromagnetic decay or by particle emission ($p,2p,\alpha$). Exploitation of these decay modes, together with high Q_β values, allow beta-decay strength distribution studies for a large number of final states in a wide energy range. However, experimental difficulties such as energy-dependent detection efficiency for γdecay and low production rates of isotopes of interest limit the decay strength studies of very exotic nuclei. In addition, the nature sets an upper energy limit in the form of the decay Q value, which is not the case in charge-exchange reactions. For this reason the charge-exchange reactions have been widely used for Fermi and Gamow-Teller transition strength studies [Ber87]. These reactions are, however, limited to nuclei close to the valley of stability. The role of deformation effects in the Gamow-Teller strength distribution has been studied recently by Frisk and Hamamoto by means of Hartree-Fock calculations [Fri95, Ham97]. The shape of the Gamow-Teller strength distribution was found to be dependent on the sign of the deformation parameter β_2. This effect could be probed by measuring the branching for the beta-delayed particle emission in the deformed nuclei near the proton drip line.

2.4.1. Selection rules for beta decay

The beta-decay Hamiltonian consists of vector (V) and axial-vector (A) terms. These interactions may contribute simultaneously to the transition probability λ, which then consists of the Fermi (F) and the Gamow-Teller(GT) matrix elements:

$$\lambda \propto g_V^2 \langle I \rangle^2 + g_A^2 \langle \sigma\tau \rangle^2 \qquad (11)$$

where g_V and g_A are the vector and the axial-vector coupling constant, respectively. Usually the experimental beta decay rate is characterized by its $\log ft_i$ value defined as:

$$\log ft_i = \log f_i\left(Z_f\ , E_{max}\right)\frac{\ln 2}{\lambda} \qquad (12)$$

where $f = f\left(Z_f\ , E_{max}\right)$ is the Fermi integral or the phase-space factor and t_i is the partial half-life of beta decay. The Fermi integral tabulated for the particular daughter nuclei with Z_f and decay energy E_{max} in ref. [Des87] has been used in this work. The log ft values can be used to classify different types of beta decay.

In Fermi beta decay, the emitted positron and neutrino have antiparallel intrinsic spins coupled to $S = 0$ and in Gamow-Teller decay the intrinsic spins are parallel and coupled to $\boldsymbol{S} = 1$. The participating particles can still carry orbital angular momentum $\boldsymbol{L}$ and thus the transition must satisfy the vector addition rules

$$\boldsymbol{I_f} = \boldsymbol{I_i} + \boldsymbol{L} \qquad \text{for Fermi-type transitions} \qquad (13)$$

$$\boldsymbol{I_f} = \boldsymbol{I_i} + \boldsymbol{L} + \boldsymbol{1} \qquad \text{for Gamow-Teller-type transitions} \qquad (14)$$

Parity of initial and final states are related as $\boldsymbol{\pi_f} = (-1)^L \boldsymbol{\pi_i}$.

***Table** 3. Beta-decay selection rules for spherical nuclei based on [Kan95]. Transitions which are not possible if either I_i or I_f is zero are in parentheses. The limits for log ft values have been taken from [Did94]. The Fermi integral has been calculated for first forbidden decay if marked with *, otherwise for allowed decay.*

Transition type	**log *ft***	***L***	**Fermi**		**Gamow-Teller**	
			ΔI	***Δπ***	***ΔI***	***Δπ***
Allowed	<5.9	0	0	No	(0),1	No
1st forbidden	>8.0*	1	(0),1	Yes	0,1,2	Yes
2nd forbidden	>10.6	2	(1),2	No	2,3	No

The fastest transitions are those with $L = 0$ and are called allowed. Transitions with $L > 0$ are called forbidden. Table 3 summarizes the selection rules for beta decay in spherical nuclei. Allowed Fermi or mixed Fermi and Gamow-Teller transitions which have log ft value between 2.9-3.7 are called superallowed.

2.4.2. Allowed Fermi beta decay

In the case of allowed approximation the vector part (Fermi) of the weak-interaction Hamiltonian reduces to the unit operator 1 in coordinate space and to the raising ($\boldsymbol{T}_+$) or the lowering operator ($\boldsymbol{T}_-$) in isospin space. Thus the square of the matrix element (Fermi strength) following from isospin algebra can be expressed as:

$$\langle 1 \rangle^2 = B(F) = T(T+1) - M_{Ti} M_{Tf} \qquad (15)$$

The Fermi matrix element vanishes unless $T_f = T_i$ and $M_{Tf} = M_{Ti} \pm 1$. Thus the allowed Fermi decay occurs only between isobaric analog states and, especially, it is the only decay mode possible for $0^+ \Rightarrow 0^+$ transitions. In other cases, the total decay strength is a combination of Fermi and Gamow-Teller strengths provided that the selection rules are fulfilled.

Pure Fermi decays can be used for testing the conserved vector current (CVC) hypothesis. This hypothesis is based on the assumption that the strength of the Fermi interaction is not affected by subnuclear degrees of freedom such as meson fields and quarks in nuclei. The CVC hypothesis can explain the constancy of the observed *ft* values for $0^+ \Rightarrow 0^+$ transitions between the $T = 1$ isobaric analog states. However, the experimental *ft* values for obtaining the strength of the Fermi interaction, g_V, have to be corrected by two effects. Radiative correction, δ_R, rises from bremssthrahlung processes inside the nucleus. The second correction is a Coulomb correction, δ_C, due to breaking of the isospin-analogue symmetry in the nuclear interaction. The latest review of $0^+ \Rightarrow 0^+$ transitions can be found in [Tow95]. In that reference, several ways to calculate the isospin-mixing correction are described. In the present work the radiative correction has been chosen to be comparable with the previous beta-decay study of ^{71}Kr, i.e. $(1 + \delta_R) = 1.026$ [Ewa81]. The correction for isospin impurity has been taken as $(1 - \delta_C) = 0.997(3)$ [Wil78].

2.4.3. Allowed Gamow-Teller beta decay

In the case of allowed decays, the relationship between the *ft* values and the transition probability can be expressed as [Bru77]:

$$ft = \frac{C}{\langle 1 \rangle^2 + \left(\frac{g_A}{g_V}\right)^2 \langle \sigma\tau \rangle^2} \tag{16}$$

where the value of the constant C = 6145(4) s is based on experimentally well-known transitions with $J_i^\pi = J_f^\pi = 0^+$ and $T_i = T_f = 1$ [Tow95] and g_A/g_V = 1.266(4) is the ratio derived from asymmetry in free neutron beta decay [Sch95].

Extreme single-particle (ESP) estimates for the square of the Gamow-Teller matrix element can be expressed as:

$$\langle \sigma\tau \rangle^2 = 6(2j_f + 1)\begin{Bmatrix} \frac{1}{2} & \frac{1}{2} & 1 \\ j_i & j_f & l \end{Bmatrix}^2 \tag{17}$$

where *{...}* is the *6j* symbol which is tabulated, for example, in [Bru77]. The Gamow-Teller transition strength is given by:

$$B(GT) = \left(\frac{g_A}{g_V}\right)^2 \langle \sigma\tau \rangle^2 \tag{18}$$

A model-independent sum rule has been derived which includes all the Gamow-Teller transitions without need for knowledge of wave functions involved [Ike62, Gaa80]:

$$\sum_f \left(\langle \sigma\tau_- \rangle^2 - \langle \sigma\tau_+ \rangle^2 \right) = 3(N - Z) \tag{19}$$

where minus sign represents β^- decay and plus sign refers to β^+ decay.

Due to the simplicity of the basic assumptions used in ESP estimates, the values appear significantly larger than the measured ones. A better agreement is found by using large-scale shell-model calculations. However, a quenching factor of ~ 0.59 in experimental strength is observed in beta decays among *sd*-shell nuclei [Bro88]. Most of this missing strength is expected to be due to configuration mixing between shell-model space and higher shells which is not necessarily taken into account in calculations. About 25% of the strength is expected to be taken away by this mixing [Ber87]. The quenching caused by configuration mixing is naturally related to the Gamow-Teller matrix element itself. On the other hand, the discrepancy between calculated and observed strength is not surprising from the point of view of CVC hypothesis which allows the possibility for g_A to be renormalized by the subnuclear degrees of freedom. These subnuclear interactions are responsible for the so-called delta(Δ) resonance at very high energies(~300 MeV) and this nucleon-delta(N-Δ) interaction could remove the strength from the lower-lying states. However, this effect has been concluded to be only of the order of few per cent [Ber87]. Recently, full *fp*-shell calculations have been performed up to A = 50 and comparison to experimental Gamow-Teller matrix elements based on beta decay measurements gives a quenching factor $q^2 = 0.554(30)$ [Mar96].

2.4.4. Charge-exchange reactions in GT-strength studies

A quenching of the Gamow-Teller strength is observed also in charge-exchange reaction studies [Ber87]. The zero-degree spectra in these reactions at intermediate energies are dominated by $\Delta L = 0$ transitions. The cross section at zero angles can be shown to be proportional to the squares of the Fermi and the Gamow-Teller matrix elements [Goo80]. The charge-exchange reactions do not have the energy limitations that beta decays have. On the other hand, experiments on charge-exchange reactions have several other limitations. They suffer from poor energy resolution compared to the decay studies. Typical resolution in *(p,n)* studies is 200-400 keV [Rap94] and for *(^{3}He,t)* reactions 140 keV has been achieved [Fuj96]. Insufficient resolution may complicate the separation of the Fermi strength from the Gamow-Teller strength. The lack of suitable target nuclides near the drip lines prevents the use of the reactions for exotic nuclei in most cases. Also, contributions due to higher-ΔL excitations as a background have to be taken into account. This is done on the basis of either theoretical calculations using distorted wave impulse approximation (DWIA) or by using extrapolation

from larger angle spectra consisting of higher-multipole contributions. To obtain absolute Gamow-Teller strength from the measured spectrum one needs a normalization which is usually done by using measured beta-decay strength for the lowest excited states.

Discrepancies between the *(p,n)* and beta-decay studies have recently been reported [Gar91, Gar95, And96]. Reasons for these disagreements can be due to deficiencies in both methods. In beta-decay studies especially the competition of beta-delayed proton and gamma decay from proton-unbound states have to be taken into account in determining the total Gamow-Teller strength distribution [Tri95]. Also *l*-forbidden contributions in beta decay have been shown to play a role in these differences [Wat85, And96].

2.4.5. Beta-delayed decay modes

Beta decay to excited states is followed by either gamma emission or charged-particle emission. In the *fp* shell the main charge-particle decay modes are proton (p), two-proton ($2p$) and alpha (α) emission of which the p emission is dominant and is discussed below. Delayed decay mode depends on the partial widths Γ_p and Γ_γ of p and γ emission, respectively.

In heavy nuclei (A > 60) the density of the final states for beta decay is too high for detailed separation of the individual transitions and the delayed-proton spectra are nearly continuous and have a bell-like shape. Figure 8 shows schematically the formation of continuous proton spectrum. At low energies the spectrum shape is determined by the competition between p and γ emission and at higher energies by the phase-space factor f.

Selection rules for p and γ decays follow from conservation of the angular momentum and can be expressed as:

p decay
$$\left|J_i - J_f\right| \pm l/2 \le L \le J_i + J_f \pm l/2 \qquad (20)$$
$$\pi_f = (-1)^L \pi_i$$

γ decay
$$\left|J_i - J_f\right| \le L \le J_i + J_f \qquad (\text{no } L = 0) \qquad (21)$$

$\Delta\pi$ = no: even electric(E), odd magnetic(M)

$\Delta\pi$ = yes: odd electric(E), even magnetic(M)

where J_i = angular momentum of the initial state, J_f = angular momentum of the final state and L = angular momentum carried by proton or photon.

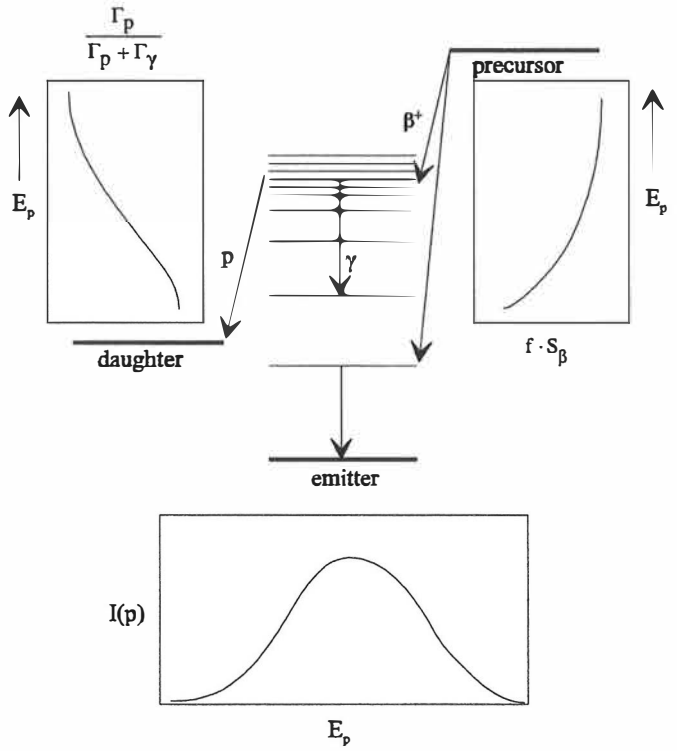

Figure 8. *Formation of the shape of beta-delayed proton spectra in heavy nuclei. Phase space factor f is included in $f \cdot S_\beta$ where S_β is the Gamow-Teller strength per energy interval. Figure is based on [Har84].*

Transition rates for both γ and p decay can be estimated. In the framework of single-particle shell model, the transition rates for gamma decay can be expressed using Weisskopf estimates [Bru77].

Transition rates for proton decay can be expressed as a product of the frequency factor ν and the penetrability P through the potential barrier [Hof89]:

$$\lambda = \nu \times P \tag{22}$$

The frequency factor can be obtained from an expression based on alpha decay of spherical nuclei [Ras66]. The penetrability is calculated as

$$P = e^{-2G} \tag{23}$$

where G = Gamow factor i.e. the integral taken over the total potential between the classical turning points R_1 and R_2 shown in Fig. 9. In this work all the proton-decay lifetimes have been calculated using the potentials described in [Hof89].

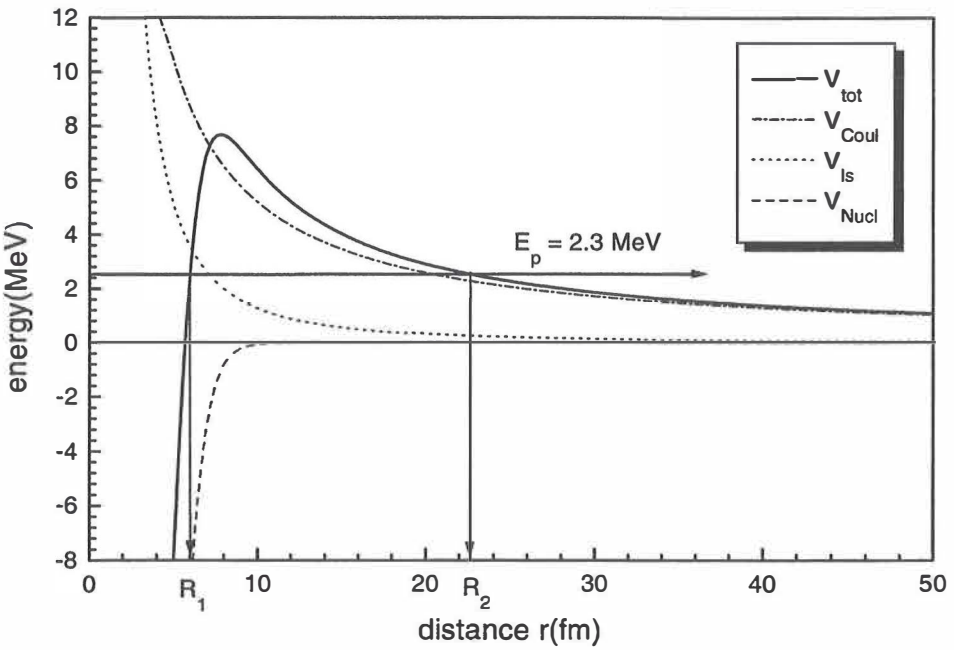

Figure 9. *Potential barrier for a L = 2 -proton inside ^{71}Br. The potential has been calculated according to [Hof89]. The integration limits i.e. turning points R_1 and R_2 are also shown for 2.3 MeV proton.*

2.4.6. Special case: mirror beta decays

A special case among β decays is the decay between mirror states in nuclei. Initial and final states in mirror transitions between M_T = -1/2 and +1/2 nuclei should have identical nuclear wave functions due to charge symmetry in nuclear forces. Possible differences in the nuclear wave functions are due to Coulomb effects. The mirror decays are special in the sense that they fulfill the selection rules of both the Fermi and the Gamow-Teller beta decay and thus they are mixed-type of decays. Since one deals with the decays between analog ground states, it can be assumed that the Fermi part of the decay is not affected by any major isospin-mixing effects due low level density near the states and the strength $B(F)$ can be calculated using eq. (15). Corrections δ_R and δ_C can be estimated to be of the same order as those for pure $0^+ \rightarrow 0^+$ decays. Determination of the Gamow-Teller matrix elements for transitions between the ground states gives immediately information about the nuclear wave functions.

2.5. Astrophysical rp process for A = 60-100

Apart from the basic nuclear structure studies, the experimental data for proton-rich nuclei can be used in astrophysical reaction flow calculations. Recently Schatz et al. [Sch98] have performed an extensive study of reaction parameters for rapid proton (*rp*) capture process above Z = 32 up to region A = 100. Due to lack of experimental information on proton-rich nuclei, the calculations had to be performed relying mostly on theoretical values of masses and half-lives. However, these calculations clearly indicate the need of complete reaction network calculations for reproducing the observed abundance patterns of elements in astrophysical objects. In particular, importance of a two-proton capture in bridging the waiting points of the *rp* process towards A = 100 was emphasized in ref. [Sch98].

In the extreme temperature and density conditions prevailing in *X*-ray bursts and supernovae, nuclear reaction time scales can be of the order of tens of seconds. Reaction flow during these conditions is called explosive hydrogen burning [Cha92]. The temperature and density conditions are typically between T_9 = 0.1-1.5 and $\rho = 10^3$-10^8 g/cm^3. In relatively low temperatures and densities the reaction flow can proceed up to HCNO cycle [Cha92]. As the

conditions get more violent a rapid proton capture process is triggered by the $^{19}Ne(p,\gamma)^{20}Na$ reaction. Above that, the reaction path is determined mainly by a competition between proton-capture reactions and beta decay, i.e. by thermonuclear reaction rates and beta-decay half-lives.

Beta-decay half-lives of nuclides along the Z = N line are quite well known up to A = 75 but in the case of proton-capture rates one has, in most cases, to rely on statistical Hauser-Feshbach calculations. These statistical calculations are based on theoretical level densities, and the transmission coefficients describing the reaction rates are calculated for each possible reaction channel [Sch98]. These statistical calculations are justified near the valley of stability, in the sense that the proton-capture reactions have quite high threshold energies and the reactions lead to the states characterized by high level density. When the temperature and the density increase, the process path will move towards the proton drip line. Due to lower threshold energies the participating states lie in the region of low level density and are clearly isolated. Thus the reaction rates are determined by individual resonances whose shapes can be described as delta functions and by non-resonant direct capture reactions. The non-resonant direct reactions exploit the low-energy tail of the resonances and the tails of bound states lying below the threshold. To obtain experimental knowledge of the properties of these states either direct measurements with radioactive beams or targets or beta-decay measurements are needed. Near the proton drip line only beta-decay experiments are possible in the *fp* shell.

The whole process is hindered in the *fp* shell by the so-called "waiting points". These occur when the proton capture towards higher masses is no longer possible due to the unbound character of the final nucleus and thus the process will wait for beta decay to continue. Figure 10 shows the concept of *rp* process in the vicinity of a waiting point.

Waiting points can be bridged by other processes such as alpha-induced reactions at light mass region [Wal81] as well as by *2p*-capture reactions [Gör95]. These *2p* captures have been shown to be even more important in the mass region A ~ 70 [Sch98] where two possible waiting-point nuclei can hinder the process, namely ^{68}Se and ^{72}Kr. The calculations in [Sch98] show that the process can continue up to A = 100 in suitable conditions and lead to twice as

large energy production as predicted previously. For that reason, experimental results for half-lives and binding energies are badly needed in the mass region A = 75 - 100.

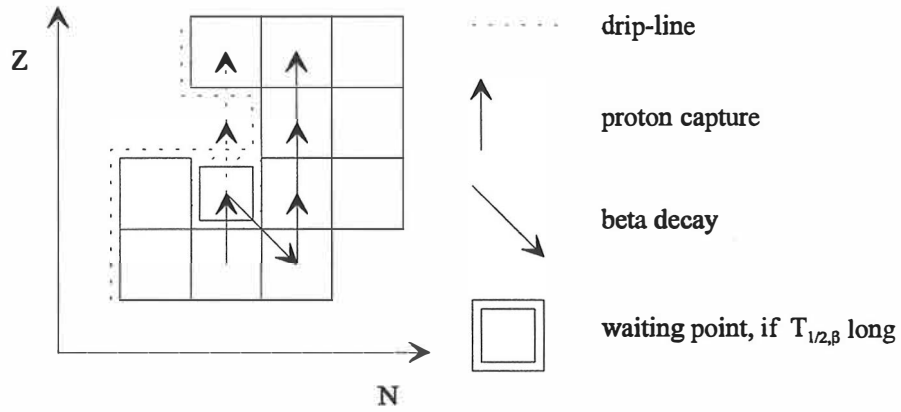

Figure 10. *Schematic view of rapid proton capture process. Dashed arrows show the possible 2p-capture path bridging the waiting points.*

3. Experimental methods

3.1. On-line mass separator facilities

Isotopes studied in this work were produced using three different mass-separator facilities in Europe. Most of the measurements were made at the ISOLDE mass-separator facility at CERN in Geneva. Other studies were performed with mass-separator IGISOL at JYFL in Jyväskylä and with the Online Mass Separator at GSI in Darmstadt. Target and ion-source combinations used differed quite drastically and special attention is paid for describing these features. A more detailed review of the ion-source techniques used in on-line mass separators can be found in [Kir81] and of the production methods used at ISOLDE in [Hag92]. Measurement setups used are discussed in connection with each facility and are summarized afterwards in a separate chapter.

3.1.1. ISOLDE at CERN

The ISOLDE facility was used to study the following isotopes near the proton drip line: ^{58}Zn, ^{70}Kr, ^{71}Kr, ^{73}Rb and ^{74}Rb. Reaction products are produced in spallation and fragmentation reactions induced by a high-energy proton beam. The original ISOLDE facility was taken into operation in 1967 [ISO70] with proton energies at 600 MeV and was reconstructed during 1990-92 to exploit the 1 GeV proton beam from the PS-Booster [Kug92]. The original task of the PS-Booster is to pre-accelerate protons supplied by a LINAC to 1 GeV energy before injection to the CERN Proton-Synchrotron (PS). Recently, the maximum energy of protons has been increased to 1.4 GeV.

Targets and ion sources used at ISOLDE must fulfill two major criteria: release of the reaction products from the target must be rapid and the ionization of the studied elements has to be efficient. These aims are usually incorporated with chemical selectivity of the system to reduce background. Due to the high penetrability of the incident protons, thick targets with lengths of the order of 20 cm and a diameter of 1.9 cm can be used [Bjø87]. The advantage of this is that the production yield can be as high as 10^{11} $s^{-1}\mu A^{-1}$ at maximum [Hag92] but it has the disadvantage of increased release times compared to thinner targets. Container material for

the target has to provide stable and non-corrosive surroundings for the target and thus the container is usually chosen to be made of refractory materials such as Ta or Re.

Reaction products are transported to the ion source via a transfer line, which also plays a role in purification of the beam. For example, cooling the transfer line reduces the amount of less volatile elements. This method, in conjunction with the plasma-discharge ion source, is especially favourable for noble gases [Bjø87]. In addition to the plasma ion source, positive (PSI) and negative surface ionization (NSI) are used. These methods are based on differences in electron affinities and ionization potentials of the elements. Usual surface materials for PSI and NSI are tungsten and LaB_6, respectively.

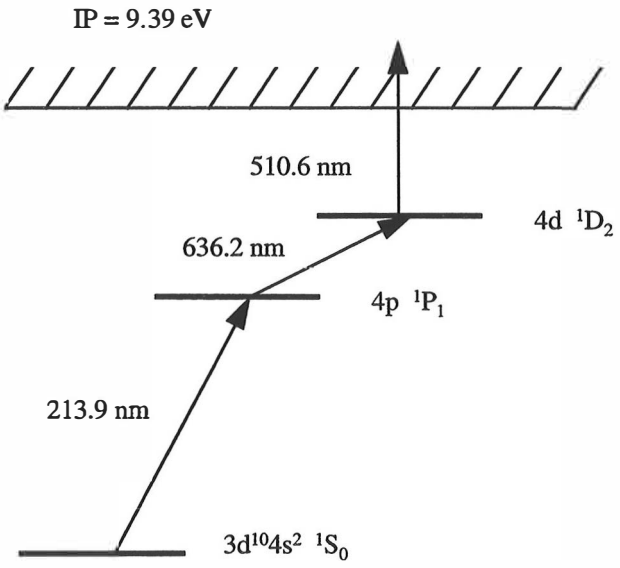

Figure 11. *Ionization scheme for Zn isotopes. Two resonant excitations are followed by non-resonant excitation into the continuum.*

A laser ion source (LIS) has been used for elements such as Ni [Jok97] and Ag [Jad97] which are difficult to produce with conventional ion sources. In this work LIS was used for the production of ^{58}Zn. Fig. 11 shows the ionization scheme used for Zn isotopes. Three laser wavelengths were used for ionization. Two of them were used to excite Zn atoms from their

atomic ground state $^1S_0$ to the $^1D_2$ state at 7.75 eV. The third laser transforms the atom to an ionic state, i.e. excites it non-resonantly over the ionization potential at 9.39 eV. Ionization efficiency for Zn achieved in this work was 5 %. More detailed information of the ionization scheme can be found in [Let97a].

Mass separation with the high-resolution separator (ISOLDE 3, presently HRS) can be used even for isobaric purification, like separating ^{37}Ca from ^{37}K [Gar91]. The mass-resolving power of the HRS has been reported to be 10600 [Kug92]. Another option is to use the General Purpose Separator (GPS) with mass-resolving power of 2400 [Kug92]. Usually the very unpleasant effect of formation of molecular sidebands due to impurities in the ion source can also be used in a controlled way to obtain pure radioactive ion beams.

The most important component in the loss of radioactive products is the decay loss due to slow release from the target. This can be optimized by choosing the target temperature sufficiently high to keep the reaction products volatile for fast release. Release of the reaction products can be measured using a combination of beta counting and half-life detection. The release from the target is characterized by a sharp rise, followed by a steep fall and a long tail. Release behaviour can be parametrized with the expression

$$P(t) = \frac{1}{N}\left(1 - e^{-t/\tau_r}\right)\left(\alpha e^{-t/\tau_f} + (1-\alpha) e^{-t/\tau_s}\right) \qquad (24)$$

where α stands for the fast fraction of the release function, τ_r, τ_f and τ_s are rise-, fast and slow fall-time constants, respectively, and N is the normalization factor. Fig. 12 shows an example of the measured release function for ^{79m}Kr. The decay losses during the release process are independent from the release behaviour. Thus, the total probability density for product i to be released and not decayed is $P(t, \lambda_i) = P(t) exp(-\lambda_i t)$. Integration of this probability density up to infinity gives the total released fraction of the product [Let97b].

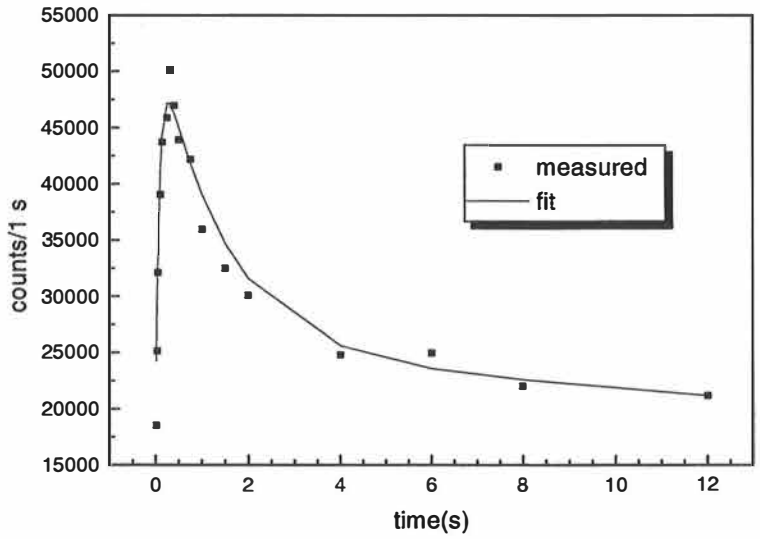

Figure 12. *Measured release curve of ^{79m}Kr fitted with the function given in Eq. (24).*

Table 4. *Targets, ion sources, release parameters, beam gate and production yields for the studied isotopes. Detailed information about the target/ion-source combinations used can be found in [Hag92]. Yields have been measured at measurement position without corrections for decay losses.*

Isotope	Target	Ion source	α	τ_r (ms)	τ_f (ms)	τ_s (s)	Beam gate (ms)	Yield (at/μC)
^{58}Zn	48 g/cm^2 Nb-foil	Laser + PSI	0.74	120	500	13	250	2.7
^{70}Kr	42 g/cm^2 Nb-foil	Plasma, cooled line	0.87	90	800	30	150	0.03
^{71}Kr	42 g/cm^2 Nb-foil	Plasma, cooled line	0.87	90	800	30	250	1.7
^{73}Rb	39 g/cm^2 Nb-foil	PSI	0.83	20	270	9	100	<0.08
^{74}Rb	39 g/cm^2 Nb-foil	PSI	0.83	20	270	9	150/300	390

A typical PS-Booster beam cycle consists of 12 proton pulses with 1.2 s time difference. The maximum intensity of the pulse is 3.2×10^{13} protons and its duration is 2.4 μs [Kug92]. This intensity results in an equivalent of 4.3 μA continuous current. During the experiments the beam of mass-separated radioactive products accelerated to 60 keV is usually accumulated for a certain time depending on the release properties of the particular element to optimize the production rate. This so-called "beam gate" is generated by an electrostatic deflector. To avoid high-voltage breakdowns during the proton-pulse impact the high voltage of the separator is brought down to zero just before the pulse impact. It is restored back to 60 kV after the impact in 10-20 ms [Kug92]. Implantation during this time is not possible and it has been shown in fig. 13 as a delay between the impact and the implantation period.

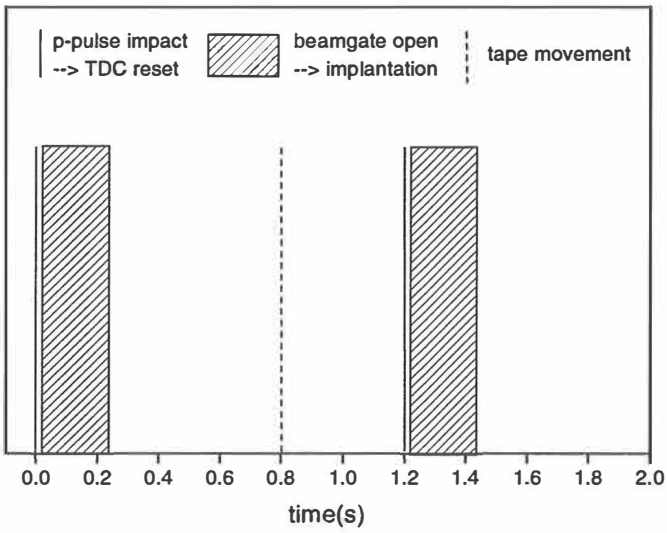

Figure 13. *Typical time structure in the ISOLDE experiment. The number of proton pulses during 14.4 s supercycle varied from 6 to 11.*

All ISOLDE experiments in the present work were performed using essentially the same measurement geometry in which the mass-separated beam was implanted into an 1/2" tape surrounded by the detector setup. The tape was movable to reduce the contribution of long-lived activities. The tape movement was related to the timing of the proton pulses so that typically the tape was moved always 800 ms after the pulse. Proton pulses resetted the TDC used to provide the time information for each event stored by the detection setup.

3.1.2. On-line Mass Separator at GSI

Decay properties of neutron deficient ^{61}Ga were studied using the On Line Mass Separator at GSI in Darmstadt [Bur97]. At GSI it is possible to use heavy-ion fusion-evaporation reactions as a production method. This provides more selective production than spallation or fragmentation reactions. Heavy-ion beams from C to U produced by the linear accelerator UNILAC can be accelerated up to 20 MeV/amu.

The GSI On-line Mass Separator exploits the so-called catcher ion-source (CIS) principle in which the fusion-evaporation reaction products are stopped in a target/catcher-foil stack of a few mg/cm^2. By heating the foils it is possible to diffuse products into an ion source. The main requirements for the production of pure radioactive beams are similar to that at ISOLDE, i.e. fast release, efficient ionization and chemical selectivity. Ion-source development at GSI has been concentrated in gaseous discharge ion sources. In the forced electron beam induced arc discharge (FEBIAD) ion source the ionizing power is based on plasma caused by electrons hitting gas molecules with a residual pressure of 10^{-4}-10^{-5} mbar [Kir76]. Small axial magnetic field is used in order to avoid immediate radial expansion of electron beam towards the anode. These ion sources can be used in the so-called bunching mode, in which the reaction products are stored by a cold surface based on adsorption properties of the element and subsequently released by heating [Kir86]. In this work FEBIAD-B2-C -type ion source was used, where no cooling, however, was performed [Kir97].

In this work Ga ions were produced, together with neighboring neutron-deficient isotopes in fusion-evaporation reactions between 121 MeV ^{36}Ar beam and 1.9 mg/cm^2 Si target . The intensity of the primary beam was typically 80 particle-nA. Singly-charged ions were extracted and subsequently mass separated by means of the GSI On-Line Mass Separator and implanted into a movable collection tape which was used to suppress the long-lived contaminants ^{61}Zn and ^{61}Cu. The tape was moved periodically after every 0.8 s collection period. The production rates for ^{61}Ga, ^{61}Zn and ^{61}Cu were $78, 4.2\times10^4$ and 5.1×10^5 at/s, respectively.

The implantation position was surrounded by two Ge detectors facing each other for gamma rays, a 4π plastic scintillator with a cylindrical geometry for positrons and a 2 mm thick plastic

scintillator in front of the other Ge detector (App. 2). The electronics were set to fire from every pair of events and 10 parameters were stored including energies and times from each detector with respect to the trigger. A time mark for each trigger signal related to the start signal of the counting period was also stored and the obtained growth-in spectrum of activity could be used for half-life analysis. The relative efficiency for the Ge detector used for determination of the branchings was obtained using internal sources of ^{56}Ni and ^{56}Co. Absolute efficiency for that detector was determined using the calibrated standard ^{60}Co source resulting in ε_{abs} = 0.95(5) % at 1.332 MeV. The efficiency of the 4π-scintillator detector was determined to be 46(4) % comparing the photopeak intensities of ^{58}Cu γrays in singles and in coincidence with the beta detector. The ^{58}Cu ions were produced in separate runs using the reactions ^{32}S + ^{nat}Si and ^{36}Ar + ^{nat}Si.

3.1.3. Heavy-ion IGISOL at JYFL

Elements above A = 80 from yttrium (Y) to palladium (Pd) are characterized by high melting points (> 1500 ° C) and the efficiency of conventional ion sources is limited by the very high temperatures needed to release these elements out of the target by diffusion. Another approach is to use gas as stopper as in the Ion-Guide Isotope Separator On-Line (IGISOL) method [Ärj85]. In this case, instead of using diffusion only for transportation, reaction products are guided to the extraction by a combination of a gas flow and a weak electric field. This approach is not limited by chemical or physical properties of the element and the fast release of even refractory elements is possible. However, using gas as a stopping material is not as efficient as solid target/stopper combinations and some losses are inevitable. Losses due to improper ionisation and diffusion to the walls of the stopping chamber limit also the total efficiency but for refractory elements the advantages of the gaseous stoppers are still indisputable.

Production rates of neutron-deficient nuclei in the mass region A = 80-88 were surveyed using the IGISOL mass separator at JYFL. The ion-guide based on-line mass-separator technique has been previously used succesfully for studying proton-rich nuclei below A = 55 via light-ion induced fusion-evaporation reactions [Äys84, Ham87, Hon87, Hon89b, Hon97a] and neutron-rich nuclei via proton-induced fission [Pen92, Lhe94, Jok94, Huh97]. This

combination usually suffers from the so-called "plasma effect" [Mor87] induced by collisions of primary heavy-ion beam and the stopping gas. A new technique has been developed at SARA/IGISOL at Lyon for the use of heavy-ion beams with an ion-guide mass separator [Ber94]. In this new method the plasma effect is reduced by separating the plasma volume from the stopping volume using a cylindrical metallic tube which conducts the primary beam through the stopping volume without interacting with the stopping gas which usually is helium.

Fig. 14 shows the geometry of the Heavy-ion version of IGISOL (HIGISOL) used in this work. Collection of the evaporation residues (EVR) is based on a large difference in angular distributions of the primary beam and EVR after a target with thickness of few mg/cm^2. The ratio of the angular half-widths α_b / α_{EVR} for the primary beam and the EVRs behind the target can be estimated as [Ber94]:

$$\frac{\alpha_b}{\alpha_{EVR}} \simeq \frac{Z_b A_b}{Z_{EVR} A_{EVR}} \qquad (25)$$

This difference arises mainly from three effects: angular spread of the projectile beam, particle evaporation from the compound nucleus and scattering of the EVRs in the target material. These effects have been discussed in detail in ref. [Ber94]. In heavy-ion reactions the EVRs have typically energies of 40-50 MeV after fusion. In this work, the thicknesses of the target (1), the entrance window (5) and the stopping gas pressure were optimized using TRIM-code [Zie85].

After passing through the entrance window, EVRs are thermalized in He-gas and ions with a charge state +1 are extracted through the nozzle (8) and the skimmer (10) using the combination of an electric field and He-flow. Using a diameter of 1.35 mm for the nozzle, the total evacuation time of the chamber is about 140 ms. For a test reaction ^{116}Cd(^{40}*Ar, 6n*)^{150}Dy an efficiency of 0.5 % was obtained relative to the number of reaction products entering the stopping chamber [Den98].

In this work the reaction $^{32}S + {}^{nat}Ni$ was used resulting in $^{90,92}Ru$ as compound nuclei. The same reaction with the energy of 150 MeV was recently used for producing ^{81}Zr and ^{85}Mo for beta-delayed proton studies [Hua97]. The beam energy in this work was chosen to be equal to their energy, i.e. 150 MeV, in the centre of the target. The energy for the maximum production cross section for ^{85}Mo in an αn channel was also confirmed by using the ALICE code [Bla76]. Target thickness was 3.7 mg/cm^2 which corresponds to nearly 100% transmission of the EVRs. The beam intensity was 125 particle-nA. The target holder was water cooled to obtain necessary heat transfer from the target. The entrance window was 1.7 mg/cm^2 thick Havar foil and the stopping pressure was 200 mbar. Half an hour test runs were performed for masses A = 80-81, 83-84 and 86-88. The mass-separated beam was implanted into the tape which was moved every 120 s to avoid accumulation of long-lived contaminants. In addition, longer runs were made for A = 82,85 to obtain more detailed spectroscopic information. Collection and decay periods for A = 82 and 85 were 60 s ON /60 s OFF and 30s ON / 30 s OFF, respectively. To maximize the counting statistics runs with only growth-in period of 60 s were also performed for both masses. The source position was surrounded by a 37 % relative efficiency Ge detector for γ-ray detection, a 10 mm thick LEGe detector for X rays and a 1 mm thick plastic scintillator for β particles.

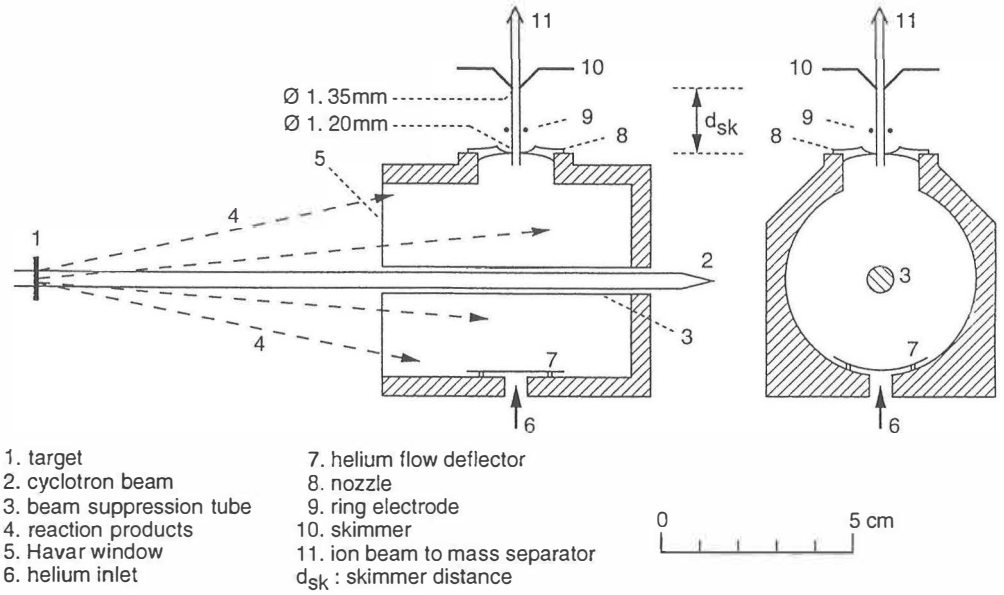

Figure 14. *Geometry of the ion guide HIGISOL used in this work [Den98].*

Fig. 15 shows the part of the nuclide chart surveyed in this experiment. Production rates of isotopes are given for each nuclei observed in atoms/s. In some cases the poor knowledge of decay properties or beta decaying isomeric states did not allow accurate determination of the branches and thus a lower limit or an estimate has been given (see figure caption). The rates have been determined by taking into account three generations of decays starting from the most exotic nucleus produced. Branching ratios used have been taken from ref. [Fir96]. Errors are induced mainly by the statistics and are of the order of 20-30 %, typically.

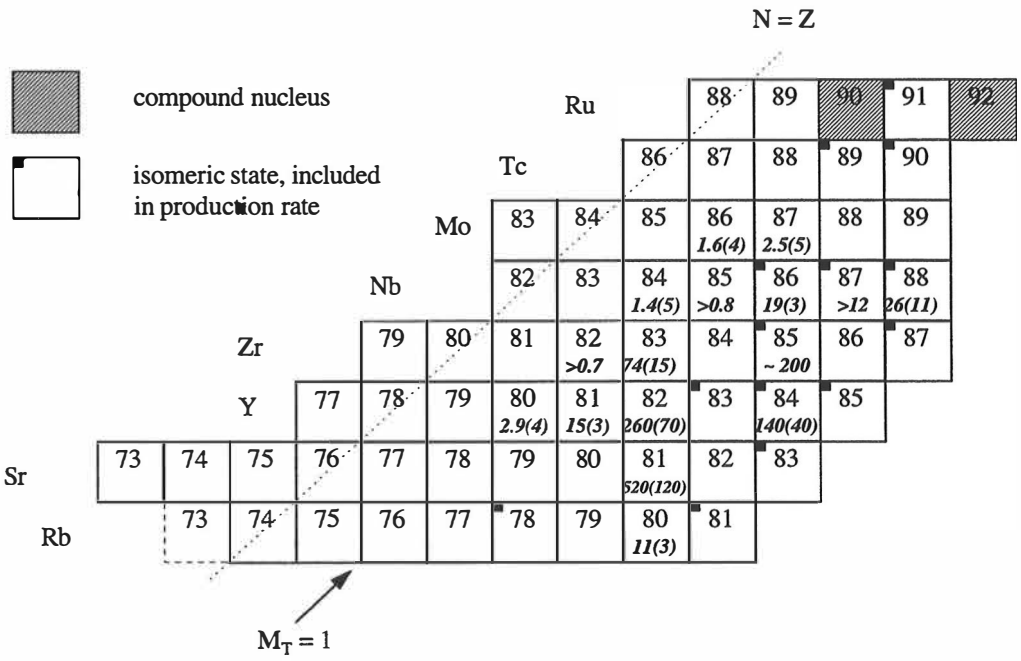

Figure 15. *Production rates of isotopes in atoms/s produced in the ^{32}S + ^{nat}Ni reaction at HIGISOL. If isomerism exists the production rate is the sum of the ground-state and isomeric-state production. Lower limits are given in the cases of ^{82}Zr, ^{85}Nb and $^{87,87m}Nb$ due to inadequate knowledge of their decay schemes. For ^{85}Zr the isomeric and the ground-state production could not be separated. The rate for ^{83}Y could not be reliably determined due to complicated feeding pattern among A = 83 isotopes. Observation of ^{84}Zr was not possible due to short collection cycle. No γ rays are emitted in the case of ^{82}Sr.*

The region is characterized by a large number of isomeric states. This disturbs a reliable determination of the production rates in some cases. Identification of the isomeric- and the

ground-state production was possible only for ^{84,84m}Y and ^{88,88m}Nb. The production of ^{84}Y was almost totally concentrated in the $J^{\pi} = 5^-$ isomer. Only about 1 % of the direct production is due to ^{84g}Y as seen by comparison of the 793 and 974 keV γ-transition intensities. All M_T = +1 nuclei between Y and Mo were produced in this work. The production is, however, concentrated to $x\alpha ypzn$ channels, for example, leading to ^{81}Sr and ^{82}Y.

Production rates can still be increased by using higher stopping gas pressure, optimizing the beam energy to be suitable for each EVR and by increasing the beam intensity. The ion-guide efficiency has been shown to increase linearly up to a 1000 mbar stopping pressure [Den98]. At this pressure, it can be estimated that the production rate would be increased by a factor of 3. All improvements described would mean that rather detailed spectroscopic studies should become possible at least for nuclei with M_T = 1/2 between Y and Tc in the near future.

3.2. Summary of detection techniques

All the experiments were performed using beta-delayed gamma-detection techniques. In some cases it was also possible to use beta-delayed proton detection with a Si-Si telescope or a special low-energy gas-Si telescope detector developed at JYFL [Hon97b].

The data were stored event-by-event allowing detailed off-line analysis with numerous gating options. Number of parameters varied from 7 to 15 depending on the experiment. The data acquisition systems used were GOOSY at ISOLDE, MBS/GOOSY at GSI and VENLA at JYFL. In addition to the event-by-event data, various set of parameters were collected in singles and multispectra/multiscaling mode at ISOLDE and GSI experiments using the SAM data acquisition system from Strasbourg. Table 5 summarizes the information about the detector setups. Geometries of the detection setups are shown in Appendix 2.

Table 5. *Summary of the measurement setups used in this work.*

Isotope	Laboratory	Detection	Detectors	#of param.
^{58}Zn	ISOLDE	$\beta\gamma$, βp, $\gamma\gamma$	ΔE_β(plastic)-E_β(Ge),E_x(Ge), E_γ(Ge), ΔE_p(gas)-E_p(Si)	13
^{61}Ga	GSI	$\beta\gamma$, $\gamma\gamma$	$\Delta E_{\beta 1}$(plastic), $\Delta E_{\beta 2}$(plastic, 4π), $E_{\gamma 1}$(Ge), $E_{\gamma 2}$(Ge)	10
^{70}Kr	ISOLDE	$\beta\gamma$, βp, $\gamma\gamma$	ΔE_β(plastic)-E_β(Ge), ΔE_p(gas)-E_p(Si), E_x(Ge), E_γ(Ge)	15
^{71}Kr	ISOLDE	$\beta\gamma$, βp, $\gamma\gamma$	ΔE_β(plastic)-E_β(Ge), ΔE_p(gas)-E_p(Si), E_x(Ge), E_γ(Ge)	15
^{73}Rb	ISOLDE	$\beta\gamma$, βp, $\gamma\gamma$	ΔE_β(plastic)-E_β(Ge), ΔE_p(Si)-E_p(Si), E_x(Ge), E_γ(Ge)	10
^{74}Rb	ISOLDE	$\beta\gamma$, βp, $\gamma\gamma$	ΔE_β(plastic)-E_β(Ge), ΔE_p(Si)-E_p(Si), E_x(Ge), E_γ(Ge)	10
A = 80-88	JYFL	$\beta\gamma$, $\gamma\gamma$	ΔE_β(plastic)-E_β(Ge),E_x(Ge), E_γ(Ge)	7

4. Results and discussion

The results of this work are presented in the following chapter by mass number in ascending order. The only exception is for Kr isotopes, for which the M_T = -1 nucleus ^{70}Kr is discussed after the other M_T = -1 nucleus ^{58}Zn and the mirror nucleus ^{71}Kr is discussed in connection with ^{61}Ga. Finally, the results from the test run for production of refractory elements are presented.

4.1. ^{58}Zn - beta decay and charge-exchange reactions

States in ^{58}Cu serve as a laboratory for studies of Gamow-Teller strength using both charge-exchange reactions and β^+ decay (Fig. 5). The allowed beta decay of ^{58}Zn feeds the same 1^+ final states in ^{58}Cu as the *(p,n)*-type charge-exchange reactions providing a direct comparison in their GT strengths. In this work beta decay of ^{58}Zn was observed for the first time at ISOLDE mass-separator facility using laser ionization. Previously, numerous charge-exchange studies have been performed using ^{58}Ni as a target, i.e. the *(p,n)*-reaction study [Rap83], the *(^{3}He,t)*-reaction studies [Aki94, Fuj96, Fuj97] and the *(^{6}Li,^{6}He)*-reaction study [Lau94].

Beta decay of ^{58}Zn is characterized by a strong $0^+ \rightarrow 0^+$ Fermi decay to its isobaric analog state at 203 keV in ^{58}Cu. In addition, the GT beta decay would populate a wide range of states with $J^\pi = 1^+$ including the ground state of ^{58}Cu. Similar decays to ^{58}Zn among the lighter nuclei are ^{42}Ti and ^{18}Ne. These β^+ emitters also have two protons outside the doubly-magic core and the ordering of the final states in their daughters is determined by the competition between $T = 0$ and $T = 1$ states. A very fast GT decay has been observed in these nuclei populating the first 1^+ state in their daughters with log *ft* values of 3.1 for ^{18}Ne and 3.2 for ^{42}Ti [Fir96].

Beta decay of ^{58}Zn

Beta decay to two low-lying excited states at 203 and 1051 keV in ^{58}Cu was observed in this work. Figure 16 shows a γ-ray spectrum in coincidence with β particles above 800 keV in energy. This energy was taken to be the threshold to reduce the background due to ^{58}Mn.

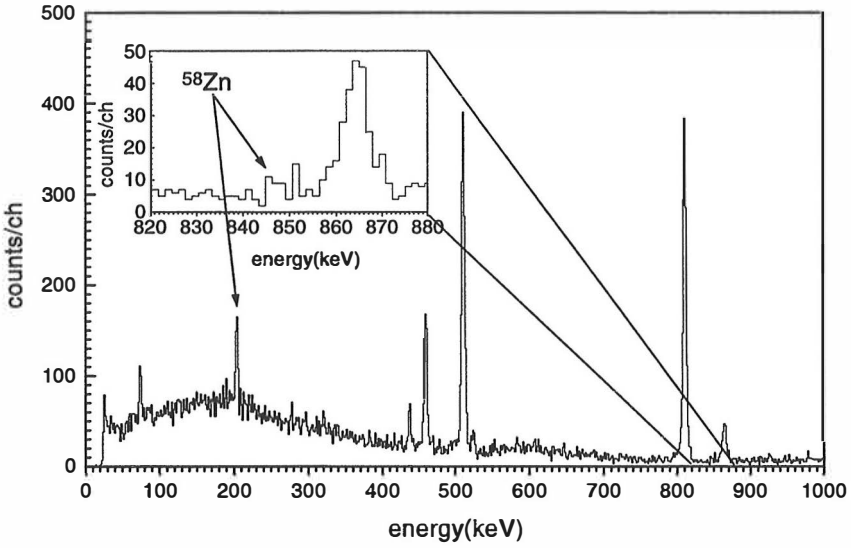

Figure 16. *Beta-gated γ-ray spectrum measured for A = 58. The spectrum shows two peaks: 203 keV and 848 keV following the β feeding to the 203 keV 0^+ and the 1051 keV 1^+ states in ^{58}Cu. Other γ rays seen are from ^{58}Mn or X rays from Pb (74 keV).*

Half-life determination based on high-energy betas could not be performed accurately due to a ^{58}Cu activity (Q_{EC} = 8563 keV) produced with equal rate. Instead of that, the β-decay half-life was determined from the multispectrum analysis of the 203 keV γ ray and was found to be 86(18) ms (Fig. 17). The measured half-life is consistent with a previous estimate of 50-80 ms based on the systematics [Har75].

Absolute branchings for the two 1^+ states were deduced assuming a pure Fermi decay to the 203 keV (J^π, T) = (0^+, 1) state. This results in ft = 3044 s [Tow95] producing a 74(16) % feeding to the IAS. Intensities of the two observed γ transitions I(203) = 100(18) and I(848) = 14(6) can be used to obtain feeding to the 1051 keV state, i.e. I_β(1051) = 12(6) %. The present

measurement setup did not allow the determination of the ground-state branch directly. The upper limit can only be given as 14 %.

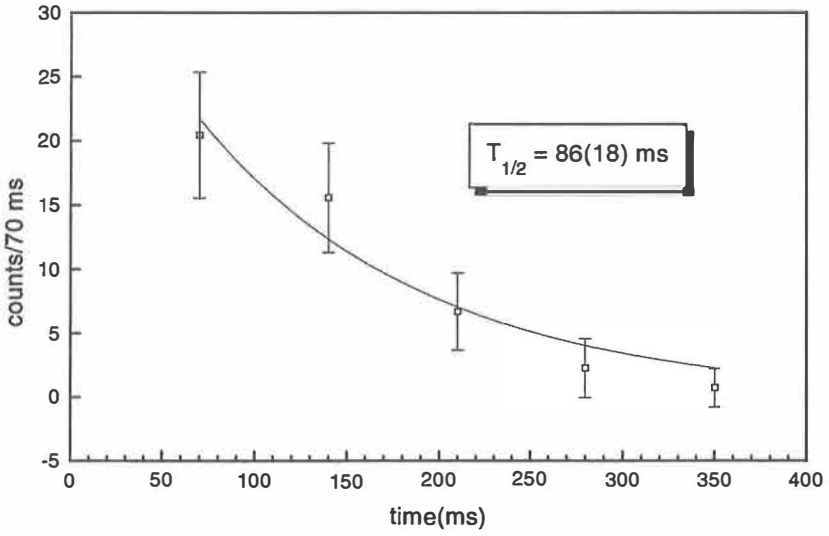

Figure 17. *Decay of 203 keV γ rays using multispectrum analysis.*

Beta-delayed protons were not observed in this work. The non-observation corresponds to an upper limit of 3 % in total branching. The upper limit for the beta-delayed proton branch, deduced from the *(p,n)* study as the feeding of the states above a proton separation energy (S_p) is 2.4 % in agreement with the present measurement. Measurement of beta-delayed protons should be a sensitive method to probe GT strength above S_p.

Discussion

The beta-decay Q value, Q_{EC} = 9370(50) keV, has been determined based on the measured mass for ^{58}Zn [Set86]. This allows a construction of the level scheme shown in Fig. 18. The log *ft* value deduced for beta decay to the 1^+ ground state in ^{58}Cu is > 4.3. This is clearly a higher value than that observed for the analogous nuclei ^{18}Ne and ^{42}Ti. In the case of ^{42}Ti, the low log *ft* value is fully reproduced by the shell-model calculation, if the observed quenching is taken into account [Miy87, Mar96]. For ^{58}Zn, shell-model calculations are not available at

this moment. However, the extreme single-particle approach should be a good approximation for the final states in these three cases, i.e. for ^{18}F, ^{42}Sc and ^{58}Cu which all have p-n pair surrounding the doubly-magic core. According to the single-particle shell model, the lowest 1^+ states in these nuclei are due to $(\pi 1d_{5/2} \otimes \nu 1d_{5/2})$, $(\pi 1f_{7/2} \otimes \nu 1f_{7/2})$ and $(\pi 2p_{3/2} \otimes \nu 2p_{3/2})$ couplings for ^{18}F, ^{42}Sc and ^{58}Cu, respectively. In the case of ^{58}Cu, the second 1^+ state is formed by an excitation of one nucleon to the $1f_{5/2}$ orbital. Configuration mixing with these 1^+ states would produce an l-forbidden contribution into the final-state wave function which would hinder the decay rate. For ^{18}F and ^{42}Sc the next 1^+ state hindering the rate is formed by excitation over two shell gaps, i.e. $(\pi 2s_{1/2} \otimes \nu 2s_{1/2})$ excitation for ^{18}F and $(\pi 2p_{3/2} \otimes \nu 2p_{3/2})$ excitation for ^{42}Sc. These states would be higher in energy compared to ^{58}Cu and the configuration mixing would be smaller.

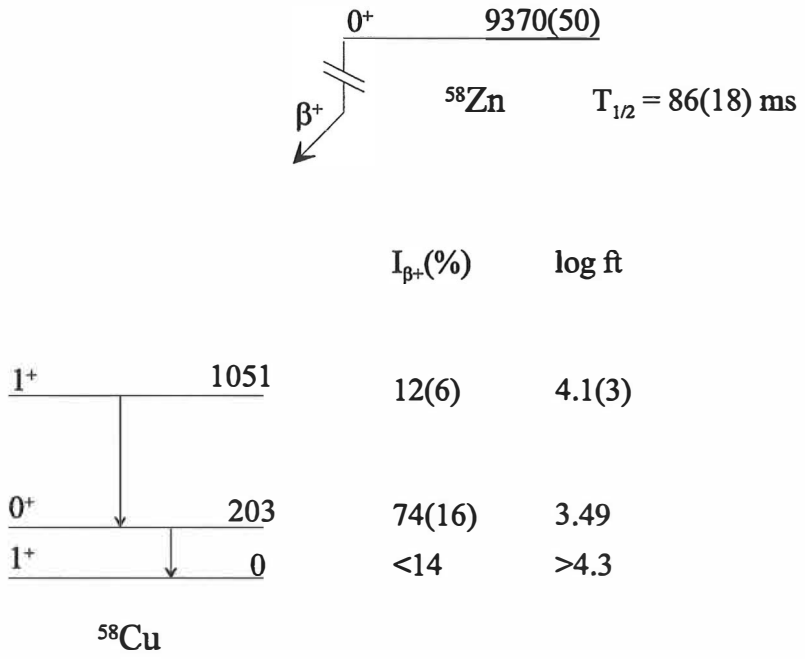

Figure 18. *Decay scheme for ^{58}Zn observed in this work. Pure allowed Fermi decay has been assumed for 0^+ --> 0^+ transition.*

Table 6 compiles the existing data of GT strengths for the 1051 keV state from charge-exchange reactions as well as from the present beta-decay study. Measured beta-decay half-life as well as calculated ones based on the results of the reaction studies are also shown. The

total half-lives show very good agreement between the reaction and decay studies as expected from the dominance of the Fermi strength *B(F)*. Also, the extracted GT strength agrees with the reaction studies within the error bars.

The absolute value from the *(p,n)*-reaction study is somewhat large compared to the result from the β decay. This is possibly due to modest resolution in the *(p,n)* study, which makes it difficult to distinguish between the 1051 keV, 203 keV and the ground states. Higher resolution obtained in the *(^{3}He,t)* study as compared to the *(p,n)* study makes possible the separation of transitions corresponding to the three lowest states and the intensity to the ground state can be accurately determined. A common procedure is to normalize this intensity by the *B(GT)* value from the inverse ground state β decay, i.e. from ^{58}Cu to ^{58}Ni. The log *ft* value for this transition has been given as 4.86(1) [Jon72] which translates into $B(GT)_{pn}$ = 0.255(2). This value has been deduced using the 511 keV annihilation peak intensity. In fact, the final result of 4.86(1) does not take into account the absolute error of 10.4 % in the total intensity [Jon72, p. 557]. Including this, the final result is $B(GT)_{pn}$ = 0.255(10) for the ground state. Improvements in accuracy for β decay of ^{58}Cu would be very welcome in the future measurements to make the normalization more reliable.

Table 6. *Compilation of GT strengths determined in previous studies and in this work for the transition to the 1^+ state at 1051 keV in ^{58}Cu. Half-lives have been calculated based on the GT strengths to individual states. Note the different notation for B(GT) than in refs. [Rap83, Fuj96, Fuj97].*

	***(p,n)* [Rap83]**	***(^{3}He,t)* [Fuj96,Fuj97]**	**this work**
$B(GT)_{1051}$	0.72(15)	0.46(10)	0.54(30)
$T_{1/2}$ (ms)	81	86	86(18)

4.2. ^{70}Kr - measurement of beta-decay half-life

In connection with the ^{71}Kr experiment, an attempt was made to measure the beta-decay half-life of another M_T = -1 nucleus ^{70}Kr at ISOLDE. This nucleus was recently observed to be proton bound in ^{78}Kr-fragmentation studies at GANIL [Bla95a]. It may have an important role

in the *rp* process as a final nucleus for a recently proposed *2p*-capture process from ^{68}Se to ^{70}Kr [Sch98]. Also, according to reaction flow calculations the path of the process can be shifted towards more proton-rich nuclei depending on the mass model used and instead of a waiting point in ^{72}Kr, the slowest beta decay along the path could be also ^{70}Kr [Sch98]. The correctness of this conclusion, however, depends on the beta-decay half-life of ^{70}Kr.

Half-life of ^{70}Kr

As an even-even nucleus ^{70}Kr has the $J^\pi = 0^+$ ground state and would decay to its $J^\pi = 0^+$ isobaric analog state in the N = Z nucleus ^{70}Br. As an odd-odd N = Z nucleus the spin and parity of the ground state of ^{70}Br is determined by a competition of this $(J^\pi, T) = (0^+, 1)$ state and a $(J, T) = (\text{odd}, 0)$ state. Two half-lives have been reported for ^{70}Br: $T_{1/2}$ = 79.1(8) ms and 2.2(2) s [Bha93]. The shorter half-life refers to the $(0^+, 1) \rightarrow (0^+, 1)$ superallowed β decay to the ground state of ^{70}Se and the longer one to the decay of the (odd, 0) state. A high decay energy of ^{70}Kr, Q_{EC} = 10.460(50) MeV [Orm97], gives the possibility to observe high-energy β particles produced mostly by the $0^+ \rightarrow 0^+$ decay. However, an almost identical decay of the $(0^+, 1)$ state in the daughter nucleus ^{70}Br having Q_{EC} = 10.35(31) MeV, has to be taken into account in the half-life determination. The problem is simplified by the fact that Br isotopes do not come out of the ion source used at ISOLDE because the water-cooled transfer line at room temperature allows only gaseous elements to be transported to the ion source [Bjø87]. This was demonstrated by collecting masses A = 72 and 73 without any sign of direct production of Br isotopes. The beam gate was chosen to be 150 ms based on the estimated half-life of ^{70}Kr (60 ms). Fig. 19 shows the decay part of the time spectrum of positrons above 1.3 MeV counted by the beta telescope. About 98 % of positrons coming from ^{70}Kr should lie above this energy limit. Observed contaminant activities ^{70}As and ^{70}Ga are long-lived: 53 min and 14 min, respectively, and they were taken into account as a constant background. The telescope consisted of a 1 mm thick plastic scintillator and a 20 mm thick planar Ge detector. Fast timing signals between the detectors were used for cleaning up the time spectrum. The time spectrum was fitted to a function:

$$N(t) = y_0 + N_{10}\left[e^{-\lambda_1 t} + \frac{\lambda_1}{\lambda_2 - \lambda_1}\left(e^{-\lambda_1 t} - e^{-\lambda_2 t}\right) + \frac{N_{20}}{N_{10}} e^{-\lambda_2 t}\right] \qquad (26)$$

where y_0 = constant for background, N_{10} = amount of Kr in the beginning of the decaying part (beam gate), N_{20} = amount of Br in the beginning of the decaying part (beam gate), λ_1 = decay constant of ^{70}Kr, λ_2 = decay constant of ^{70}Br (fixed to correspond to the half-life of ^{70}Br).

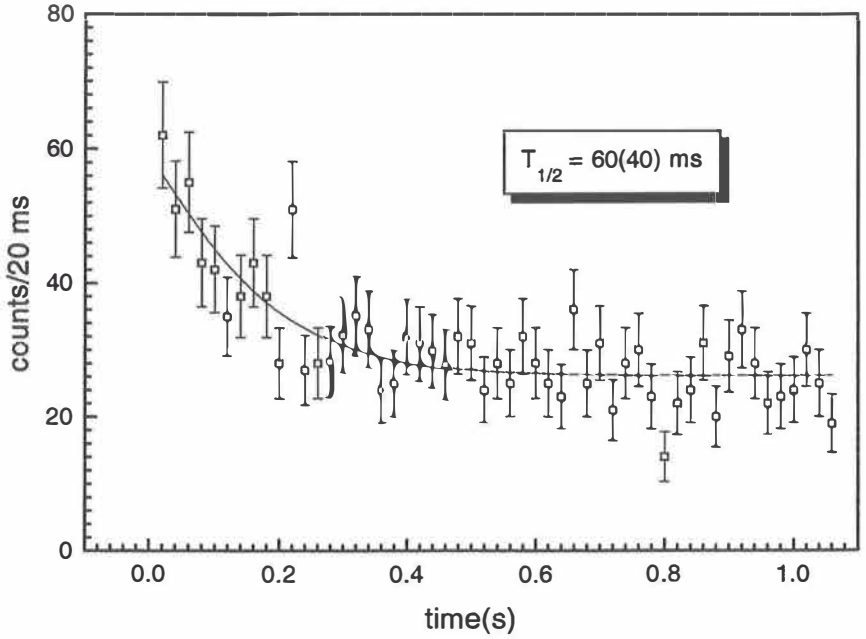

Figure 19. *Time distribution of beta decays in the chain ^{70}Kr-^{70}Br-^{70}Se. The measuring time was 27 h and the beam gate was set to be 150 ms.*

Equation (26) takes into account the decay of ^{70}Kr and the production and the decay of ^{70}Br as a daughter of ^{70}Kr. As an input the fitting procedure needs the ratio of Br and Kr at the beginning of the fitting region, i.e. at the time of the beamgate. This has been simulated using the knowledge of the release parameters from Table 4 including 20% errors. The final value for the half-life has been obtained using an iterative method which consisted of three steps: a) assumed initial value of $T_{1/2,i}$, b) simulation of the ratio Br/Kr and c) fit for the half-life. The process was repeated until the final value converged. Initial values ranging from 40 to 90 ms resulted in the final value of $T_{1/2}$ = 60(40) ms for the beta-decay half-life of ^{70}Kr.

Discussion

The obtained half-life can be compared with the result from recent QRPA-calculations which give $T_{1/2}$ = 390 ms [Möl97, Sch98]. The disagreement in $T_{1/2}$ in comparison with the theoretical value is very significant and would lead to a much faster reaction flow in the mass region A ~ 70 than calculated in ref. [Sch98]. The beta-decay half-life can be estimated assuming superallowed Fermi beta decay of ^{70}Kr. Assuming the value Q_{EC} = 10.459(50) MeV from the recent shell-model Coulomb-energy calculation [Orm97], $B(F)$ = 2 and C = 6145(4) s one obtains $T_{1/2}$ = 61 ms. This estimate supports the result obtained in this work. Another prediction using QRPA calculations by Hirsch et al. agrees with the measured result giving $T_{1/2}$ = 55 ms [Hir93].

According to Hartree-Fock calculations performed for deformed nuclei near the proton drip line, deformation would drive most of the Gamow-Teller strength on to proton unbound states [Fri95]. No evidence for β-delayed γ or p decay from ^{70}Kr was found in this experiment. The Si detector thickness of 300 μm allowed β-delayed proton detection up to 6 MeV. Upper limit for b_p can be estimated based on two counts seen in the "proton region" in the ΔE-E spectrum of the gas-Si telescope detector resulting in 1.3 %.

4.3. Beta decay of M_T = -1/2 nuclei ^{61}Ga and ^{71}Kr

Determination of the ground-state Gamow-Teller matrix elements for mirror transitions in the *fp* shell allows direct comparison to model predictions. Shell-model calculations for the mirror nuclei have been performed up to A = 57 [Miy87, Sem96, Mar96]. Above A = 60, only predictions for the decay energies have been possible. The extrapolated values for the decay energies do not show the typical smooth behaviour of experimental energies observed between the closed shells of A = 40 and 56 (Fig.1). This emphasizes the need for more experimental data to guide extrapolations. Studies of mirror β decays in the *fp* shell have been possible earlier up to ^{59}Zn [Hon81] and in the upper *fp* shell for ^{67}Se [Bau94]. Experiments performed in this work for ^{61}Ga and ^{71}Kr partly fill the unknown gap between these nuclei and extend the studies of beta decays between mirror nuclei towards the end of the *fp* shell.

4.3.1. ^{61}Ga - extending the mirror-decay systematics

Beta-delayed gamma decay of ^{61}Ga

Up to now, ^{61}Ga has been observed and its beta-decay half-life measured using fragmentation of ^{78}Kr [Moh91, Win93]. However, no other information about its decay properties have been reported. On the other hand, the final states for beta decay below 2.3 MeV in ^{61}Zn are well-known [Chu92]. Spin and parity assignments are based on $n\gamma$ and $\gamma\gamma$ angular correlation measurements [Smi82, Sch89]. Relative gamma intensities are also known as well as conversion coefficients for low-energy transitions. Due to the relatively low production rate and strong ground-state feeding, only the strongest γ transition de-exciting a certain level could be observed in the present work. The deduced beta-decay branching ratios in this work are based on the previously known γ branching ratios from the populated states [Thi84] and the intensities determined from the present beta-decay data.

Figure 20 shows a γ-ray spectrum observed at A = 61. Four γ transitions of 88, 123, 418, and 755 keV were assigned to the β decay of ^{61}Ga based on the known γ transitions in ^{61}Zn. Intensity determination of the 88 keV peak following the beta decay of ^{61}Ga was disturbed by K_β X rays of Pb. However, the contribution from the K_β X rays could be determined based on the intensities observed in the calibration spectrum at A = 56. The 88 keV mixed $E2$+$M1$ transition is also highly converted with a measured total conversion coefficient of α = 0.59(48) [Chu92] and this correction induces an additional error into the beta feeding. The 752/755 keV doublet is due to γ transitions following the beta decays of ^{61}Zn and of ^{61}Ga, respectively. The intensity of the 752 keV peak was obtained by using the 690 keV peak from beta decay of ^{61}Zn as a reference. The final intensity for the 755 keV peak of ^{61}Ga was obtained after subtracting this contribution from the total intensity of the 752/755 keV doublet.

In Table 7, the observed γ transitions following the beta decay of ^{61}Ga are shown. The intensities have been determined using the beta-gated (4π detector) γ -ray spectrum in anticoincidence with a plastic scintillator placed in front of the Ge detector. In this way a

spectrum free from positron summing was obtained. Only the upper limits for the intensities of the 938 and the 1362 keV γ transitions could be determined in the absence of clearly resolved peaks. Half-life estimates using growth-in curves for beta-delayed gamma transitions have been also given. Although the accuracies remain modest due to the low counting statistics, the values differ significantly from the values of contaminant activities ^{61}Zn and ^{61}Cu which have half-lives of 89.1 s and 3.4 h, respectively [Chu92]. Beta-decay half-life for ^{61}Ga has been measured to be 150(30) ms using the A1200 radioactive-beam facility at MSU [Win93]. In the following calculations the previous value was used.

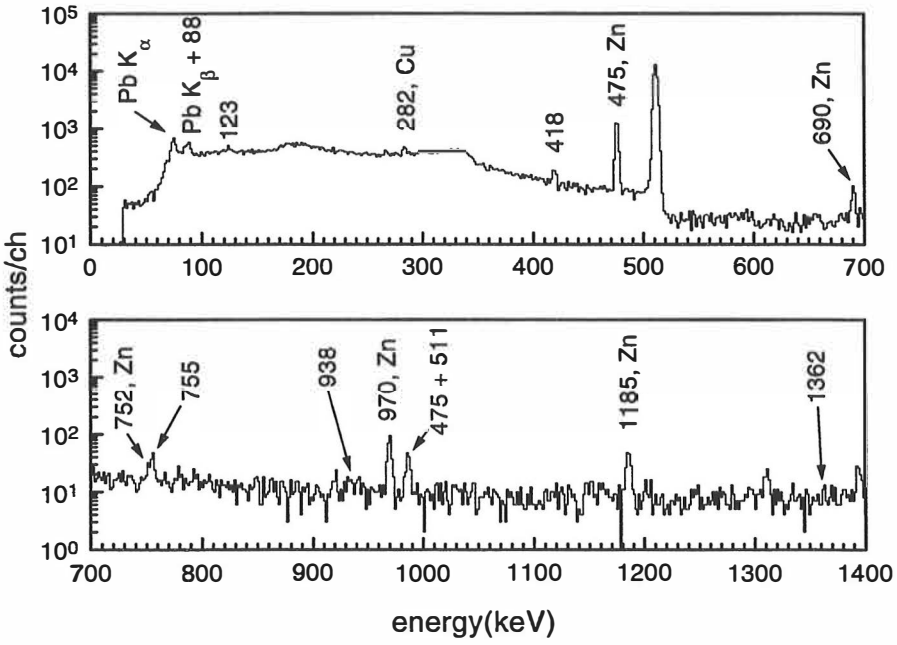

Figure 20. *Beta-delayed γ-ray spectrum for A = 61. Peaks originating from the beta decay of ^{61}Ga are marked with their energies. The other lines come from the beta decays of ^{61}Zn and ^{61}Cu. Collection time was 4 h.*

Total beta intensity for ^{61}Ga was determined as an integral of the 150(30) ms component of the time spectrum for the observed positrons in the 4π scintillator. The time spectrum was fitted with a two component growth-in curve by fixing the half-lives for ^{61}Ga and ^{61}Zn. A

constant offset was included taking into account the long-lived ^{61}Cu activity and a randomly distributed background. Integrals of these curves gave the relative beta intensities produced during the measurement for each nuclei. The absolute beta intensity for ^{61}Ga was obtained by scaling the relative intensity using the absolute intensity of the 475 keV peak from the beta decay of ^{61}Zn. This results in 84(20)% feeding to the ground state of ^{61}Zn. This is in agreement with the other ground state feedings observed in the *fp* shell for the mirror decays. The large error limit is mainly due to the large error limit in the half-life of ^{61}Ga which has to be taken into account in the fitting procedure as well as in the integration. Obtained branchings and the resulting log *ft* values are shown in the decay scheme (Fig. 21). Corrections for internal conversion have been made for the 88, 123 and 418 keV transitions [Chu92].

Table 7. *Relative intensities of the γ rays observed in the beta decay of ^{61}Ga. Only upper limits are given for the 938 and 1362 keV transitions. Half-life estimates obtained from fits to the growth-in periods from 0 to 800 ms are shown for some cases. The level energies have been taken from [Chu92].*

E_γ(keV)	E_i(keV)	J_i^π	E_f(keV)	J_f^π	$T_{1/2}$(ms)	I_γ(rel.units)
87.6(10)	88.40(10)	1/2$^-$	0	3/2$^-$	210(220)	250(70)
122.9(10)	123.75(10)	5/2$^-$	0	3/2$^-$	-	120(30)
418.4(8)	418.10(15)	3/2$^-$	0	3/2$^-$	140(70)	100(14)
754.5(12)	756.02(18)	5/2$^-$	0	3/2$^-$	60(70)	79(13)
938	937.7(4)	1/2$^-$	0	3/2$^-$	-	<11
1362	1362.3(4)	3/2$^-$,5/2$^-$	0	3/2$^-$	-	<13

The atomic-mass evaluation for 1995 [Aud95] gives Q_{EC} = 8.992(200) MeV for the beta decay of ^{61}Ga. A shell-model calculation for Coulomb-energy differences taking into account isospin-nonconserving (INC) interaction gives a slightly higher value Q_{EC} = 9.262(50) MeV [Orm97]. The latter value is in close agreement with the other two commonly used mass predictions of Jänecke-Masson [Jän88] and the microscopic-macroscopic model of Möller &Nix [Möl95], which give 9.220 and 9.330 MeV, respectively. Also, the calculated half-life for the $0^+ \rightarrow 0^+$ beta emitter ^{62}Ga based on the Coulomb-energy calculations of ref. [Orm97]

is in good agreement with the measured value. Thus, the Q_{EC} value from [Orm97] was adopted for further use.

Discussion

The proposed decay scheme for ^{61}Ga is shown in Fig. 21. The scheme is similar to those of the other mirror nuclei in the *fp* shell and is dominated by a strong ground-state feeding. The GT matrix element for the ground-state decay $\langle\sigma\tau\rangle = 0.35(34)$ is much smaller than the extreme single-particle estimate assuming the $2p_{3/2}$ --> $2p_{3/2}$ -transition $\langle\sigma\tau\rangle_{ESP} = 1.29$. This reduction of the Gamow-Teller ground-state matrix element relative to the single-particle estimate is typical for the *fp*-shell nuclei and has its origin in configuration mixing.

Shell-model calculations for light Zn isotopes using the MSDI interaction have been performed by Van Hienen et al. [Van76]. In these calculations ^{56}Ni was used as an inert core without any possibility for $1f_{7/2}$ excitations. MSDI two-body matrix elements were adjusted to reproduce the energy levels of Ni and Cu isotopes in the region A = 57-68. Calculations for occupation numbers of the ground states of Zn isotopes resulted in increasing configuration mixing of the $2p_{3/2}$, $1f_{5/2}$ and $2p_{1/2}$ orbits when going towards the proton drip line. For the ground state of ^{61}Zn, the occupation probabilities of the orbitals above were 0.50, 0.35 and 0.15, respectively.

All beta transitions imply allowed character. The observed feedings to the $1/2^-$ state at 88 keV and to the $5/2^-$ states at 124 and 756 keV fix the ground state of ^{61}Ga to be $J^\pi = 3/2^-$ and it is in accordance with the standard shell-model configuration (Fig. 4). This is also expected from the $J^\pi = 3/2^-$ character of the ground state of the mirror nucleus ^{61}Zn. Calculations of log *ft* values for beta decays of odd-A Ga isotopes between A = 63-67 by Van Hienen et al. gave satisfactory results compared to experiments, except for the $3/2^-$ --> $5/2^-$ transitions. This shows only valence nucleon excitations to be insufficient for explaining these transitions. The discrepancies were qualitatively explained by the importance of particle-hole excitations of the ^{56}Ni core. Similar, but quantitative results have been obtained in the case of ^{57}Cu for which the $3/2^-$ --> $5/2^-$ transitions have been shown to be fully explained by 3p-2h -excitations [Sem96].

A lack of shell-model studies for beta decay of ^{61}Ga do not allow direct comparisons between the experiment and calculations.

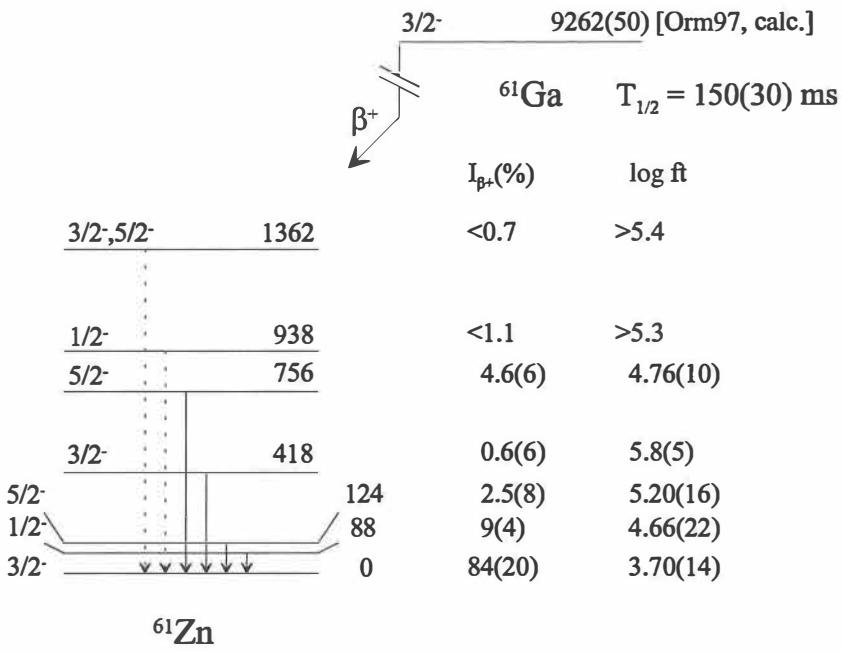

Figure 21. *Proposed decay scheme for ^{61}Ga. The observed γ transitions are shown by the solid arrows. The dashed arrows show transitions for which only upper limits have been given. The Q_{EC} value has been taken from the shell-model calculation in [Orm97].*

4.3.2. ^{71}Kr - mirror beta decay in the upper fp shell

The A ~ 70 region is fascinating due to expected collective effects in mid-shell nuclei. In fact, due to deformation, a large fraction of Gamow-Teller strength is predicted to be located within Q_{EC} windows for light Kr isotopes and would then be probed by beta decay [Fri95]. In addition to ^{61}Ga, another mirror decay studied in this work is ^{71}Kr. Its first observation by beta decay resulted only in a half-life determination [Ewa81]. The recent fragmentation study of ^{78}Kr at GANIL lead to the observation of a weak β-delayed proton branching in ^{71}Kr as well as in ^{67}Se and ^{75}Sr [Bla95b]. The latter experiment resulted in significantly shorter half-life compared to the first beta-decay measurement.

Delayed radiation

The experiment was performed at ISOLDE in connection with the search for two other light Kr isotopes ^{70}Kr and ^{69}Kr. Since both β-delayed γ and proton emission is possible in this region, the measurement setup was designed to cover all decay modes (see Table 5). Fig. 22 shows β-gated γ-ray spectra for two different time intervals to emphasize the production of ^{71}Kr. Based on the known levels in ^{71}Br [Arr90, Bha93] and the fact that the relative intensities of the peaks correspond to in-beam studies [Arr90] the observed γ rays at 198 and 207 keV are assigned to β decay of ^{71}Kr. Table 8 shows the relative intensities of these transitions as well as upper limits for other non-observed but possible γ transitions.

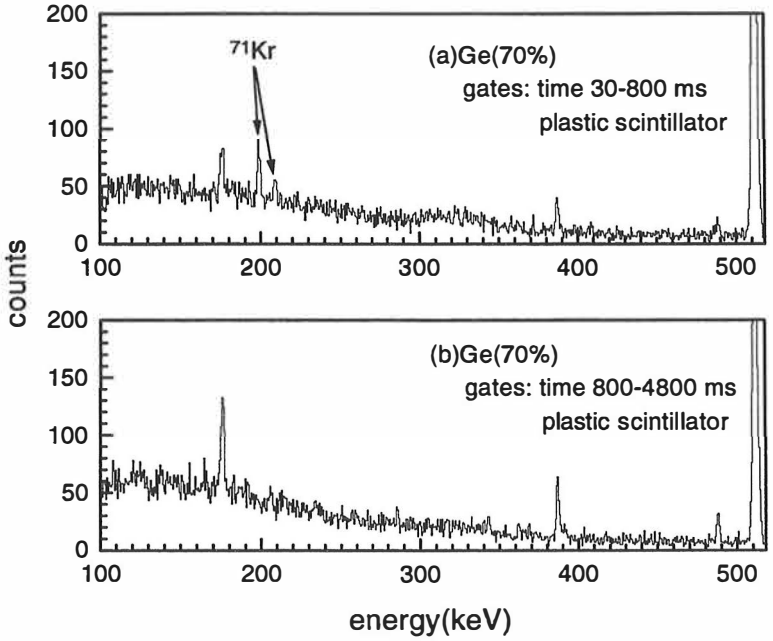

Figure 22. *Beta-gated γ-ray spectra measured for A = 71. (a) Spectrum from the time period 30-800 ms after the proton pulse from PS-Booster shows the population of the first excited state of ^{71}Br at 207 keV. (b) Background spectrum from the period of 801- 4800 ms.*

Table 8. *Intensities of the observed gamma transitions and upper limits for the unobserved expected transitions in ^{71}Br and ^{70}Se.*
a) Following the βp decay to the first excited state in ^{70}Se. Represents an upper limit of all beta decays of ^{71}Kr.

E_γ [keV]	I_γ [rel. unit]	J_i	J_f	in
198	100(11)	$(3/2)^-$	$(1/2^-)$	^{71}Br
207	36(6)	$(3/2)^-$	$(5/2)^-$	^{71}Br
262	< 8	$(3/2^-)$	$(5/2)^-$	^{71}Br
599	< 10	$(7/2^-)$	$(3/2^-)$	^{71}Br
945	< 1%[a)]	2^+	0^+	^{70}Se

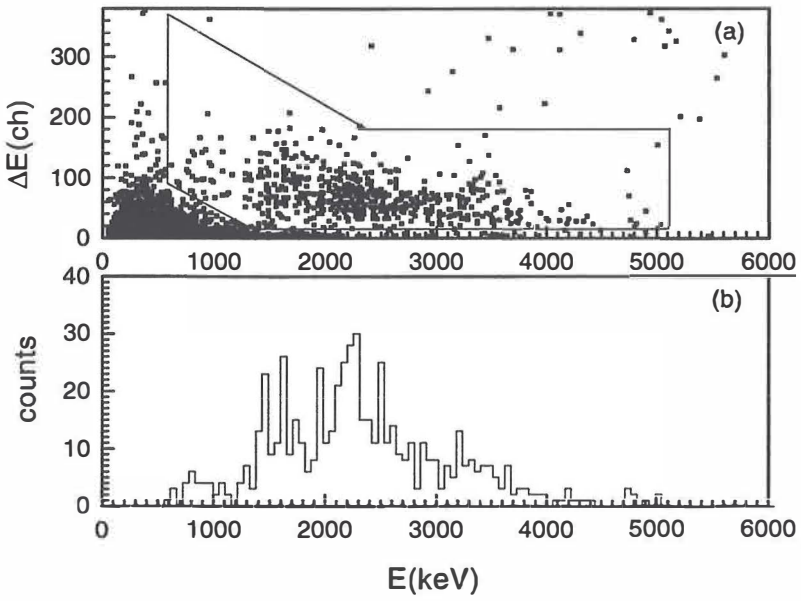

Figure 23. *Beta-delayed protons observed at mass A = 71. (a) Total ΔE_{gas}-E_{Si} matrix with a window set for protons. (b) Projected proton spectrum.*

Beta-delayed proton (βp) decay was also observed in this work. Protons were detected with a low-energy gas-Si telescope detector [Hon97b] with a resolution of 30 keV. The result is

shown in Fig. 23. The spectrum is bell-shaped as is typical for nuclei with A > 60. Due to modest statistics, detailed analysis is not possible. However, the spectrum clearly shows a maximum at the energy of 2.3 MeV. Proton-gamma coincidence selection did not give any evidence for βp emission to populate the 945 keV 2^+ state in ^{70}Se and only an upper limit of 1% could be determined (Table 8). Branching to proton-unbound states was determined to be 3.4(13) %. The value is lower than that observed in the fragmentation study i.e. 5.2(6) % [Bla95b] but the two values are consistent within the error limits. The absolute value for the beta-delayed proton branching ratio given in [Publ.2] is slightly lower, i.e. 2.1(7) %, for ^{71}Kr. This difference is due to the fact that the electron capture to the proton unbound states was not properly taken into account in [Publ.2]. However, the results are the same within the error bars and the difference does not affect the final conclusions on the beta decay of ^{71}Kr.

Beta-decay half-life and the Q_{EC} value

The half-life for ^{71}Kr has been measured earlier by beta decay to be 97(9) ms [Ewa81]. A recent study relying on βp detection resulted in $T_{1/2} = 64^{+8}_{-5}$ ms [Bla95b] in clear disagreement with the earlier value. In this work the observation of β-delayed protons and high-energy positrons allowed the half-life measurement to be performed in two different ways. The weighted average of the results shown in Fig. 24 gives $T_{1/2}$ = 100(3) ms in agreement with the previous value measured with the mass-separated source. The reason for the disagreement between this result and the result of the fragmentation experiment is not understood.

The beta-decay Q_{EC} value of ^{71}Kr is given by the systematics to be 10.49(42) MeV [Aud95]. In this work the Q_{EC} value was measured to be 10.14(32) MeV based on the endpoint of the beta spectrum [Publ.2]. These two values are consistent with each other. The experimental value determined in this work has been used in further calculations.

Using the measured γ-transition and p intensities, the β branchings could be determined and are given in Table 9. The total beta intensity was obtained from the short-lived component of the time spectrum of the positrons. The strongest observed background contributions due to ^{71}Zn and ^{71}As were taken into account using a constant offset since they are long-lived, 2.45 min and 65.3 h, respectively. In addition, ^{71}Br is also present following the decay of ^{71}Kr but it also has a long half-life of 21.6 s. Thus, the amount is negligible. The constant offset was

determined by fitting a single exponential plus constant background into the region of 250 - 800 ms in the time spectrum of the positrons.

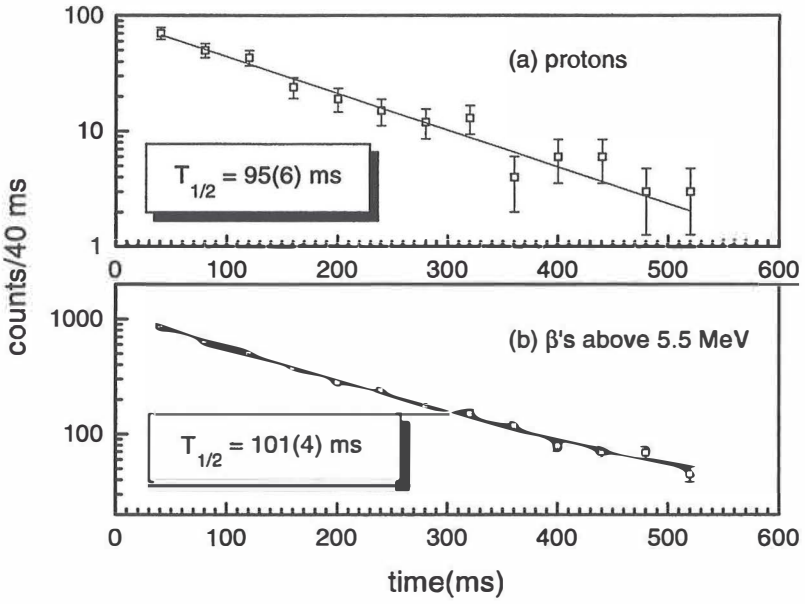

Figure 24. *Half-life determinations using (a) beta-delayed protons and (b) high-energy positrons. The energy limit 5.5 MeV for the positrons was chosen to correspond to the endpoint energy of the daughter nucleus ^{71}Br.*

Table 9. *Beta decay of ^{71}Kr to the levels of ^{71}Br. [a] Not seen, estimated upper limit.*

E_γ [keV]	J^π	I_β [%]	log *ft*	$\lvert\langle\sigma\tau\rangle\rvert$
0	$(5/2)^-$	80.8(24)	3.72(7)	0.31(20)
207	$(3/2)^-$	15.8(14)	4.38(8)	0.40(4)
262	$(3/2^-)$	$< 1^{a)}$	> 5.6	
806	$(7/2^-)$	$< 1.1^{a)}$	> 5.4	
p unbound		3.4(13)		

Discussion

The ground state of ^{71}Br has been deduced to be J^{π} = (3/2,5/2,7/2)$^-$ based on its allowed β decay to the 5/2$^-$ ground state in ^{71}Se [Hag82]. In addition, based on the angular distribution of the *M2* γ transition de-exciting the 9/2$^+$ isomeric state at 759 keV, the ground state of ^{71}Br has been proposed to be 5/2$^-$ [Arr90]. In further discussions we adopt the value of (5/2)$^-$ as also given in a recent compilation [Bha93]. Assuming charge symmetry to be still valid in this mass region the ground-state spin and parity is (5/2)$^-$ also in ^{71}Kr. The decay scheme based on the discussion above and the observed feedings given in Table 9 are presented in Fig. 25.

A large ground-state branch $b_{g.s.}$ = 80.8(24) % is as expected for mirror nuclei. In addition to the (5/2)$^-$ ground state, the adopted level scheme includes few other states as possible final states for the allowed GT beta decay. A state at 207 keV would explain the two observed γ transitions. The strong allowed β feeding to this state is consistent with a J^{π} = (3/2)$^-$ assignment. The order in the cascade of 198 keV and 9 keV (unobserved) transitions, left unanswered by in-beam work [Arr90], could not be directly measured in this work. However, an intermediate state at 198 keV with J^{π} = 1/2$^-$ would not be fed by allowed β decay and it would be fed very weakly also by the 9 keV γ transition from the 207 keV level compared to a direct transition to the ground state. Assuming pure *M1* transitions the ground-state transition should be a factor of 12000 stronger. Thus, the J^{π} = (1/2$^-$) state most likely lies at 9 keV in ^{71}Br.

Beta feeding to the J^{π} = (3/2$^-$) state at 262 keV was not observed. This could be an indication of a particular configuration of this state which would hinder the β decay. In fact, the low-energy structure in ^{71,73}Br has been explained to rise from shape coexistence including oblate ground-state and prolate rotational ΔJ = 2 band built on a 3/2$^-$ state [Gri92]. In ^{71}Br the band head is at 207 keV and, based on the well-known Alaga rule for the beta decay to rotational states, it is estimated that 0.8 % feeding is expected to populate the (7/2$^-$) state at 899 keV. The sensitivity of the setup was not good enough to test this prediction and only an upper limit of 1.1 % could be obtained for the branching.

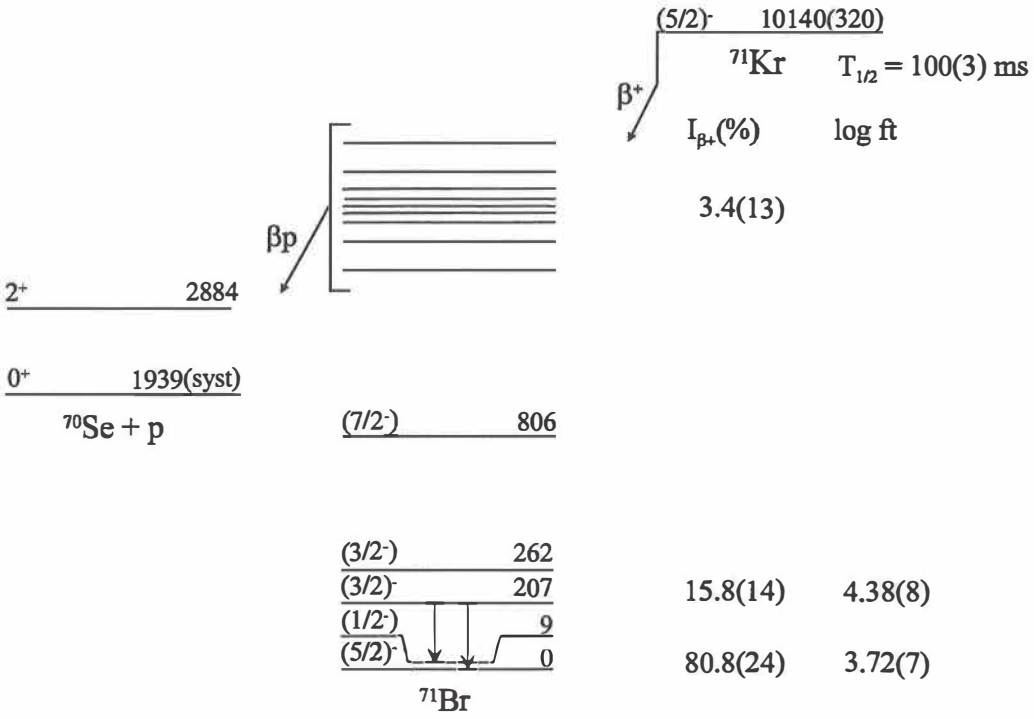

Figure 25. *Proposed decay scheme for ^{71}Kr.*

A low-energy 5/2⁻,1/2⁻ doublet has also been observed in ^{73}Br but in reverse order. Based on not very definite spin-parity assignments of ^{71}Br states and on Hartree-Fock calculations with a deformed potential, a different low-energy structure has been proposed for the daughter nucleus [Ham97]. The calculation supports the formation of a low-lying 3/2⁻,1/2⁻ doublet with oblate shape. In this work, the possible beta decay to the low-lying 9 keV level could not be separated from the ground-state feeding. If the ground state would be $J^{\pi} = 1/2^-$, it would make the observed allowed beta decay of ^{71}Br to the ground state of ^{71}Se questionable [Hag82]. Another member of the proposed doublet, the $J^{\pi} = 3/2^-$ state, as the ground state is possible, if the angular distribution measurement of Arrison et al. for the 759 keV $9/2^+$ --> $(5/2)^-$ transition is disregarded. The mirror symmetry requires a nearly similar low-lying structure for ^{71}Kr as well. Due to a small energy difference between the members of the doublet and possible deviations caused by the Coulomb interaction the ordering could be reversed in comparison to ^{71}Br. Results obtained in this work do not contradict the $1/2^-$ ground-state assignment to ^{71}Kr since strong β feeding to the 9 keV state would still be possible.

4.3.3. Systematics of mirror nuclei in the fp shell

The decay studies performed for ^{61}Ga and ^{71}Kr allow the systematics of the ground-state Gamow-Teller matrix elements to be extended towards the region where collective effects are expected to dominate over single-particle behaviour. Fig. 26 shows a comparison of the experimental ground-state GT matrix elements in the *fp* shell and the available results of the shell-model calculations for the $1f_{7/2}$ nuclei. The experimental values have been obtained using Eqs. (15,16) and the latest data compilations of Nuclear Data Sheets. Ground-state Gamow-Teller matrix elements determined for both ^{61}Ga and ^{71}Kr continue the systematics of the previously known isotopes.

The ground-state GT matrix elements for ^{61}Ga and ^{71}Kr, 0.35(34) and 0.31(20), respectively, are consistent with the trend observed in the *fp* shell. Large errors in the values for ^{61}Ga, ^{67}Se and ^{71}Kr are mainly due to large uncertainties in the Q_{EC} values and in the half-lives, except for ^{71}Kr for which the half-life was accurately measured in this work. Cases of ^{45}V, ^{47}Cr, ^{59}Zn and ^{67}Se might suffer from additional uncertainties due to the procedures for the total intensity determination in these cases [Hor82, Bur85, Hon81b and Bau94, respectively]. A recent full *fp*-shell calculation [Mar96] reproduces the observed GT matrix elements for the mirror nuclei ^{41}Sc, ^{45}V, ^{47}Cr and ^{49}Mn with a quenching factor q^2 ranging from 0.55 to 0.77. It should be noted that calculations with restricted model spaces [Miy87] give good results for mid-$1f_{7/2}$-shell nuclei such as ^{47}Cr. Above A = 60, experimental difficulties, rising mainly from low production cross sections, increase the uncertainties and a meaningful comparison with shell-model calculations has to wait for detailed spectroscopic studies.

In the case of ^{67}Se, two half-lives have been reported: 107(35) ms [Bau94] and 60^{17}_{-11} ms [Bla95b]. The latter value obtained in fragmentation of ^{78}Kr would increase the value of the GT matrix element very close to the single-particle value $\langle \sigma\tau \rangle_{ESP} = 0.845$. To compensate for this increase a Q_{EC} value of ~ 11.5 MeV would be required which is significantly larger than the value Q_{EC} = 9.87 MeV obtained by Coulomb-energy calculation [Jän88] and also the value Q_{EC} = 10.15(22) MeV from ref. [Aud95]. Thus, the measured half-lives in [Bla95b] seem to be systematically too short compared with the general trend expected in the *fp* shell.

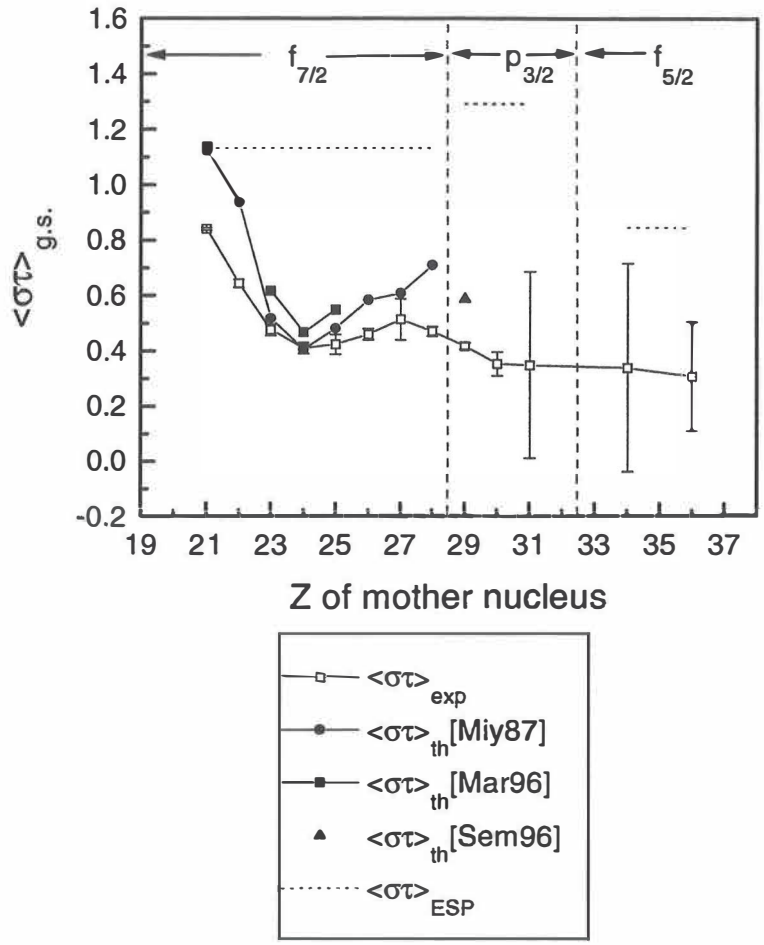

Figure 26. *Systematics of ground-state Gamow-Teller matrix elements in the fp shell.*

Total integrated GT strengths in studied nuclei are about 10 % from the sum rule limit of $\sum_f \langle \sigma\tau_+ \rangle^2 > 3$ for mirror nuclei. Similar values have been obtained for other *fp*-shell mirror nuclei with A = 45-59. However, these values can be used only to compare the sensitivity of the measurements instead of drawing any solid conclusions about the GT strength distribution since most of the experiments have been performed using beta-delayed gamma spectroscopy in absence of the possibility for more sensitive beta-delayed proton detection. Beta-delayed proton spectroscopy has been exploited only for ^{59}Zn [Hon81b], ^{67}Se [Bla95b] and ^{71}Kr. The

total β strength fragmented to proton-unbound states for ^{59}Zn is around 50 %, although the absolute feeding to these states is only 0.23 % [Hon81b]. In the case of ^{61}Ga, the proton separation energy of the emitter ^{61}Zn is fairly high, i.e. S_p = 5290(16) keV compared to S_p = 3418(1) keV for ^{59}Cu. Thus, the probability for proton emission should be lower. Beta-delayed proton branching is approximately proportional to the fifth power of the available energy window $(1-S_p/Q_{EC})$. For ^{61}Ga, this estimate leads to b_p = 0.03 %. In the case of ^{59}Zn, the low mass of ^{58}Ni due to the magic proton number Z = 28 lowers the proton separation energy causing a relatively high beta-delayed proton branch compared to ^{61}Ga.

4.4. Search for M_T = -1/2 nucleus ^{73}Rb

^{73}Rb plays a crucial role in determining the endpoint of the *rp*-process path. Provided that this nucleus is proton unbound the *rp* process would have to wait for the beta decay of ^{72}Kr with $T_{1/2}$ = 17.2 s before continuing towards higher masses. Due to its long β-decay half-life compared to the time scale of the *rp* process, ^{72}Kr would become a waiting-point nucleus where the process is slowed down or even terminated. A faster way of proceeding beyond the waiting points was proposed recently [Gör95]. This reaction is a sequential *2p*-capture process which could bridge the waiting point at ^{72}Kr through a chain ^{72}Kr -> ^{73}Rb -> ^{74}Sr.

Previous studies

An earlier measurement searching for the beta decay of ^{73}Rb has set an upper limit for the production rate for this nucleus to be 1 atom/s at the ISOLDE/SC facility [Aur77] indicating its unbound character. Fragmentation studies at MSU with ^{78}Kr beam on a ^{58}Ni target also support this result, detecting only ^{74}Rb ions but not ^{73}Rb [Moh91]. However, this could be partly explained by a drop in the production cross section from ^{74}Rb to ^{73}Rb since the reduction factors in producing similar isotope pairs ^{66}As-^{65}As and ^{70}Br-^{69}Br were of the order of 100 and the observed number of ^{74}Rb was rather low. Based on this argument, an experiment to search for the β and proton decay was performed at ISOLDE-facility at CERN [Oin95, Publ.1]. In a recent experiment at GANIL it was possible to set an upper limit for the

proton-decay half-life for ^{73}Rb to around 100 ns also indicating a proton-unbound character [Bla95a].

ISOLDE search for ^{73}Rb

The detector setup with a scintillator-Ge telescope detector described in Table 6 allowed detection of high-energy positrons up to 10 MeV. It also included proton detection with a 20 μm Si ΔE and 500 μm Si E telescope detector as well as γ- and *X*-ray detection. The beam gate was open for 100 ms after each proton impact from the PS-Booster. Fig. 27 shows the β spectra observed at masses A = 73 and 74. High-energy β particles observed in the mass A = 74 spectrum are due to beta decay of ^{74}Rb, which has a half-life of $T_{1/2}$ = 64.9(5) ms. Beta decay energies as given by [Aud95] for these Rb isotopes are Q_{EC} = 10.62(50) MeV for ^{73}Rb and Q_{EC} = 10.44(44) MeV for ^{74}Rb. The partial β-decay half-life for ^{73}Rb would thus be nearly equal to that of ^{74}Rb. Low-energy β particles in the A = 73 spectrum can be explained by the production of neutron-rich isobars ^{73}Ga and ^{73}Zn which have β-decay endpoint energies of less than 4.5 MeV. Comparing the ratio of the observed high-energy β events above 5 MeV at both masses, and correcting for measurement times, one can determine the ratio of the yields to be Y(^{73}Rb)/Y(^{74}Rb) = 2×10^{-4}. Taking into account the production rate of ^{74}Rb this gives for the production rate of ^{73}Rb an upper limit of 0.08 at/μC. This value is ten times lower than in the previous study of ref. [Aur77].

Non-observation of the ground-state proton decay gives an additional limit for the production rate. A search for the proton decay was limited to proton energies above 300 keV due to the energy loss continuum of β particles in the thin ΔE detector of the proton telescope. Assuming 100 % proton branch this translates to upper limit of 8×10^{-4} protons/μC.

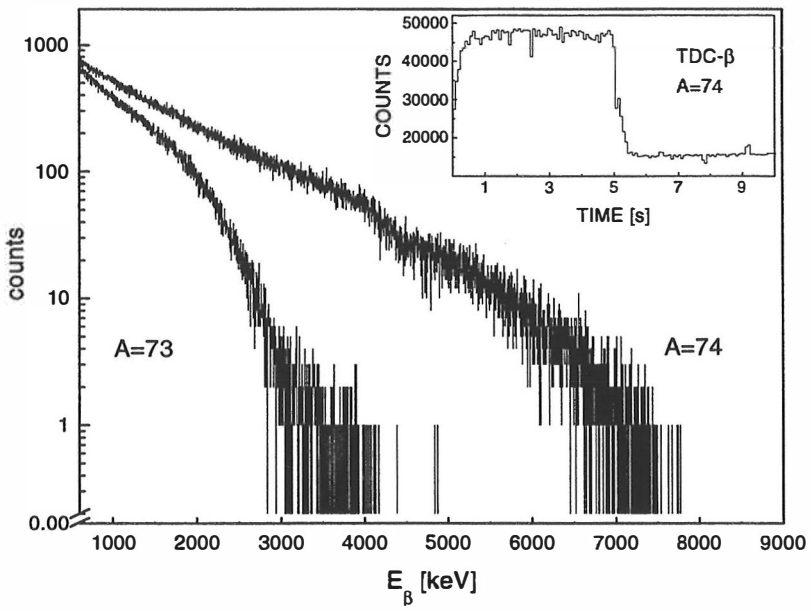

Figure 27. *Beta spectra observed at masses A = 73,74 with the planar Ge detector. Measurement times in the β spectra were 16 h for A =73 and 4.8 h for A = 74. The inset shows the β-gated time spectrum of A = 74 events with time structure described in previous chapter. The area above the flat backgound in time region 0 - 5.5 s was used for determining the production rate of ^{74}Rb.*

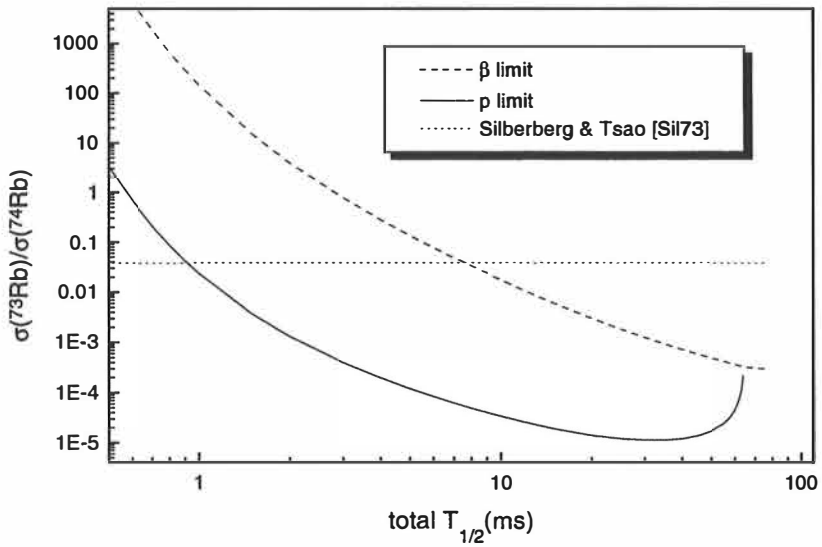

Figure 28. *Measured upper limits of the cross-section ratio of ^{73}Rb to ^{74}Rb as a function of assumed total half-life of ^{73}Rb.*

Discussion

The ground-state proton decay of ^{73}Rb would decrease the total half-life and thus increase decay losses when extracting the ions out from the target due to release behaviour. This has been taken into account in Fig. 28, in which the upper limit of the cross-section ratio $\sigma(^{73}\text{Rb})/\sigma(^{74}\text{Rb})$ deduced from the experiment is given as a function of a total half-life of ^{73}Rb both for the beta and proton measurements. In this analysis the partial beta-decay half-life of ^{73}Rb was assumed to be the same as the half-life of ^{74}Rb. The dotted line is the calculated cross-section ratio based on the semiempirical formula of Silberberg and Tsao [Sil73].

The beta-detection sensitivity is not sufficient to establish the unbound character of ^{73}Rb based on cross-section ratio for $T_{1/2} < 8$ ms due to decay losses. The proton-detection limit is sensitive down to $T_{1/2} \sim 0.9$ ms where the decay would be totally dominated by the proton decay with $E_p \sim 300$ keV [Hof89]. An estimated half-life of about 100 ns based on fragmentation studies corresponds to a proton energy of about 500 keV assuming that proton decay is associated with an $L = 1$ transition ($3/2^- \rightarrow 0^+$) and about to 650 keV for an $L = 3$ transition ($5/2^- \rightarrow 0^+$). In principle, the measurement of the lifetime of the ground state of ^{73}Rb is possible via β decay of ^{73}Sr.

4.5. Beta decay of Z = N nucleus ^{74}Rb

The ground state of ^{74}Rb with $(J^\pi, T) = (0^+, 1)$ decays by a pure Fermi transition to the ground state of ^{74}Kr. Thus, it provides a test for the CVC hypothesis [Orm95]. However, this requires an accurate knowledge of the beta-decay energy and half-life. As an odd-odd nucleus with N = Z, this nucleus is expected to be characterized by two low-lying levels: one with $(J^\pi, T) = (0^+, 1)$ i.e. the ground state and the other with $(J, T) = (\text{odd}, 0)$. Isomeric character of the latter state is possible if large differences in initial and final state wave functions hinder γ transitions. Also, decay by relatively slow β emission might become possible.

In connection with the search for ^{73}Rb at ISOLDE we also looked for a possible β-decaying $T = 0$ isomer in ^{74}Rb. An earlier study based only on beta detection by D'Auria et al. [Aur77]

provided an upper limit of 1% for the production cross section of a $T = 0$ isomer in respect to the production cross section of the ground state. All beta decays of J = odd state in ^{74}Rb would finally lead to population of the 455 keV 2^+ state in the daughter nucleus ^{74}Kr. Also, beta decay of such state would be much slower than the ground-state Fermi decay. Therefore a run was made using 5 s ON/6 s OFF beam cycles. The proton pulses were produced randomly during the 5 s BEAM ON period within a 14.4 s supercycle. The individual beam-on period, i.e. the beam gate, after a particular proton pulse was 300 ms. This kind of time structure allowed half-life measurements for both the ground and possible isomeric state. Decay of the positrons emitted by the isomeric state could be detected during the 6 s BEAM OFF period. The half-life for the ground-state decay was measured using the plastic β counter in singles mode to achieve high statistics. This measurement was performed separately with the SAM acquisition system and with a different timing sequence so that the time spectrum was reset after every proton pulse. A single exponential fit assuming a constant background at mass A = 74 resulted in a value of $T_{1/2}$ = 64.1(8) ms in excellent agreement with the previously published value of 64.9(5) ms [Aur77].

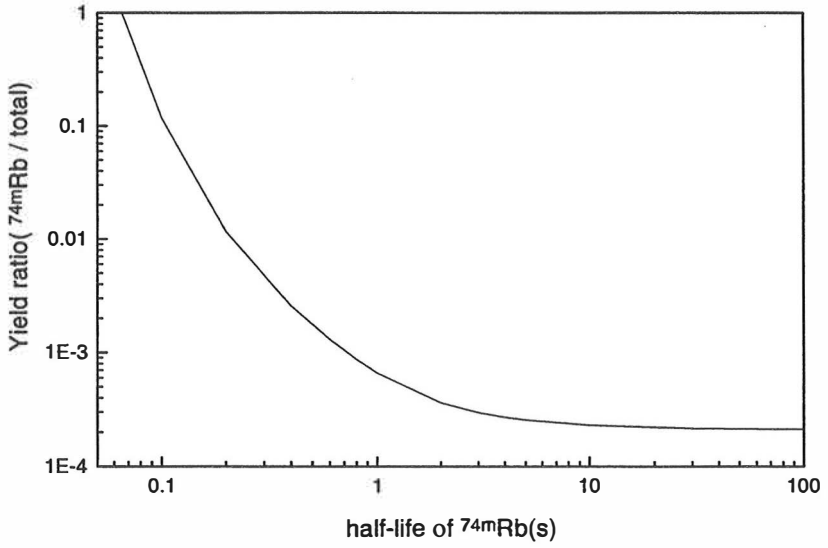

Figure 29. *The experimental upper limit for the yield ratio of ^{74m}Rb with T = 0 to total beta decays of ^{74}Rb as a function of beta-decay half-life of the isomer. Dependence of decay losses on assumed half-life have been taken into account.*

The search for a 455 keV γ ray in coincidence with high-energy positrons above 1.5 MeV as an indication of beta-decaying isomer proved unsuccessful. Comparing the time distributions of positrons with energies above 5.5 MeV in BEAM ON and BEAM OFF periods it was possible to obtain an upper limit for production of beta-decaying isomeric state. Only one event was observed 460 ms after the end of the BEAM ON period compared to total events of N_{tot} = 7038 during the whole collection period. Fig. 29. shows the upper limit of the portion of the isomeric beta decay from the total production rate of high-energy betas (^{74g}Rb) as a function of beta-decay half-life of the isomeric state.

Discussion

The production rate of the isomeric state is only 0.1 % of the total intensity of ^{74}Rb above $T_{1/2}(^{74m}\text{Rb})$ ~ 0.7 s. In the vicinity of $T_{1/2}(^{74g}\text{Rb})$ = 64.9 ms, the comparison of the intensities based only on the beta detection is meaningless due to non-separable beta-decay components of the isomeric and the ground state as well as to a competition of the gamma and beta emission from the isomeric state. Decay of the possible isomeric state has also been recently looked for by using delayed particle-γ-γ coincidences [Rud96]. No isomeric γ rays with energies greater than 50 keV were found. These results indicate that the T = 1 interaction is the dominant part of the n-p interaction in the case of ^{74}Rb.

Nine best-known Fermi beta decays for testing the CVC hypothesis have accuracies better than 0.2 % in their *ft* values [Tow95]. In the case of ^{74}Rb, this would require an order of 0.1 ms and 1 keV in accuracy in $T_{1/2}$ and Q_{EC}, respectively. Even a moderate improvement in the value of beta-decay half-life would need high counting statistics with a high detection efficiency and long collection time. With conventional spectroscopic methods, as beta-decay endpoint-energy measurements, the 1 keV accuracy in Q_{EC} value is impossible to reach and will remain as a future challenge for mass measurements based on other techniques.

4.6. Survey experiment for A = 80-88

Due to the refractory character of elements from Y to Pd progress in experimental decay studies of short-lived isotopes with A > 80 has been very slow during the past 15 years. From the astrophysical point of view, this region has become recently more interesting because the *2p*-capture reaction has been shown to provide a potential bridge for the *rp* process to continue beyond A = 70 [Sch98]. Given suitable conditions, the reaction flow could continue up to A = 100 and would follow closely the N = Z line. In this region, nucleons start to fill the $1g_{9/2}$ orbital and strong deformation will break the *(2j + 1)* degeneracy allowing several positive parity states to be formed in addition to negative parity states originating from the *fp* shell. Depending on their energy and available final states for decay, the states may be isomeric. Indeed, several gamma- and beta-decaying isomers have been found, especially in Y, Zr, Nb and Mo isotopes, closer to the valley of stability.

Production rates of nuclides made in this test experiment using the Heavy-ion version of the IGISOL facility (HIGISOL) indicate that spectroscopic studies near N = Z line are possible in the mass region A > 80. After the improvements suggested in Chapter 3 have been carried out, the estimated increase of the production rates will make studies of nuclei near N = Z line possible with very high selectivity. In the following the results of HIGISOL runs with long collection times at masses A = 82 and 85 are discussed.

4.6.1. Improved results for ^{82}Y

The high production rate of ^{82}Y made it possible to resolve the question of differences in results of two previous beta-decay experiments [Lis81, Del82]. Lister et al. [Lis81] used reactions ^{60}Ni(^{24}*Mg,pn*)^{82}Y and ^{60}Ni(^{28}*Si,αpn*)^{82}Y with beam energies of 90 and 110 MeV, respectively, whereas a reaction ^{54}Fe(^{32}*S,3pn*)^{82}Y with a beam energy of 123 MeV was used in the work of Della Negra et al. [Del82]. In both experiments the He-jet technique was used and the half-life, Q_{EC} value and relative gamma intensities were measured. The half-life of ^{82}Y was measured to be 9.5(0.4) s in ref. [Lis81] and 9.5(0.5) s in ref. [Del82]. However, relative intensities measured for the 602 keV γ transition were in serious disagreement in these works.

Beta-delayed gamma spectroscopy

A β-gated gamma spectrum measured at A = 82 is shown in Fig. 30. Previously observed γ transitions at energies 573, 602, 737 and 1176 keV following the β decay of ^{82}Y were clearly seen. In addition, beta feeding to the 2^+ state at 1865 keV in ^{82}Sr was observed for the first time. The state decays by γ emission with energies of 689, 1291 and 1865 keV. The transition with the energy of 1291 keV was found to decay with a half-life of 11^{+14}_{-4} s, which corresponds to ^{82}Y decay. A gamma peak at 1311 keV was also seen but it can be completely explained to be caused by summing of 573 and 737 keV peaks. Emission of a γ ray with this energy would be inconsistent with the $J^\pi = 0^+$ assignment for the 1311 keV state based on *(p,t)*-reaction studies [Bal73].

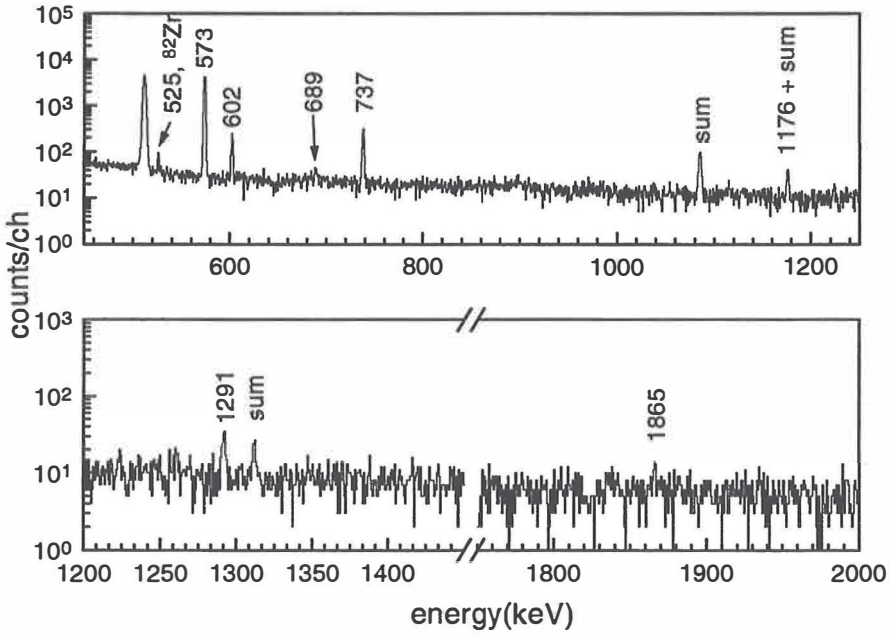

Figure 30. *Beta-gated gamma-ray spectrum measured for A = 82. Total collection time was 11 h including 7.1 h collection with 60 s ON / 60 s OFF as well as 3.9 h collection with 60 s ON beam cycles. All peaks except the one at 525 keV are due to the decay of ^{82}Y.*

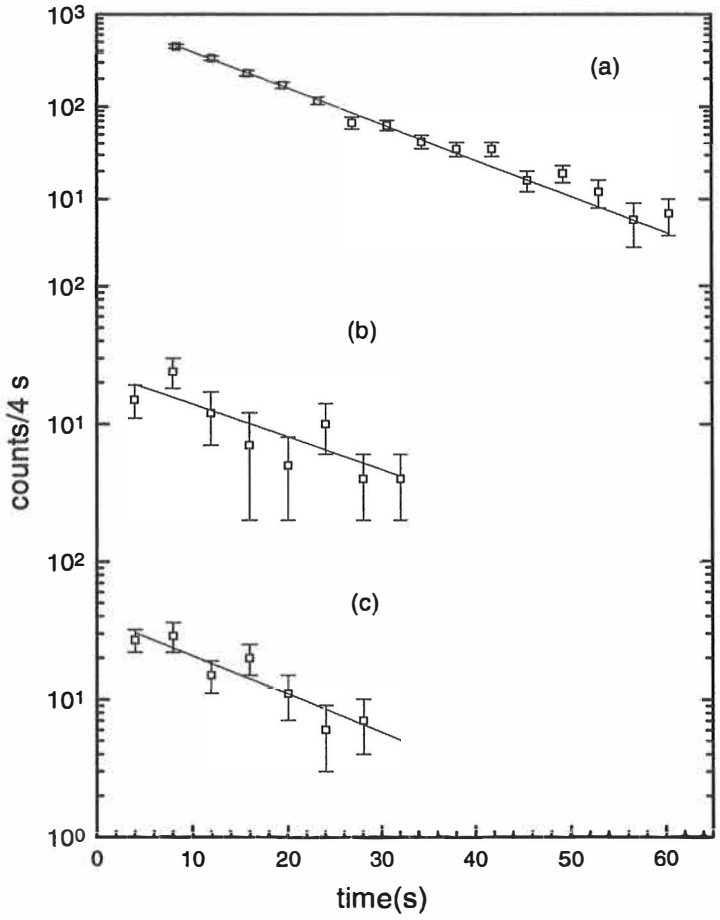

Figure 31. *Decay curves for (a) 573 keV, (b) 602 keV and (c) 737 keV beta-gated gamma transitions at A = 82.*

The decay curves for the β-gated 573, 602 and 737 keV γ transitions are displayed in Fig. 31. Fitting of a single exponential to decay of the 573 keV peak resulted in $T_{1/2}$ = 8.30(20) s which is in disagreement with the earlier values. Low statistics in the cases of 602 keV and 737 keV transitions increases the fitting error limits. However, the obtained values of 13(5) and 11(3) s for the 602 and 737 keV γ rays, respectively, are consistent with the value for the most intense transition of 573 keV. Since the γ-ray spectrum is almost exclusively dominated by ^{82}Y, it is

reasonable to use a single-component fit for determining the half-life associated with the 511 keV annihilation peak and with beta decay observed by a thin scintillator. Thus, only a constant background was assumed in these cases. The resulting half-life values 7.64(33) s and 7.75(7) s, respectively, are lower than the value based on the 573 keV γ transition. However, these results support the existence of a shorter-lived component in A = 82 compared to the previous experiments. Since the decay of ^{82}Zr might distort the half-life analysis when using only positrons as well as 511 keV annihilation quanta, the value of 8.30(20) s is adopted.

Relative intensities and fitted half-lives for the observed γ rays are given in Table 10. Previously published values for the intensities are shown for comparison. Discrepancy in results from the different experiments is most evident in the intensity of the 602 keV transition.

Table 10. *Compilation of γ transitions following beta decay of ^{82}Y. In addition, γ rays with energies of 127, 247, 398 and 525 keV were observed, but their intensities did not allow any $T_{1/2}$ determination. These γ rays have been previously assigned to decay of ^{82}Zr [Lia82].*
a) deduced from the growth-in to decay ratio.

E(keV)	Relative intensity			$T_{1/2}$(s)
	[Lis81]	[Del82]	this work	this work
β's				7.75(7)
511				7.64(33)
573.4(3)	100	100	100(7)	8.30(20)
601.9(3)	41	13(1)	4.4(4)	13(5)
688.9(4)			0.5(3)	
737.3(3)	9	9(1)	8.5(7)	11(3)
1175.9(6)	4	~2	0.9(3)	7^{+24}_{-3} a)
1291.0(6)			1.6(3)	11^{+14}_{-4} a)
1865.3(15)			0.5(3)	

Ground-state feeding for ^{82}Y was estimated to be about 75 % in ref. [Del82]. The value was based on a number of recoils counted using the time-of-flight method. Assuming the same

ratio of the 573 keV peak intensity to the total number of ions as in ref. [Del82], the ground-state feeding is estimated to be 75(25) %.

Discussion

The intensity ratio of the γ rays de-exciting the 1176 keV state is $I(602)/I(1176) = 4.9(17)$. A recent in-beam experiment resulted in a consistent ratio of 4.2(9) [Tab94]. However, the latest compilation has adopted a totally different value of 9.6(10) [Kin95] which more or less equals that given in the oldest β-decay work of Lister et al. [Lis81]. In the work of Lister et al., the gamma intensities were determined using reactions ^{60}Ni(^{24}*Mg,pn*)^{82}Y and ^{60}Ni(^{28}*Si,αpn*)^{82}Y. In addition, the relative intensities of the 573 keV and 602 keV transitions given in [Lis81] are also in disagreement with the present study. The He-jet system used could not separate neighboring masses and thus, in the case of the latter reaction, the decay of a *3pn*-channel product ^{84m}Y could increase the measured gamma intensity for 602 keV. In their work, the half-life was determined using the 573 keV transition, which should give a value consistent with ours. However, the results do not agree. The half-life based on time-of-flight mass spectrometry of the recoils [Del82] could include contributions from neighboring masses, which exclusively have longer half-lives and thus should give an apparently longer half-life for ^{82}Y. In contrast to previous investigations the mass resolving power in the present work was good enough to separate neighboring masses. In fact, no neighboring mass contaminations were observed in the production rate tests in the studied mass region between A = 80 and 88.

The existence of isomeric states in nuclei close to the N = Z = 40 shell closure is common. The systematics of known odd-odd yttrium isotopes suggests the existence of an isomeric state in ^{82}Y as most of the isotopes between ^{84}Y and ^{100}Y have been observed to be characterized by isomeric states. In addition, other odd-odd $M_T = 2$ nuclei from ^{74}Br to ^{94}Rh exhibit isomerism. However, no clear evidence for an isomer in ^{82}Y with a significantly different half-life from that of ^{82g}Y was found.

The decay scheme for ^{82}Y is shown in Fig. 32. All the known final states for the allowed Gamow-Teller beta decay are populated below 2 MeV. The 2^+ state at 2195 keV observed in *(p,t)*-reaction study [Bal73] was not seen in the present work.

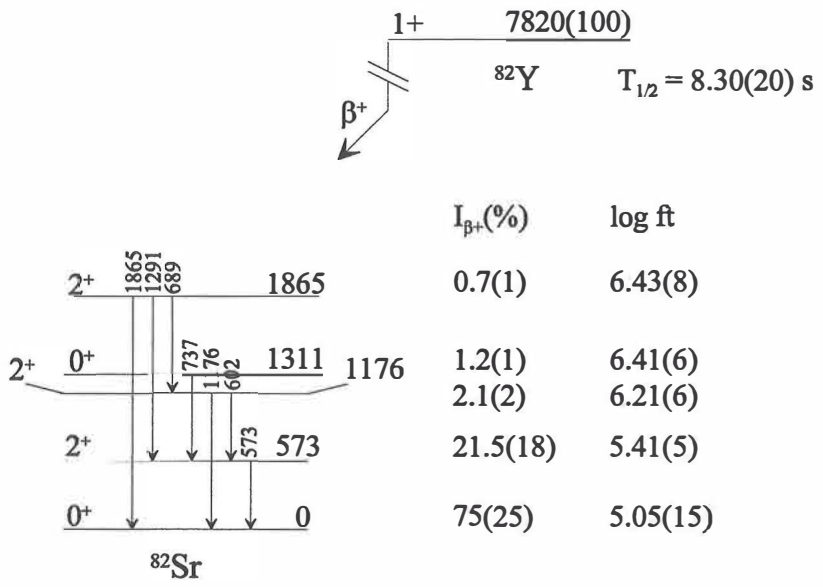

Figure 32. *Updated decay scheme for ^{82}Y.*

Gamma-ray peaks previously assigned to the decay of ^{82}Zr were also observed, but insufficient statistics prevented any half-life analysis. Also, the knowledge of low-lying final states in ^{82}Y is too poor for any assignments. The production of ^{82}Zr shows, however, the power of the HIGISOL method for producing neutron-deficient Zr isotopes even with modest stopping efficiency.

4.6.2. Observation of new transitions in A = 85

Production of neutron-deficient A = 85 nuclides was studied in a 7 h long experiment. A special emphasis on this test was put on studying the production of recently observed ^{85}Mo. The study of Huang et al. [Hua97], based on beta-delayed proton decay, reported recently a half-life of 3.2(2) s for ^{85}Mo. No beta-delayed gamma rays related to ^{85}Mo were observed in this study. A gamma-ray spectrum recorded in this is shown in Fig. 33. In addition to the well-

known γ transitions following beta decays of ^{85}Nb and ^{85,85m}Zr, several earlier unidentified peaks were observed. Of these transitions, the ones with the energies of 484 and 759 keV are intense enough for a half-life determination.

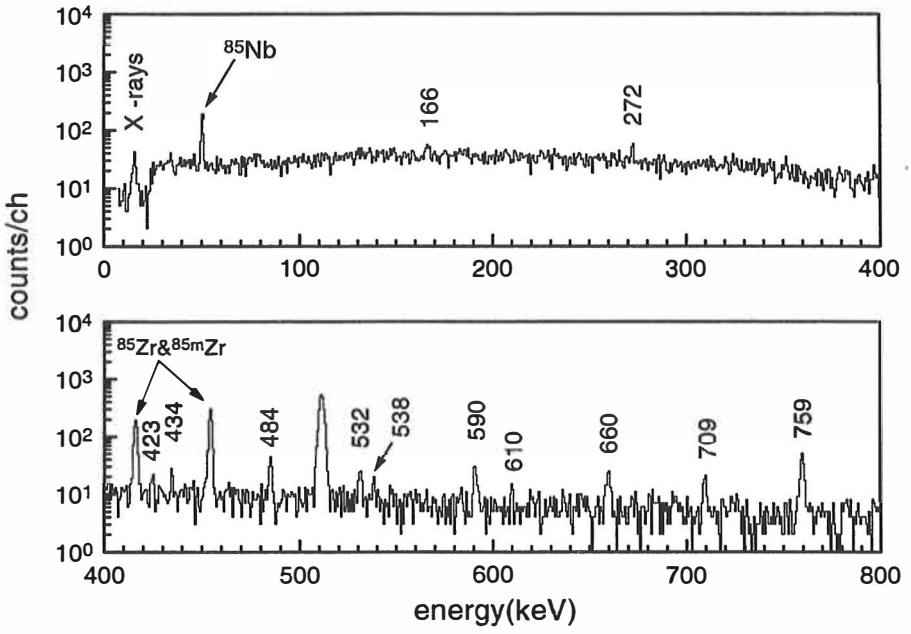

Figure 33. *Beta-gated gamma ray spectrum for A = 85. The previously unknown γ transitions are labelled by their energies. Total measurement time was 7.4 h, consisting of 2.8 h with 60 s collection period and 4.6 h with a 30 s ON followed by a 30 s OFF period.*

Single-component fits including the 60 s growth-in and the 30 s decay periods of the 759 keV γ peak resulted in a weighted average of 12(5) s for the half-life. Similar half-life of 10.9(3) s has been observed for ^{85m}Zr, but no γ transition of this energy was reported [Buc92]. In that work Zr activity was obtained in spallation reactions produced by a 280 MeV ^{3}He beam on a ^{nat}Mo target. A clean Zr source was produced as ZrF_3^+ ions using on-line mass separation. From the gamma transitions observed in the work of Bucurescu et al. [Buc92], only the two strongest ones with energies of 416 and 454 keV were observed in the present work. The 759 keV transition cannot be associated with the decay of ^{85}Mo or ^{85}Nb due to their different half-lives of 3.2(2) s and 20.9(7) s, respectively. The beta decay of ^{85}Nb has been previously

studied by using the ^{58}Ni($^{32}S,\alpha p$)^{85}Nb reaction at a bombarding energy of 105 MeV [Kur88]. Only one beta-delayed gamma transition with an energy of 50 keV was observed in that work. This transition was seen also in the present work.

A possible origin for the 759 keV γ transition is a β-decaying isomer in ^{85}Nb or in ^{85}Mo. Existence of an isomer in ^{85}Nb is supported by the systematics of odd-A Nb isotopes between ^{87}Nb and ^{99}Nb all of which have been observed to have low-lying 1/2$^-$ isomeric states. This state can be explained by an extreme single-particle shell model to be due to an odd proton in the $2p_{1/2}$ orbital, while the 9/2$^+$ ground state originates from an odd proton in the $1g_{9/2}$ orbital. Additional support for the isomeric state is given by the systematics of odd-A N = 44 isotones from ^{79}Br to ^{83}Y. In these nuclei the ground-state spin and parity are determined by competition between long-lived 9/2$^+$ and 3/2$^-$ states. Similar arguments are valid in the case of ^{85}Mo. An estimate for the ratio of the production rates for ^{85}Mo and ^{85}Nb can be calculated using the computer code ALICE. This indicates the production cross section of ^{85}Mo to be 15 times larger compared to ^{85}Nb for the reaction and bombarding energy used. Remembering the observed high production rate of $J^\pi = 5^-$ isomer ^{84m}Y, similar enhanced production of the isomeric state could be possible also for A = 85 leading to a high production rate for ^{85m}Mo. Only available in-beam study of a daughter nucleus ^{85}Nb has resulted in observation of a ΔJ = 2 band built on the (9/2$^+$) ground state [Gro91]. These transitions could not be observed in the present work.

In the case of the 484 keV transition, the ratio of intensities during the growth-in and decay periods leads to a value of $T_{1/2} = 4^{+8}_{-2}$ s. This value is consistent with the reported half-life of ^{85}Mo. However, due to large error limits this transition can be connected with the beta decay of ^{85m}Nb or ^{85m}Mo as well. The origin of other observed and unknown γ rays cannot be determined due to insufficient statistics and limited knowledge of the level structures of ^{85}Nb and ^{85}Zr. However, these peaks are most likely associated with beta decays of ^{85}Mo, ^{85m}Mo or ^{85m}Nb since β-delayed γ transitions in other nuclei in this mass chain are well known.

5. Summary and outlook

Neutron deficient nuclei in the *fp* shell have been studied in this work using beta-delayed proton and gamma-ray spectroscopy. Experiments have been performed using the ISOLDE mass-separator facility at CERN as well as the On-Line Mass Separator at GSI. In addition, a test experiment has been performed at the IGISOL mass separator at JYFL to gain experience on the possibilities for spectroscopic studies in the vicinity of the Z = N = 40 sub-shell closure and beyond with heavy-ion reactions. These studies provide new information on the basic beta-decay properties of the nuclei involved and enlarge the experimental database for the modelling of the astrophysical *rp*-process path.

Beta decays of $M_T = -1$ nuclei ^{58}Zn and ^{70}Kr were observed for the first time in this work. The decay of ^{58}Zn offers a unique possibility to compare Gamow-Teller transition strengths obtained in the beta-decay measurements and charge-exchange reactions. The Gamow-Teller strength determined from the β decay of ^{58}Zn was found to be in good agreement with the results from both *(p,n)*- and *(^{3}He,t)*-reaction studies. Slow Gamow-Teller beta decay was observed to populate the $J^\pi = 1^+$ ground state in ^{58}Cu compared to the fast transitions found in the analoguous nuclei ^{18}Ne and ^{42}Ti. In the framework of the single-particle shell model, hindrance in the beta decay indicates a mixture of the $1f_{5/2}$ orbital in the ground-state wave function of ^{58}Cu. The beta-decay half-life has been measured for ^{70}Kr to be 60(40) ms. This differs significantly from the value of 390 ms used in the *rp*-process path calculations and stresses the importance of experimental data in modelling the astrophysical processes. The reaction flow due to the short half-life of ^{70}Kr is drastically enhanced compared to the model calculations.

Beta-delayed γ spectroscopy has been employed for the first time in studies of the mirror beta decays of ^{61}Ga and ^{71}Kr. The results help in extending the systematics of the Gamow-Teller ground-state matrix elements towards the end of the *fp* shell. The obtained GT matrix elements in the upper *fp* shell are consistent with the trend observed above Z = 28. Decreasing trend towards the end of the *fp* shell is expected due to increase of collectivity as the number of valence nucleons increases. Both nuclei possess a large ground-state feeding typical of mirror decays in which both Fermi and Gamow-Teller operators contribute. The half-life of

^{71}Kr has been measured to be 100(3) ms. This result clarifies the discrepancy observed recently [Bla95b]. A significant beta-delayed proton branch has been observed in ^{71}Kr confirming the discovery using fragmentation as a production method.

The proton drip line has been crossed for Rb isotopes. Non-observation of ^{73}Rb in beta-decay studies is consistent with the results obtained in fragmentation studies. The search for the (J, T) = (odd, 0) isomeric state in ^{74}Rb was unsuccessful as was the case also in the in-beam experiments [Rud96]. The use of ^{74}Rb for testing the CVC hypothesis would require very accurate mass measurements for ^{74}Kr and ^{74}Rb beyond reach with conventional spectroscopic methods.

Production of refractory elements in the region A = 80-88 close the proton drip line has been proven possible with the new HIGISOL technique. This combination of heavy-ion fusion-evaporation reactions and the ion-guide technique is a powerful tool to extend the spectroscopic studies along the proton drip line towards ^{100}Sn. Using the reaction ^{32}S + ^{nat}Ni with a bombarding energy of 165 MeV it was possible to produce all short-lived M_T = +1 isotopes with A = 80-86. In addition, a high production rate for ^{82}Y allowed an improved spectroscopic studies of this nuclide. Existence of an isomeric state in ^{82}Y could not be ruled out. A survey for A = 85 showed a large number of previously unknown γ transitions following β decays of ^{85,85m}Mo or/and ^{85m}Nb. The prospects of continuing the studies near sub-shell closure of Z = N = 40 look extremely promising.

Recent developments in both experimental and theoretical side of the field are increasingly touching the region studied in this work. Full shell-model calculations will still be limited to lower masses for years, but other approaches indicate interesting features to be present. The position of the Gamow-Teller giant resonance in N ~ Z nuclei has been predicted to depend on the shape of the nucleus using Hartree-Fock calculations in a deformed potential [Ham97]. This would show up as an enhancement in beta-delayed proton emission from these states for certain deformation and thus would serve as a sign for the oblate or prolate shape of the nucleus. Possible tests for this prediction would be measurements of absolute β-delayed proton branches in the vicinity of N = Z = 40, especially in ^{80,81}Zr. Experimental developments concerning radioactive ion-beam (RIB) facilities will certainly push the level of

knowledge still higher in the near future. Although, even with the RIB facilities, one has to struggle with low production rates due to low beam intensities in spite of the higher production cross sections. So, development and upgrading of the present facilities should not be forgotten. This work shows the capabilities of the present generation facilities as well as introduces one new method for reaching radioactive refractory isotopes near the $N = Z = 40$ sub-shell closure.

References

[Aki94] H.Akimune, I.Daito, Y.Fujita, M.Fujiwara, M.B.Greenfield, M.N.Harakeh, T.Inomata, J.Jänecke, K.Katori, S.Nakayama, H.Sakai, Y.Sakemi, M.Tanaka, and M.Yosoi, Nucl. Phys. A **569**(1994)245c.

[And96] B.D.Anderson, A.R.Baldwin, P.Baumann, B.A.Brown, F.Didierjean, C.C.Foster, L.A.C.Garcia, A.Huck, A.Knipper, R.Madey, D.M.Manley, G.Marguier, M.Ramdhane, H.Ravn, C.Richard-Serre, G.Walter and J.W.Watson, Phys. Rev. C **54**(1996)602.

[Ant84] M.S.Antony and A.Pape, Phys. Rev. C **30**(1984)1286.

[Ant97] M.S.Antony, A.Pape and J.Britz, At. Data Nucl. Data Tables **66**(1997)1.

[Arr90] J.W.Arrison, T.Chapuran, U.J.Hüttmeier and D.P.Balamuth, Phys. Lett. B **248**(1990)39.

[Aud95] G.Audi, A.H.Wapstra, Nucl. Phys. A **595**(1995)409.

[Aue83] N.Auerbach, Phys. Rep. **98** no. **5**(1983)1.

[Aur77] J.M.D'Auria, L.C.Carraz, P.G.Hansen, B.Jonson, S.Mattsson, H.L.Ravn, M.Skarestad and L.Westgaard and The ISOLDE Collaboration, Phys. Lett. B **66**(1977)233.

[Bal73] J.B.Ball, J.J.Pinajian, J.S.Larsen and A.C.Rester, Phys. Rev. C **8**(1973)1438.

[Bau94] P. Baumann, M. Bounajma, A. Huck, G. Klotz, A. Knipper, G. Walter, G. Marguier, C. Richard-Serre, H. Ravn, E. Hagebö, P. Hoff and K. Steffensen, Phys. Rev. C **50**(1994)1180.

[Ben85] T.Bengtsson and I.Ragnarsson, Nucl. Phys. A **436**(1985)14.

[Ber87] G.F.Bertsch and H.Esbensen, Rep. Prog. Phys. vol. **50**, no. **6**(1987)607.

[Ber94] R. Beraud, A.Emsallem, A.Astier, R.Bouvier, R.Douffait, Y.Le Coz, S.Morier, A.Wojtasiewicz, Yu.A.Lazarev, I.V.Shirokovsky, I.N.Izosimov, D.Barneoud, J.Genevey, A.Gizon, R.Guglielmini, G.Margotton, J.L.Vieux-Rochaz, Nucl. Instr. and Meth. in Phys. Res. A **346**(1994)196.

[Bha93] M.R.Bhat, Nucl. Data Sheets **68**(1993)117.

[Bjø87] T.Bjørnstad, E.Hagebo, P.Hoff, O.C.Jonsson, E.Kugler, H.L.Ravn, S.Sundell, B.Vosicki and the ISOLDE Collaboration, Nucl. Instr. and Meth. in Phys. Res. B **26**(1987)174.

[Bla76] M.Blann, University of Rochester, USERDA Report COO-3494-29, unpublished (1976).

[Bla95a] B.Blank, S.Andriamonje, S.Czajkowski, F.Davi, R.Del Moral, J.P.Dufour, A.Fleury, A.Musquere, M.S.Pravikoff, R.Grzywacz, Z.Janas, M.Pfützner, A.Grewe, A.Heinz, A.Junghans, M.Lewitowicz, J.-E.Sauvestre and C.Donzaud, Phys. Rev. Lett. **74**(1995)4611.

[Bla95b] B.Blank, S.Andriamonje, S.Czajkowski, F.Davi, R.Del Moral, C.Donzaud, J.P.Dufour, A.Fleury, A.Grewe, R.Grzywacz, A.Heinz, Z.Janas, A.Junghans, M.Lewitowicz, A.Musquere, M.S.Pravikoff, , M.Pfützner and J.-E.Sauvestre Phys. Lett. B **364**(1995)8.

[Boh69] A.Bohr and B.Mottelson, Nuclear Structure vol.1, W.A.Benjamin, New York (1969).

[Bre90] D.S.Brenner, C.Wesselborg, R.F.Casten, D.D.Warner and J.-Y.Zhang, Phys. Lett. B **243**(1990)1.

[Bro88] B.A.Brown and B.H.Wildenthal, Ann. Rev. Nucl. Part. Sci. **38**(1988)29.

[Bru77] P.J.Brussaard and P.W.M.Glaudemans, Shell-Model Applications in Nuclear Spectroscopy, North-Holland, Amsterdam (1977).

[Buc92] D.Bucurescu, M.S.Rapaport, C.F.Liang, P.Paris and G.Cata-Danil, Z. Phys. A **342**(1992)403.

[Bur85] T.W.Burrows, J.W.Olness and D.E.Alburger, Phys. Rev. C **31**(1985)1490.

[Bur97] K.Burkard, R.Collatz, M.Hellström, Z.Hu, W.Hüller, O.Klepper, R.Kirchner, E.Roeckl, K.Schmidt, M.Shibata and A.Weber, Nucl. Instr. and Meth. in Phys. Res. B **126**(1997)12.

[Cas85] R.F.Casten, Nucl. Phys. A **443**(1985)1.

[Cau94] E.Caurier, A.P.Zuker, A.Poves and G.Martinez-Pinedo, Phys.Rev. C **50**(1994)225.

[Cha92] A.E.Champagne and M.Wiescher, Ann. Rev. Nucl. Part. Sci. **42**(1992)39.

[Chu92] Z.Chunmei, Nucl. Data Sheets **67**(1992)271.

[Com83] E.Comay and J.Jänecke, Nucl.Phys. A **410**(1983)103.

[Del82] S.Della Negra, H.Gauvin, D.Jacquet and Y.Le Beyec, Z.Phys. A **307**(1982)305.

[Den98] P.Dendooven, R.Beraud, E.Chabanat, A.Emsallem, A.Honkanen, M.Huhta, J.C.Wang, A.Jokinen, G.Lhersonneau, M.Oinonen, H.Penttilä, K.Peräjärvi and J.Äystö, accepted for publication in Nucl. Instr. and Meth. in Phys. Res. (1998).

[Des87] P.Dessagne and C.Miehé, CRN Report No. CRN PN 87-08(1987).

[Des88] Ph.Dessagne, Ch.Miehe, P.Baumann, A.Huck, G.Klotz, M.Ramdhane, G.Walter and J.M.Maison, Phys. Rev. C **37**(1988)2687.

[Did94] F.Didierjean and G.Walter, CRN Report No. CRN PN 94-01(1994).

[Ehr51] J.B.Ehrman, Phys.Rev. **81**(1951)412.

[Ewa81] G.T.Ewan, E.Hagberg, P.G.Hansen, B.Jonson, S.Mattsson, H.L.Ravn and P.Tidemand-Petersson, Nucl. Phys. A **352**(1981)13.

[Fir96] R.B.Firestone, S.Y.F.Chu, V.S.Shirley, C.M.Baglin and J.Zipkin, Table of Isotopes, 8th Edition, John Wiley & Sons, New York (1996).

[Fri95] F.Frisk, I.Hamamoto and X.Z.Zhang, Phys. Rev. C **52**(1995)2468.

[Fuj96] Y.Fujita, H.Akimune, I.Daito, M.Fujiwara, M.N.Harakeh, T.Inomata, J.Jänecke, K.Katori, H.Nakada, S.Nakayama, A.Tamii, M.Tanaka, H.Toyokawa and M.Yosoi, Phys. Lett. B **365**(1996)29.

[Fuj97] Y.Fujita, private communication, (1997).

[Gaa80] C.Gaarde, J.S.Larsen, M.N.Harakeh, S.Y.Van Der Werf, M.Igarashi, A.Müller-Arnke, Nucl. Phys. A **334**(1980)248.

[Gar66] G.T.Garvey and I.Kelson, Phys.Rev.Lett. **16**(1966)197.

[Gar91] A.Garcia, E.G.Adelberger, P.V.Magnus, H.E.Swanson, O.Tengblad, D.M.Moltz and the ISOLDE Collaboration, Phys. Rev. Lett. **67**(1991)3654.

[Gar95] A.Garcia, E.G.Adelberger, P.V.Magnus, H.E.Swanson, D.P.Wells, F.E.Wietfeldt, O.Tengblad and the ISOLDE Collaboration, Nucl. Phys. A **51**(1995)R439.

[Goo80] C.D.Goodman, C.A.Goulding, M.B.Greenfeld, J.Rapaport, D.E.Bainum, C.C.Foster, W.G.Love and F.Petrovich, Phys. Rev. Lett. **44**(1980)1755.

[Gri92] A.G.Griffiths, C.J.Ashworth, J.Rikovska, N.J.Stone, J.P.White, I.S.Grant, P.M.Walker, W.B.Walters, Phys. Rev. C **46**(1992)2228.

[Gro91] C.J.Gross, K.P.Lieb, D.Rudolph, M.A.Bentley, W.Gelletly, H.G.Price, J.Simpson, D.J.Blumenthal, P.J.Ennis, C.J.Lister, Ch.Winter, J.L.Durell, B.J.Varley, Ö.Skeppstedt and S.Rastikerdar, Nucl. Phys. A **535**(1991)203.

[Gör95] J.Görres, M.Wiescher and F.-K.Thielemann, Phys. Rev. C **51**(1995)392.

[Hag82] E.Hagberg, J.C.Hardy, H.Schmeing, H.C.Evans, U.J.Schrewe, V.T.Koslowsky, K.S.Sharma and E.T.Clifford, Nucl. Phys. A **383**(1982)109.

[Hag92] E.Hagebo, P.Hoff, O.C.Jonsson, E.Kugler, J.P.Omtvedt, H.L.Ravn and K.Steffensen, Nucl. Instr. and Meth. in Phys. Res. B **70**(1992)165.

[Ham87] H.Hama, M.Yoshii, K.Taguchi, T.Ishimatsu, T.Shinozuka and M.Fujioka, Proceedings of the 5th International Conference on Nuclei far from Stability, Rousseau Lake, Ontario, Canada, American Institute of Physics (1987)p.650.

[Ham97] I.Hamamoto, Gamow-Teller Beta Decays in Drip-line, Proceedings of the International Symposium on New Facet of Spin Giant Resonances in Nuclei, Tokyo, Japan, November 17-20(1997).

[Har75] J.Hardy, AECL-5032(1975)p.17.

[Har84] J.C.Hardy and I.S.Towner, J. Phys.(Paris) C **4**(1984)417.

[Har84] P.E.Haustein, At. Data Nucl. Data Tables **39**(1988)185.

[Hey94a] K.L.G.Heyde, The Nuclear Shell Model, 2nd Edition, Springer-Verlag, Berlin, Heidelberg, New York (1994).

[Hey94b] K.L.G.Heyde, Basic Ideas and Concepts in Nuclear Physics, IOP Publishing Ltd, Bristol, Philadelphia (1994).

[Hir93] M.Hirsch, A.Staudt, K.Muto and H.V.Klapdor-Kleingrothaus, At. Data Nucl. Data Tables **53**(1993)165.

[Hof89] S.Hofmann, Proton Radioactivity, Contribution to Particle Emission from Nuclei, edited by M.Ivascu and D.N.Poenaru, CRC Press, Boca Raton, USA (1989).

[Hon81a] J.Honkanen, PhD Thesis, Research Report No.17, Department of Physics, University of Jyväskylä (1981).

[Hon81b] J.Honkanen, M.Kortelahti, K.Eskola and K.Vierinen, Nucl. Phys. A **366**(1981)109.

[Hon82] J.Honkanen, J.Äystö, M.Kortelahti, K.Eskola, K.Vierinen and A.Hautojärvi, Nucl. Phys. A **380**(1982)710.

[Hon87] J.Honkanen, V.Koponen, H.Hyvönen, P.Taskinen, J.Äystö and K.Ogawa, Nucl. Phys. A **471**(1987)489.

[Hon89] J.Honkanen, V.Koponen, P.Taskinen, J.Äystö, K.Eskola, S.Messelt and K.Ogava, Nucl. Phys. A **496**(1989)462.

[Hon97a] A.Honkanen, P.Dendooven, M.Huhta, G.Lhersonneau, P.O.Lipas, M.Oinonen, J.-M.Parmonen, H.Penttilä, K.Peräjärvi, T.Siiskonen and J.Äystö, Nucl. Phys.A **621**(1997)689.

[Hon97b] A.Honkanen, M.Oinonen, K.Eskola, A.Jokinen and J.Äystö, Nucl. Instr. and Meth. in Phys. Res. A **395**(1997)217.

[Hon98] A.Honkanen, PhD Thesis, Research Report No. 3/1998, Department of Physics, University of Jyväskylä (1998).

[Hor82] P.Hornshøj, J.Kolind and N.Rud, Phys. Lett. B **116**(1982)4.

[Hua97] W.X.Huang, R.C.Ma, X.J.Xu, Y.X.Xie, Z.K.Li, Y.X.Ge, Y.Y.Wang, T.M.Zhang, X.F.Sun, G.M.Jin and Y.X.Luo, Z. Phys. A **359**(1997)349.

[Huh97] M.Huhta, PhD Thesis, Research Report No.1/1997, Department of Physics, University of Jyväskylä (1997).

[Ike62] K.Ikeda, S.Fujii, J.I.Fujita, Phys. Lett. **2**(1962)169.

[ISO70] The ISOLDE Isotope Separator Facility at CERN(ed. by A.Kjellberg and G.Rudstam), CERN 70-3(1970).

[Jad97] Y.Jading, R.Catherall, V.N.Fedoseyev, A.Jokinen, O.C.Jonsson, T.Kautzsch, I.Klöckl, K.-L.Kratz, E.Kugler, J.Lettry, V.I.Mishin, H.L.Ravn, F.Scheerer, O.Tengblad, P.Van Duppen, W.B.Walters, A.Wöhr and the ISOLDE Collaboration, Nucl. Instr. and Meth. in Phys. Res. B **126**(1997)76.

[Joh92] C.W.Johnson, S.EW.Koonin, G.H.Lang and W.E.Ormand, Phys. Rev. Lett. **69**(1992)3157.

[Jok94] A.Jokinen, PhD Thesis, Research Report No.3/1994, Department of Physics, University of Jyväskylä (1994).

[Jok97] A.Jokinen, A.H.Evensen, E.Kugler, J.Lettry, H.L.Ravn, P.Van Duppen, N.Erdmann, Y.Jading, S.Köhler, K.-L.Kratz, N.Trautmann, A.Wöhr, V.N.Fedoseyev, V.I.Mishin, V.Tikhonov and the ISOLDE Collaboration, Nucl. Instr. and Meth. in Phys. Res. B **126**(1997)95.

[Jon72] H.W.Jongsma, A.G.Da Silva, J.Bron and H.Verheul, Nucl. Phys. A **179**(1972)554.

[Jän66] J.Jänecke, Phys. Rev. **147**(1966)735.

[Jän88] J.Jänecke and P.J.Masson, At. Data. Nucl. Data Tables **39**(1988)265.

[Kan95] J.Kantele, Handbook of Nuclear Spectrometry, Academic Press, London (1995).

[Kel66] I.Kelson and G.T.Garvey, Phys. Lett. **23**(1966)689.

[Kin95] M.M. King and W.-T. Chou, Nucl. Data Sheets **76**(1995)285.

[Kir76] R.Kirchner and E.Roeckl, Nucl. Instr. and Meth. **133**(1976)187.

[Kir81] R.Kirchner, Nucl. Instr. and Meth. **186**(1981)275.

[Kir86] R.Kirchner, O.Klepper, D.Marx, G.-E.Rathke and B.Sherrill, Nucl. Instr. and Meth. in Phys. Res. A **247**(1986)265.

[Kir97] R.Kirchner, private communication (1997).

[Kug92] E.Kugler, D.Fiander, B.Jonson, H.Haas, A.Przewloka, H.L.Ravn, D.J.Simon, K.Zimmer and the ISOLDE Collaboration, Nucl. Instr. and Meth. in Phys. Res. B **70**(1992)41.

[Kur88] T.Kuroyanagi, S.Mitarai, B.J.Min, H.Tomura, Y.Haruta, K.Heiguchi, S.Suematsu and Y.Onizuka, Nucl. Phys. A **484**(1988)264.

[Lan93] G.H.Lang, C.W.Johnson, S.E.Koonin and W.E. Ormand, Phys. Rev. C **48**(1993)1518.

[Lau94] H.Laurent, S.Gales, D.Beaumel, G.M.Crawley, J.E.Finck, S.Fortier, J.M.Maison, C.P.Massolo, D.J.Mercer, J.S.Winfield, G.H.Yoo, Nucl. Phys. A **569**(1994)297c.

[Let97a] J.Lettry, R.Catherall, V.Fedoseyev, G.J.Focker, G.Huber, O.C.Jonsson, E.Kugler, M.Koizumi, U.Köster, V.I.Mishin, H.Ravn, V.Sebastian, C.Tamburella and the ISOLDE collaboration, to be published in Proc. of ICIS97 (1997).

[Let97b] J.Lettry, R.Catherall, P.Drumm, P.Van Duppen, A.H.M.Evensen, G.J.Focker, A.Jokinen, O.C.Jonsson, E.Kugler, H.Ravn and the ISOLDE Collaboration, Nucl. Instr. and Meth. in Phys. Res. B **126**(1997)130.

[Lhe94] G.Lhersonneau, B.Pfeiffer, K.-L.Kratz, J.Äystö, T.Enqvist, P.P.Jauho, A.Jokinen, J.Kantele, M.Leino, J.M.Parmonen and H.Penttilä, Phys. Rev. C **49**(1994)1379.

[Lia82] C.F.Liang, P.Paris, D.Bucurescu, S.Della Negra, J.Obert and J-C.Putaux, Z. Phys. A **309**(1982)185.

[Lis81] C.J.Lister, P.E.Haustein, D.E.Alburger and J.W.Olness, Phys. Rev. C **24**(1981)260.

[Mar96] G.Martinez-Pinedo, A.Poves, E.Caurier and A.P.Zuker, Phys. Rev. C **53**(1996)R2602.

[Mar97] G.Martinez-Pinedo, A.P.Zuker, A.Poves and E.Caurier, Phys. Rev. C **55**(1997)187.

[Miy87] H.Miyatake, K.Ogawa, T.Shinozuka and M.Fujioka, Nucl. Phys. A **470**(1987)328.

[Moh91] M.F.Mohar, D.Bazin, W.Benenson, D.J.Morrissey, N.A.Orr, B.M.Sherrill, D.Swan, J.A.Winger, A.C.Mueller and D.Guillemaud-Mueller, Phys. Rev. Lett. **66**(1991)1571.

[Mor87] K.Morita, T.Inamura, T.Nomura, J.Tanaka, H.Miyatake, M.Fujioka, T.Shinozuka, M.Yoshii, H.Hama, K.Taguchi, K.Sueki, Y.Hatsukawa, K.Furuno and H.Kuto, Nucl. Instr. and Meth. in Phys. Res. B **26**(1987)406.

[Mot55] B.R.Mottelson and S.G.Nilsson, Phys. Rev. **99**(1955)1615.

[Möl81] P.Möller and J.R.Nix, Nucl.Phys. A **361**(1981)117.

[Möl95] P.Möller, J.R.Nix, W.D.Myers and W.J.Swiatecki, At. Data Nucl. Data Tables **59**(1995)185.

[Möl97] P.Möller, J.R.Nix and K.-L.Kratz, At. Data Nucl. Data Tables **66**(1997)131.

[Naz96] W.Nazarewicz, J.Dobaczewski, T.R.Werner, J.A.Maruhn, P.-G.Reinhard, K.Rutz, C.R.Chinn, A.S.Umar and M.R.Strayer, Phys.Rev. C **53**(1996)740.

[Nil55] S.G.Nilsson, Mat. Fys. Medd. Dan. Vid. Selsk. **29**(1955)no.16.

[Oin95] M.Oinonen, P.Bauman, F.Didierjean, P.Hoff, A.Huck, A.Jokinen, A.Knipper, G.Lhersonneau, M.Leino, G.Marguier, K.Mezilev, Yu.Novikov, A.Popov, C.Serre, P.Van Duppen, G.Walter and J.Äystö, JYFL Annual Report 1994, (1995) p.20.

[Orm95] W.E.Ormand and B.A.Brown, Phys. Rev. C **52**(1995)2455.

[Orm97] W.E.Ormand, Phys. Rev. C **55**(1997)2407.

[Pen92] H.Penttilä, PhD Thesis, Research Report No.1/1992, Department of Physics, University of Jyväskylä (1992).

[Rap83] J.Rapaport, T.Taddeucci, T.P.Welch, C.Gaarde, J.Larsen, D.J.Horen, E.Sugarbaker, P.Kontz, C.C.Foster, C.D.Goodman, C.A.Goulding and T.Masterson, Nucl. Phys. A **410**(1983)371.

[Ras66] J.O.Rasmussen, Alpha Decay, Alpha-, Beta- and Gamma-Ray Spectroscopy vol. I, edited by K.Siegbahn, North-Holland, Amsterdam (1966).

[Rud96] D.Rudolph, C.J.Gross, J.A.Sheikh, D.D.Warner, I.G.Bearden, R.A.Cunningham, D.Foltescu, W.Gelletly, F.Hannachi, A.Harder, T.D.Johnson, A.Jungclaus, M.K.Kabadiyski, D.Kast, K.P.Lieb, H.A.Roth, T.Shizuma, J.Simpson, Ö.Skeppstedt, B.J.Varley and M.Weiszflog, Phys. Rev. Lett. **76**(1996)376.

[Sat97] W.Satula, D.J.Dean, J.Gary, S.Mizutori and W.Nazarewicz, Phys. Lett. B **407**(1997)103.

[Sch95] K.Schreckenbach, P.Liaud, R.Kossakowski, H.Nastoll, A.Bussiere and J.P.Guillaud, Phys. Lett. B **349**(1995)427.

[Sch98] H.Schatz, A.Aprahamian, J.Görres, M.Wiescher, T.Rauscher, J.F.Rembges, F.-K.Thielemann, B.Pfeiffer, P.Möller, K.-L.Kratz, H.Herndl, B.A.Brown and H.Rebel, Phys. Rep. **294** No. **4**(1998)167.

[Set86] K.K.Seth, S.Iversen, M.Kaletka, D.Barlow, A.Saha and R.Soundranayagam, Phys. Lett. B **173**(1986)397.

[Sil73] R.Silberberg and C.H.Tsao, Astroph. J. Suppl. **25**(1973)315.

[Smi82] P.J.Smith, L.P.Ekström, F.Kearns, P.J.Twin and N.J.Ward, J.Phys. G **8**(1982)281.

[Str67] V.M.Strutinsky, Nucl.Phys. A **95**(1967)420.

[Thi84] J.M.Thirion, G.Chouraqui, T.H.Müller and M. Port, Z. Physik A **317**(1984)329.

[Tho51] R.G.Thomas, Phys.Rev. **81**(1951)148.

[Tow95] I.S.Towner, E.Hagberg, J.C.Hardy, V.T.Koslowsky and G.Savard, Proc. of the 1st International Conference on Exotic Nuclei and Atomic Masses ENAM-95, Arles, France, June 19-23(1995).

[Tri95] W.Trinder, E.G.Adelberger, Z.Janas, H.Keller, K.Krumboltz, V.Kunze, P.Magnus, F.Meissner, A.Piechaczek, M.Pfützner, E.Roeckl, K.Rykaczewski, W.-D.Schmidt-Ott and M.Weber, Phys. Lett. B **349**(1995)267.

[Van76] J.F.A. Van Hienen, W. Chung and B.H. Wildenthal, Nucl. Phys. A **269**(1976)156.

[Wal81] R.K.Wallace and S.E.Woosley, Astrophys. J. **45**(1981)389.

[Wat85] J.W.Watson, W.Pairsuwan, B.D.Anderson, A.R.Baldwin, B.S.Flanders, R.Madey, R.J.McCarthy, B.A.Brown, B.H.Wildenthal and C.C.Foster, Phys. Rev. Lett. **55**(1985)1369.

[Wil78] D.H.Wilkinson, A.Gallman and D.E.Alburger, Phys. Rev. C **18**(1978)401.

[Win93] J.A.Winger, D.P.Bazin, W.Benenson, G.M.Crawley, D.J.Morrissey, N.A.Orr, R.Pfaff, B.M.Sherrill, M.Thoennessen, S.J.Yennello and B.M.Young, Phys. Rev. C **48**(1993)3097.

[Zie85] J.F.Ziegler, J.P.Biersack and U.Littmark, TRIM-code, The Stopping and Range of Ions in Matter, Vol. 1, ed. J.F.Ziegler, Pergamon Press, New York (1985).

[Ärj85] J.Ärje, J.Äystö, H.Hyvönen, P.Taskinen, V.Koponen, J.Honkanen, A.Hautojärvi and K.Vierinen, Phys. Rev. Lett. **54**(1985)99.

[Äys84] J.Äystö, J.Ärje, V.Koponen, P.Taskinen, H.Hyvönen, A.Hautojärvi and K.Vierinen, Phys. Lett. B **138**(1984)369.

Appendices

Appendix 1.

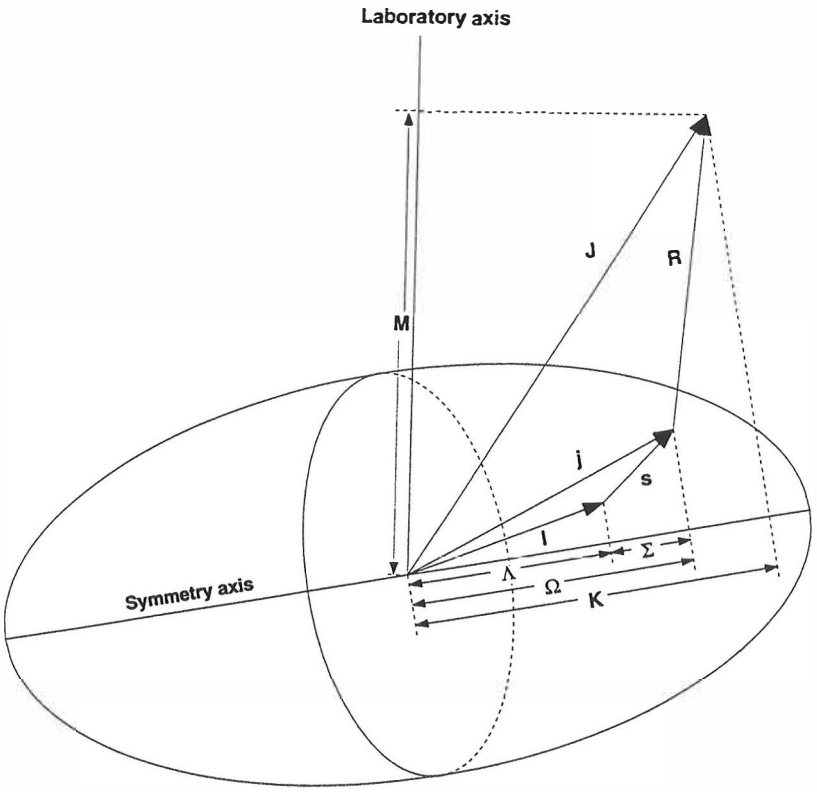

Figure A1. *Asymptotic quantum numbers for the deformed shell model [Fir96]. N is the principal oscillator number and determines the parity of the orbital as* $\pi = (-1)^N$, n_z *is the number of nodes along the symmetry axis z,* Λ *is the projection of the orbital angular momentum* $\boldsymbol{l}$ *on the symmetry axis. The whole nucleonic system must have conserved total angular momentum* $\boldsymbol{R}$ *which has a projection K on the symmetry axis. In the case of axial symmetry,* $K = \Omega$. *Since j looses its meaning in a deformed potential, mixing between the states with different nlj configuration is possible provided that the states have the same projection* Ω.

Appendix 2.

a)

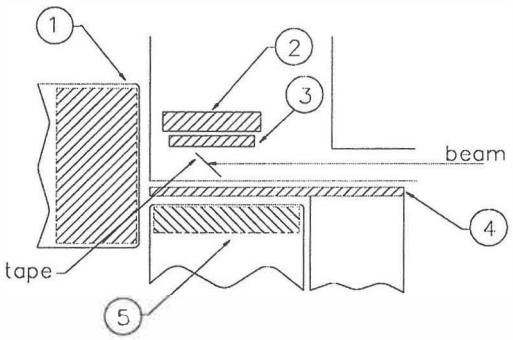

b)

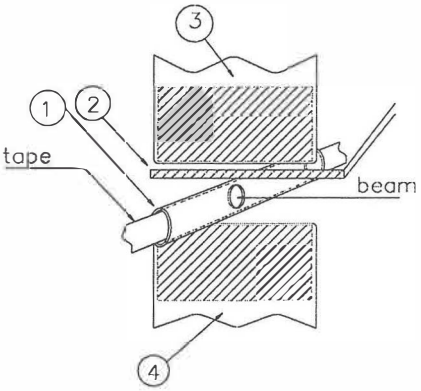

c)

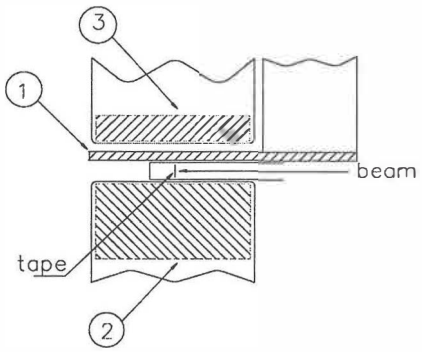

Figure A2. *Measurement setups used in this work.*
a) *Setup used at ISOLDE. 1) E_γ, HPGe(70 %), 2) E_p, 500 μm Si, 3) ΔE_p, 20 μm Si or 10 torr CF_4 gas-detector, 4) ΔE_β, 1.75 mm plastic scintillator, 5) E_X and E_β, 10 or 20 mm planar HPGe, low gain for β's and high gain for X-rays.*
b) *Setup used at GSI. 1) $\Delta E_\beta(1)$, cylindrical 2 mm 4π- plastic scintillator, 2) $\Delta E_\beta(2)$, 1.75 mm plastic scintillator, 3) $E_\gamma(1)$, HPGe(70 %), 4) $E_\gamma(2)$, HPGe(70 %).*
c) *Setup used at IGISOL. 1) $\Delta E_\beta(2)$, 1 mm plastic scintillator, 2) E_γ, HPGe(37 %), 4) E_X, 10 mm planar LEGe.*